LUNDS UNIVERSITET

Department of Physics

Division of Mathematical Physics

Theoretical Light Matter Dynamics Group (TLMD)

Two-photon Rabi oscillations in hydrogen: A theoretical study of effective Hamiltonian approaches

Master Thesis

Jakob Bruhnke

Supervisor: Jan Marcus Dahlström

Co-Supervisor: Axel Stenquist

Degree: Master of Science

Project duration: 8 months

Examination date: May 23, 2024

Abstract

In this thesis, the effective Hamiltonian formalism is studied and applied to two-photon Rabi oscillations in hydrogen.

The process occurs when two photons are absorbed or emitted simultaneously. There exist various approaches to model two-photon transitions. In this thesis, we single out essential quantum states using the projection operator technique and solve for the exact dynamics in this essential subspace of the total Hilbert space. The non-essential states are *adiabatically eliminated*; their contributions are included perturbatively via the resolvent formalism in form of level-shifts and effective couplings to the essential states. Through this, an *effective Hamiltonian* in the essential subspace is obtained.

In the first part of the thesis, it will be shown how this effective Hamiltonian formalism reveals fascinating ties between the *Markov approximation* and the *pole approximation*. Furthermore, higher-order corrections will be discussed. A novel expansion of the resolvent operator is proposed, which in a special case allows for the analytical determination of a second-order effective Hamiltonian.

In the second part, two-photon Rabi oscillations in hydrogen are studied using effective Hamiltonians. Rabi oscillations are a coherent process in which a quantum system, driven by monochromatic radiation, periodically oscillates between two states. Thus, complete population transfer between the states is enabled. When driven by two photons, we speak of two-photon Rabi oscillations. While it is known that two-photon Rabi oscillations cannot be driven between the 1s and 2s state due to ionisation, it will be shown that two-photon Rabi oscillations are indeed possible drive between the 1s and 3s/d states. While the 3s state ionises rapidly, the 3d state couples strongly enough to the 1s ground state to facilitate two-photon Rabi oscillations. The mechanism is explained with bright and dark states.

With ever stronger free-electron lasers and the near-future prospect of attosecond pump-probe experiments (with both extreme ultraviolet and X-ray pump and probe pulses), multi-photon processes by short-wavelength radiation are bound to become more and more accessible and relevant. Therefore, this thesis may serve as a foundation for the theoretical description of novel light-matter interaction phenomena in the near future.

Abbreviations

BWPT	Brillouin-Wigner Perturbation Theory
CIS	Configuration-Interaction Singles
ECS	Exterior Complex Scaling
EDA	Electric Dipole Approximation
FEL	Free-Electron Laser
GRSPT	General Rayleigh-Schrödinger Perturbation Theory
ODE	Ordinary Differential Equation
RWA	Rotating Wave Approximation
SFA	Strong-Field Approximation
STIRAP	Stimulated Raman Adiabatic Passage
SVEA	Slowly-Varying Envelope Approximation
TDCIS	Time-Dependent Configuration Interaction Singles
TDSE	Time-Dependent Schrödinger Equation
TISE	Time-Independent Schrödinger Equation
UV	Ultraviolet
XUV	Extreme Ultraviolet

Contents

Introduction

The study of light-matter interaction is central to our understanding of the universe and has led to many technological breakthroughs that define our everyday lives, such as photography, lasers, LEDs, integrated circuits (manufactured using optical lithography), solar cells, and fiber communications. From a physicist's point of view, we witnessed a scientific revolution in the last century, which was enabled through quantum theory [1–3]: Whereas before, light-matter interaction had to be described macroscopically through properties such as the polarisation, susceptibility or absorption coefficients, quantum theory allows us to describe the microscopic world of interactions with single atoms, molecules, nano structures, and solids.

On the quantum scale, light enables us to control electrons inside matter. In the last century, spurred by experimental advances and theoretical progress – perhaps most notably the invention of the laser [4] – the ability of physicists and chemists to exert such control has grown and led to the blossoming of many subfields. The basis of quantised light-matter interaction was laid out by Einstein already in 1916 when he proposed rate equations for three elementary processes: absorption, stimulated emission and spontaneous emission [5]. Absorption and stimulated emission are two sides of the same coin: It is the excitation or de-excitation of an electron by an electromagnetic field. In the language of quantum optics, the electron absorbs or emits a photon of frequency angular ω to bridge an energy gap $\hbar\omega$. These processes can be described semi-classically with the wave description of light. Spontaneous emission is a more complex effect arising from vacuum fluctuations and requires a quantum optics description [6]. For this thesis, it is rather unimportant, except that the lifetime due to spontaneous emission provides a very strict limit on the coherent processes observable in matter.

This thesis is concerned with the theoretical description of multiphoton processes in quantum systems, with exact applications to hydrogen atoms. Multiphoton transitions are a phenomena distinctly quantum in nature. Instead of absorbing one photon of frequency ω to bridge the energy gap $\hbar\omega$, Maria Göppert-Mayer postulated already in 1931 that it should be possible to absorb, or emit, two photons of frequency $\omega/2$ simultaneously to bridge the same gap [7]. Exactly 30 years later, two experiments independently verified her prediction [8, 9]. Since then, multiphoton transitions have become central to not only nonlinear optics [10], but also to strong-field physics [11, 12], attosecond science [13], two-photon and Raman spectroscopy [6], and recently neutral-atom quantum computing [14–16].

A particularly fascinating quantum effect is Rabi oscillations [17], which encapsulates the process in which the electronic population oscillates between two quantum states, thus enabling complete population transfer between the states [6]. Rabi oscillations are perhaps the most prototypical non-perturbative effect in quantum dynamics, and they constitute one of the most

studied and well-known processes in quantum systems. They are at the cornerstone of quantum computers [18, 19] and have found many mature applications, perhaps most notably in nuclear magnetic resonance spectroscopy and magnetic resonance imaging, which are invaluable tools in analytical chemistry [20] and medicine [21], respectively. For a long time, their observation was only possible in the long-wavelength regime. Recently, the development of seeded free-electron lasers (FEL) led to Rabi oscillations being observed in the extreme ultraviolet (XUV) regime for the first time [22].

In combining the phenomena of two-photon transitions and Rabi oscillations, we arrive at the niche phenomenon of two-photon Rabi oscillations. These were first driven with microwave radiation [23–25] and recently in the NIR regime in Helium [26], as well as the optical and ultraviolet (UV) regimes in heavier atoms such as Rubidium [27–30]. The extension of Rabi oscillations into the multiphoton regime promises to combine the ability to completely transfer population to a target state with the possibility to reach dipole-forbidden and highly excited long-lived states [14, 26, 31, 32]. It is the accurate modelling of two-photon Rabi oscillations in hydrogen that forms the core of this thesis.

The theoretical description of multiphoton transitions is multifaceted, and many textbooks and monographs devote chapters to the topic. Excellent resources valuable for this thesis include Lindgren's and Morrison's *Atomic Many-Body Theory*, Faisal's *Theory of Multiphoton Processes* [33], Akulin's and Karlov's *Intense Resonant Interactions in Quantum Electronics* [34], or Cohen-Tannoudji's, Dupont-Roc's, and Grynberg's *Atom-Photon Interactions* [35]. As a resource on more recent physics, Joachain's, Kylstra's, and Potvliege's *Atoms in Intense Laser Fields* can be recommended [11].

The toolkit of physicists to model multiphoton transitions starts at ordinary time-dependent perturbation theory [11, 33, 36], which is a capable tool at moderate intensities and can, for example, describe non-resonant multiphoton ionisation [37]. Modeling more complicated phenomena, such as resonant multiphoton ionisation, and describing higher intensities, requires more effort. A particularly popular concept has been that of *effective Hamiltonians*, introduced in nuclear physics by Feshbach in 1958 [38, 39]. Applied to multiphoton transitions, the idea is to take the essential quantum states participating in the multiphoton transition and describe their interactions non-perturbatively [33]. At the same time, the influence of other states is described perturbatively and will yield contributions to the energies (in the form of Stark shifts and ionisation rates) and the couplings (in the form of effective multiphoton couplings and imaginary Rabi frequencies) [33, 40, 41]. Effective Hamiltonians can be obtained using many different approaches, ranging from working in the interaction picture in a rotating frame (i.e. within the *rotating wave approximation* (RWA) [6]) and adiabatically eliminating non-essential states [32, 42–48], employing *Floquet theory* [11, 34, 41, 49–52] or working with the *resolvent operator* with the *projection operator technique* [35, 40, 53–55].

In this thesis, we will use non-Hermitian Floquet theory [51, 52] and the effective Hamiltonian formalism [33] to model two-photon Rabi oscillations in hydrogen. The results are benchmarked by numerically exact simulations for hydrogen within the dipole approximation. It has been previously shown that two-photon Rabi oscillations between the 1s and metastable 2s state in hydrogen cannot be observed [56]. The model presented in this thesis reproduces this important

result. A novel finding in this thesis is that there exist, however, parameter regimes in which two-photon Rabi oscillations between the 1s and 3s/3d states can be driven successfully in hydrogen. We can describe them using a 3-level effective Hamiltonian, which through a bright and dark state analysis can be approximated by an effective 2-level bright system.

Two-photon Rabi oscillations require a theoretical deep-dive into an approximation that is central to multiphoton transitions: *adiabatic elimination* [57]. When the intermediate states in multiphoton transitions are sufficiently non-resonant, their influence on the overall dynamics can be approximated as adiabatic. This means that their average amplitudes vary slowly, so that only their instantaneous amplitudes matter for the essential states dynamics. Neglecting the history of the intermediate states constitutes an assumption of Markovianity. With the development of stimulated Raman adiabatic passage (STIRAP) [58], adiabatic elimination has become quite popular. However, there have been concerns on the validity of common implementations of adiabatic elimination [59, 60], the relationship of adiabatic elimination and the RWA [61, 62], as well as discussions about possible higher-order extensions and generalisations [60, 63–68]. An essential conclusion of this thesis is that the assumption of Markovianity is directly reflected in the pole approximation of the resolvent operator formalism, in which the energy landscape around the resonance is approximated as flat. Furthermore, going beyond the pole approximation allows for the description of higher-order processes in adiabatic elimination, yielding higher-order effective Hamiltonians [33, 36]. Previous proposals were based on either iterative or perturbative procedures [33, 60, 69–75]. In this thesis, a novel *ansatz* for an expansion of the resolvent operator will be shown. For a special case, this *ansatz* allows us to analytically calculate the second-order effective Hamiltonian.

The thesis is thus split into three parts. In Chapter 1, the theory of semi-classical light-matter interaction is laid out, focusing on Floquet theory and the resolvent formalism. As a minimalistic case study, the three-level ladder system is presented, in which two-photon Rabi oscillations can, through adiabatic elimination, be modeled via a 2-level effective Hamiltonian. In preparation for the next chapter, different implementations of adiabatic elimination are discussed. In Chapter 2, a comprehensive theory of higher-order adiabatic elimination within the resolvent formalism is presented and put into context with a recent publication of Paulisch *et al.* [60]. Lastly, in Chapter 3, a model system capable of describing intense, coherent multiphoton processes in hydrogen is presented, relying on non-Hermitian Floquet theory and the effective Hamiltonian formalism. After a case study of the well-explored 1s-2s two-photon transition in hydrogen, our physical core result of two-photon Rabi oscillations between the 1s and 3s/3d states is discussed in detail. Finally, in 1983, Holt *et al.* calculated effective Hamiltonian parameters for the resonant two-, three-, and four-photon ionisation in hydrogen [41]. Since their study, computational capabilities have improved, and thus, updated and supplemental parameters will be presented. The thesis concludes with separate summaries of Chapters 2 and 3.

The following two pages contain condensed flowcharts (Fig. 1 and 2) summarising the contributions of this thesis (analytical and conceptual contributions shaded blue, computational contributions shaded green). Furthermore, the concepts and results from the literature that are most central to this thesis are summarised (shaded red) and, through arrows, related to the research of the thesis. These flowcharts may serve as a guide when reading Chapters 2 and 3.

Flowchart for Chapter 2: Higher-order adiabatic elimination in the resolvent formalism

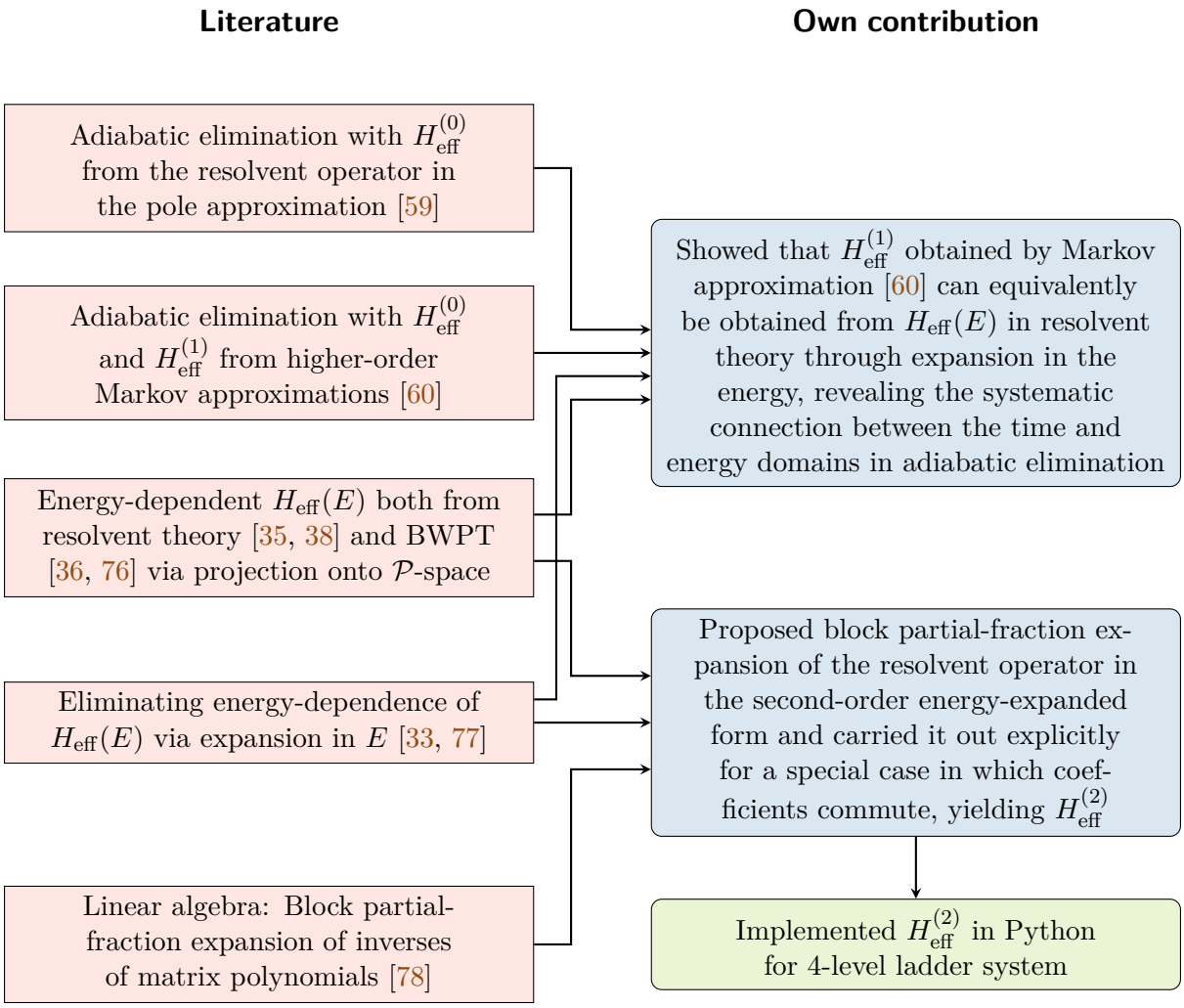

Figure 1: Flowchart for the contributions made in Chapter 2 and how they relate to the literature (indicated by arrows). Literature is shaded red, analytical contributions blue, and computational contributions green.

Flowchart for Chapter 3: Two-photon Rabi oscillations in hydrogen

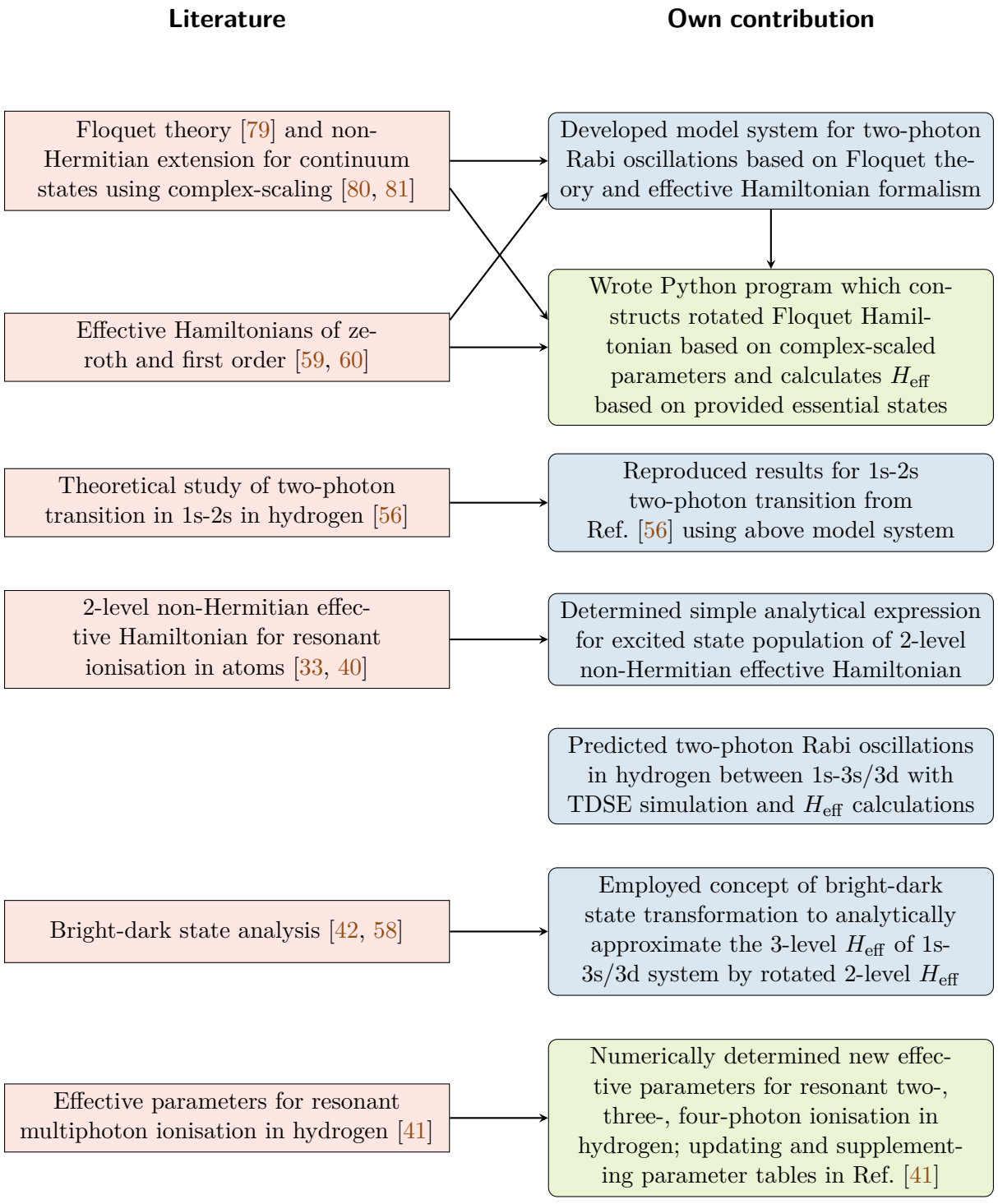

Figure 2: Flowchart for the contributions made in Chapter 3 and how they relate to the literature (indicated by arrows). Literature is shaded red, analytical or conceptual contributions blue, and computational contributions green.

1 Interaction of a quantum system with an electromagnetic field

The study of light-matter interaction is, first and foremost, applied quantum mechanics [82–84]. We will thus start at the beginning, Schrödinger's equation, in Section 1.1, and then progress to the semiclassical Hamiltonian of a quantized atom and classical field, in Section 1.2. For periodic Hamiltonians, such as the semiclassical Hamiltonian for a monochromatic field, Floquet theory, introduced in Section 1.3, provides an approach to obtain the coupled set of ordinary differential equations (ODE) for the state amplitudes where the coefficients are time-independent. The resolvent operator formalism and projection operator technique, introduced in Section 1.4, allow the exact description of the quantum dynamics of essential Hilbert subspaces, providing a pathway beyond ordinary time-dependent perturbation theory. Fundamental concepts of multi-photon light-matter dynamics will be demonstrated via the textbook example of a two-photon Rabi cycling three-level ladder system in Section 1.5. Different approaches to the adiabatic elimination of the intermediate state will be presented, ranging from naïve to rigorous. Finally, in Section 1.6, the treatment of ionisation is discussed, in which a decaying quantum system is described via non-Hermitian effective Hamiltonians.

Atomic units ($\hbar = m_e = e = 4\pi\epsilon_0 = 1$) are used.

1.1 The Schrödinger equation

In quantum theory, physical observables are represented by Hermitian operators acting on quantum states $|\Psi\rangle$ in a Hilbert space $\mathcal{H}$. The dynamics of a quantum system can be expressed in equivalent "pictures", e.g. the Schrödinger picture, Heisenberg picture, or interaction picture. These different pictures yield the same physics and differ only in their mathematical formalism. In the present work, the Schrödinger picture is used. The quantum states $|\Psi(t)\rangle$ are then time-dependent, while the operators are time-independent [84]. The dynamics of $|\Psi(t)\rangle$ is governed by the time-dependent Schrödinger equation (TDSE) [3]

$$\mathrm{i}\frac{\mathrm{d}}{\mathrm{d}t}|\Psi(t)\rangle = H|\Psi(t)\rangle\,, \tag{1.1}$$

where H is the Hamilton operator, which is the operator associated with the energy of the quantum system. Note that for an open system, such as one that results from including a classical radiation field, the Hamiltonian might be explicitly time-dependent [84].

1.2 The Hamiltonian of an atom in an electromagnetic field

Maxwell's equations [85] describe the dynamics of the electric field $\boldsymbol{\mathcal{E}}(\mathbf{r},t)$ and magnetic field $\boldsymbol{\mathcal{B}}(\mathbf{r},t)$. Through a scalar potential $\phi(\mathbf{r},t)$ and vector potential $\boldsymbol{\mathcal{A}}(\mathbf{r},t)$, these fields can be expressed as [86]

$$\boldsymbol{\mathcal{E}}(\mathbf{r},t) = -\boldsymbol{\nabla}\phi(\mathbf{r},t) - \frac{1}{c}\frac{\partial}{\partial t}\boldsymbol{\mathcal{A}}(\mathbf{r},t) \tag{1.2}$$

$$\boldsymbol{\mathcal{B}}(\mathbf{r},t) = \boldsymbol{\nabla} \times \boldsymbol{\mathcal{A}}(\mathbf{r},t). \tag{1.3}$$

Due to the derivatives appearing in Eq. (1.2) and (1.3), there is a certain freedom in choosing ϕ and $\boldsymbol{\mathcal{A}}$, referred to as gauge ambiguity. The gauge transformations read

$$\phi \to \phi - \frac{1}{c}\frac{\partial}{\partial t}\chi \quad \text{and} \quad \boldsymbol{\mathcal{A}} \to \boldsymbol{\mathcal{A}} + \boldsymbol{\nabla}\chi, \tag{1.4}$$

where $\chi(\mathbf{r},t)$ is an arbitrary scalar field that is twice continuously differentiable. Classical electromagnetism is *gauge invariant* under these transformations [86].

It can be shown that quantum mechanics is gauge invariant too, and thus, there are various equivalent ways of including an electric and magnetic field in quantum mechanics [84]. In light-matter interaction, popular choices are the *length gauge* [7, 87] and the *velocity gauge* [33, 88]. There is an ongoing debate about the impact of gauges in the context of strong-field physics, especially regarding the strong-field approximation (SFA). While quantum mechanics is gauge-invariant, the invariance is not guaranteed when approximations are introduced [89–94]. For this thesis, the debate is not relevant since the SFA is not made and, crucially, the result of the model systems presented in this work can always be compared to both velocity gauge and length gauge TDSE simulations.

Often in light-matter interaction, one may neglect the interaction with the magnetic field [6] since the magnetic dipole moment is more than 100 times weaker than the electric dipole moment [95]. Just as common-place is the *electric dipole approximation* (EDA), introduced by Maria Göppert-Mayer [7], which consists of neglecting the spatial variation of the field quantities, i.e. $\boldsymbol{\mathcal{E}}(\mathbf{r},t) \to \boldsymbol{\mathcal{E}}(t)$, etc. [84]. Note that neglecting the magnetic field is occasionally regarded as part of the EDA [89]. The EDA is intuitive given that the characteristic length scale of atoms is in Ångström ($10^{-10}\,\mathrm{m}$), while the wavelength of visible light is approximately $10^{-7}\,\mathrm{m}$ [82]. It fails at high intensities (where relativistic and magnetic effects have to be accounted for) as well as high and (perhaps counter-intuitively) low frequencies [96, 97]. In this thesis, the magnetic coupling will be neglected, and the EDA applied throughout.

For a field-free system, described by the Hamiltonian H_0, adding the radiation field $V(t)$ within the electric dipole approximation is accomplished as follows:

$$H(t) = H_0 + V(t) = H_0 + \begin{cases} \mathbf{r}\cdot\boldsymbol{\mathcal{E}}(t), & \textit{length gauge}, \\ \mathbf{p}\cdot\boldsymbol{\mathcal{A}}(t) + \frac{\boldsymbol{\mathcal{A}}^2(t)}{2}, & \textit{velocity gauge}. \end{cases} \tag{1.5}$$

These Hamiltonians describe the system interacting with a classical radiation field [82, 84].

1.3 A brief introduction to Floquet theory

In this section, the theoretical framework of how to describe a quantum system under periodic excitation is reviewed. The period is denoted $\tau = 2\pi/\omega$. This theory is today known as (quantum) Floquet theory and was first explored by Shirley, 1965 [79]. It is well-established and covered in many textbooks, e.g. Ref. [34, 57]. Floquet theory describes physics beyond the RWA [6, 11]. The RWA is an extensively-used approximation in light-matter interaction [43, 44, 98, 99]. It is based on the neglect of fast-oscillating (i.e. off-resonant) terms in the Hamiltonian. For multiphoton processes that require summation over many off-resonant states, the RWA can easily break down [62, 100–102].

Floquet theory is concerned with the time evolution of a quantum system with periodic Hamiltonian $H(t) = H_0 + V(t)$ where $V(t) = V(t+\tau)$. Let us assume excitation by a linearly polarized plane wave in length gauge, $V(t) = z\mathcal{E}_0 \cos(\omega t)$.[1] In the TDSE, we expand $|\Psi(t)\rangle = \sum_m c_m(t)\,|m\rangle$ into the orthonormal field-free basis spanned by $|m\rangle$ and project onto a field-free eigenstate from left, $\langle n|$:

$$\mathrm{i}\frac{\mathrm{d}}{\mathrm{d}t}c_n(t) = E_n c_n(t) + \mathcal{E}_0 \cos(\omega t)\sum_m z_{nm} c_m(t). \tag{1.6}$$

Here, we used $\langle n|m\rangle = \delta_{nm}$, $H_0\,|n\rangle = E_n\,|n\rangle$, and defined $z_{nm} \coloneqq \langle n|z|m\rangle$. Despite the periodic Hamiltonian, the amplitudes $c_n(t)$ are not periodic themselves. Within Floquet theory we can however expand the coefficients $c_n(t)$

$$c_n(t) = \sum_{k=-\infty}^{\infty} c_{n,k}(t)\mathrm{e}^{\mathrm{i}k\omega t}, \tag{1.7}$$

where the expansion coefficients $c_{n,k}(t)$ are periodic, i.e. $c_{n,k}(t) = c_{n,k}(t+\tau)$. The existence of these periodic expansion coefficients is guaranteed by the Floquet theorem [57]. Note that while Eq. (1.7) may look like a Fourier series, it is not since the $c_{n,k}(t)$ are time-dependent. However, the index k is still referred to as the Fourier component [33] or harmonic index. For our purposes, it helps to interpret k as an occupation number, i.e. the number of photons associated with a quantum state. This is possible since Floquet theory can be formulated as a limiting case of quantum optics [33].

The task is now to determine $c_{n,k}(t)$. To this end, let us insert Eq. (1.7) into Eq. (1.6). Equating the terms with the same harmonic k [34], we obtain

$$\mathrm{i}\frac{\mathrm{d}}{\mathrm{d}t}c_{n,k}(t) = (E_n + k\omega)c_{n,k}(t) + \frac{\mathcal{E}_0}{2}\sum_m z_{nm}\left[c_{m,k+1}(t) + c_{m,k-1}(t)\right]. \tag{1.8}$$

Comparing Eq. (1.6) and Eq. (1.8), we see that the transformation is both advantageous and disadvantageous. The disadvantage is that instead of one equation per n, we now have to solve one equation per n *and* per k. Thus, where for a two-level system there were two equations to be solved, we now have to solve $2k$ equations. Since the sum over k in Eq. (1.7)

[1] Many-mode fields can also be treated using Floquet theory [34, 51, 103–106]. Pulse envelopes can be included within the slowly-varying envelope approximation (SVEA) [33]; the same applies to time-dependent phases, known as pulse chirp effects.

goes from $-\infty$ to ∞, we are technically dealing with infinitely many equations [107]. Luckily, the equations for k can usually be truncated considerably so that only a few remain that contain the essential physics. The considerable advantage is that we transformed a set of coupled ODEs with time-dependent coefficients (due to the $\cos(\omega t)$) to a set of coupled ODEs with constant coefficients (diagonals $E_n + k\omega$ and off-diagonals $\mathcal{E}_0 z_{nm}/2$) [34, 57]. This is helpful for the pursuit of analytical solutions, as well as for numerical approaches.

On another note, we immediately notice the selection rule

$$k \to k \pm 1, \tag{1.9}$$

which means that the photon number is only allowed to decrease or increase by one in the course of one transition. The amplitude $c_{m,k+1}(t)$ corresponds to stimulated emission while $c_{m,k-1}(t)$ to absorption. In many situations, only one of these processes conserves energy. Omitting the other fast-oscillating amplitude is known as the RWA. The presence of these counter-rotating terms in Eq. (1.8) shows how Floquet theory gives access to physics beyond the RWA.

Due to the similar structure of Eq. (1.6) and (1.8), the latter is sometimes called the Floquet-Schrödinger equation, with the corresponding Floquet Hamiltonian $H^{(F)}$ [33]. The Floquet Hamiltonian yields itself to a perturbative interpretation of the kind

$$H^{(F)} = H_0^{(F)} + V^{(F)}, \tag{1.10}$$

where the Floquet states $|n, k\rangle$ are the eigenstates of $H_0^{(F)}$, while $V^{(F)}$ represents the perturbation. Without going into more detail, it can be shown that working with the Floquet-Schrödinger equation, and thus the Floquet Hamiltonian and Floquet states, does not pose new challenges: The Floquet Hamiltonian is Hermitian, the Floquet states span an orthonormal basis, and the time-evolution operator constructed using the Floquet Hamiltonian is unitary, fulfills the time-transition property, $U(t, t_0) = U(t, t_1)U(t_1, t_0)$, and the normalisation, $U(t_0, t_0) = 1$ [33].

1.4 The resolvent operator formalism

While ordinary time-dependent perturbation theory is useful for treating off-resonant multiphoton processes, it easily breaks down for resonant phenomena due to singularities [33]. Thus, more powerful procedures are necessary. In this thesis, multiphoton processes will be described via the resolvent operator formalism [38, 39] in conjunction with the projection operator technique [39, 108]. The resolvent formalism is a reformulation of quantum mechanics in the energy domain. Through projection of the resolvent operator onto a subset of states deemed essential, the dynamics of the multiphoton-resonant states can be described non-perturbatively, while the influence of non-essential states is included parametrically in the form of level-shifts and effective couplings [33, 35, 109]. This section paraphrases *Atom-Photon Interactions* of Cohen-Tannoudji *et al.* [35].

1.4.1 The resolvent operator

Let the Hamiltonian of our system be given by $H = H_0 + V$. Since the derivations leading to the resolvent operator make use of the time-evolution operator in exponential form, i.e. $U(t,t') = \mathrm{e}^{-\mathrm{i}H(t-t')}$, the Hamiltonian needs to be time-independent. Thus, Floquet Hamiltonians synergize well with the resolvent operator formalism because the explicit time-dependence of the field is removed [33].[2]

The resolvent operator is denoted by

$$G(z) = \frac{1}{z - H}, \tag{1.11}$$

where $z \in \mathbb{C}$. The resolvent is not defined on the spectrum of H, since this would lead to singularities. $G(z)$ is related to the time evolution operator, $U(\tau)$, $\tau \coloneqq t - t'$, of a quantum system via

$$U(\tau) = \frac{1}{2\pi\mathrm{i}} \int_{C_+ \cup C_-} \mathrm{d}z\, \mathrm{e}^{-\mathrm{i}z\tau} G(z), \tag{1.12}$$

where $C_\pm$ are the integration contours, corresponding to two infinitely close parallel lines above and below the real axis, oriented from right to left (C_+) and from left to right (C_-) [35]. Thus, knowledge of the resolvent gives access to the time evolution of a system.

1.4.2 The projection operator technique

The full Hamiltonian $H = H_0 + V$ is complicated and to obtain $G(z)$ from Eq. (1.11), we need to invert the full Hamiltonian. In order to obtain the time evolution from Eq. (1.12) via the residue theorem, we furthermore need to find the eigenvalues of H. For large Hilbert spaces, this problem is intractible. However, in multiphoton transitions, the only states with significant population – and thus the only states of interest to us – are the multiphoton-resonant states. Through the projection operator technique, we project onto the subspace of the Hilbert space which is spanned by these essential states and thus obtain the effective dynamics of the essential states, described by an effective Hamiltonian [39, 108].

For a given Hilbert space $\mathcal{H}$, we denote the subspace of essential states as $\mathcal{P}$ (also called the *model space* [110, 111]) and the subspace of non-essential states as $\mathcal{Q} = \mathcal{P}^\perp$. The two subspaces are orthogonal complements of each other and thus their direct sum spans the entire Hilbert space, $\mathcal{H} = \mathcal{P} \oplus \mathcal{Q}$. The operators that project onto $\mathcal{P}$ and $\mathcal{Q}$ are denoted by P and Q respectively. The projector P satisfies $P = P^\dagger$ and $P^2 = P$, analogously $Q = Q^\dagger$ and $Q^2 = Q$, and $PQ = QP = 0$.

The resolvent operator in the model space $\mathcal{P}$ is given by

$$PG(z)P = \frac{P}{z - PH_0P - PR(z)P}, \tag{1.13}$$

where $R(z)$ is called the *level-shift operator*,

$$R(z) = V + V\frac{Q}{z - QHQ}V. \tag{1.14}$$

[2] Actually, the Floquet Hamiltonian arises from the semiclassical resolvent theory [33].

$PR(z)P$ describes the interaction between the $\mathcal{Q}$-space and the model space by giving contributions to the energies (in light-matter interaction, these are dynamical Stark shifts) and introducing effective couplings on the off-diagonals. Note that by defining an effective Hamiltonian (also called the Feshbach operator [38]),

$$H_{\text{eff}}(z) = PH_0P - PR(z)P, \tag{1.15}$$

the resolvent in Eq. (1.13) becomes structurally be equivalent to Eq. (1.11). Thus, $H_{\text{eff}}(z)$ serves as the effective Hamiltonian in the model space, where the coupling from $\mathcal{Q}$ to $\mathcal{P}$ is contained exactly within $R(z)$. $H_{\text{eff}}(z)$ reproduces a subset of the exact eigenvalues of the full Hamiltonian H. The dependence on the energy prevents us from employing this Hamiltonian in the time-independent Schrödinger equation (TISE), $EP|\Psi\rangle = H_{\text{eff}}(E)P|\Psi\rangle$ (where we set $z \equiv E$). Instead, we will have to resort to approximations for $R(z)$, which aim at eliminating the z-dependence.

Lastly, it can also be shown that the resolvent can couple from $\mathcal{P}$ to $\mathcal{Q}$ as

$$QG(z)P = \frac{Q}{z - QHQ}QVPG(z)P. \tag{1.16}$$

To interpret $QG(z)P$, one must read from right to left. We first propagate in $\mathcal{P}$ using $PG(z)P$ and then couple to the non-essential subspace $\mathcal{Q}$ via QVP, where we obtain the dynamics of the non-essential states by propagating under $\mathcal{Q}$-space Hamiltonian QHQ. Thus, via Eq. (1.16), the dynamic of the non-essential states can be obtained by first calculating the dynamics of the essential states, then coupling to the non-essential states and finally propagating in $\mathcal{Q}$ using QHQ. Note that these previous derivations are exact and non-perturbative. They are a reformulation of time-dependent quantum mechanics in the energy domain for time-independent Hamiltonians.

1.4.3 Expansion of the level-shift operator

In perturbation theory, the perturbation V is taken as sufficiently small to expand in it. Within the resolvent formalism, this is carried out by perturbatively expanding the level-shift operator in powers of V [108], yielding the perturbation series

$$\begin{aligned} R(z) \approx V + V\frac{Q}{z - H_0}V + V\frac{Q}{z - H_0}V\frac{Q}{z - H_0}V \\ + V\frac{Q}{z - H_0}V\frac{Q}{z - H_0}V\frac{Q}{z - H_0}V + \dots \,. \end{aligned} \tag{1.17}$$

Note that we simplified $Q[z - QH_0Q]^{-1} = Q[z - H_0]^{-1}$ since $[Q, H_0] = 0$ and $Q^2 = Q$.[3]

While Eq. (1.17) may seem rather abstract, we may consider the effective interaction $PR(z)P$, which in the expanded form of Eq. (1.17) lends itself to a clear physical interpretation: The number of V appearing in any term corresponds to the number of exchanged photons that take part in a process. Due to the P projectors in front of and behind $R(z)$, the start and end point of the multiphoton processes are always essential states while, due to the Q projectors in Eq. (1.17),

[3] Q projects on the field-free non-essential states, which are eigenstates of H_0.

all intermediate states are necessarily non-essential.

1.5 Three-level ladder system and adiabatic elimination

In this section, the interaction of a three-level ladder system with a linearly polarized electric field will be studied. This system offers the most simple semi-classical description of a two-photon process [34, 107]. As such, three-level systems have been studied in depth in the context of lasers [112–115], spectroscopy [116, 117], quantum cryptography [118], and STIRAP [119].

First, Floquet theory will be employed to yield the amplitude equations within the RWA [34]. For such a simple system, this may seem unnecessary since one could swiftly derive these equations in the interaction picture [57]. However, the problems tackled in Chapter 3 rely on the Floquet Hamiltonian and therefore, it is instructive to use it here. For large detunings of the intermediate state, one can through various implementations of adiabatic elimination obtain 2-level effective Hamiltonians. The naïve approach, which is a typical procedure (see e.g. Ref. [66, 120–122]), will be discussed in Section 1.5.2. Its shortcomings are summarised in Section 1.5.3. Formal adiabatic elimination within the resolvent formalism is presented in Section 1.5.4. Paulisch *et al.* proposed a higher-order adiabatic elimination procedure based on Markov approximations in the time domain [60]; their approach is shown in Section 1.5.5.

1.5.1 The coupled equations of the three-level ladder system

The three-level ladder model consists out of three states, $|a\rangle$, $|v\rangle$, and $|b\rangle$, with energies $E_{a/v/b}$ respectively. The states are coupled via an electric field $\mathcal{E}_0 \cos(\omega_0 t)$ with frequency ω_0. The system is depicted in Figure 1.1a). Thinking in terms of Floquet theory (see Section 1.3), we can associate the ground state $|a\rangle$ with N photons, yielding the Floquet state $|a, N\rangle$. When we transition from $|a\rangle$ to the intermediate state $|v\rangle$, we absorb one photon, yielding $|v, N-1\rangle$ and analogously the upper state $|b, N-2\rangle$. The Floquet states have similar energies, differing only in the one-photon detuning Δ and the two-photon detuning δ, as illustrated in Figure 1.1b).

By only considering these three resonant Floquet states, we discard infinitely many Floquet states. In particular, exclusion of the four states $|a, N-2\rangle$, $|v, N+1\rangle$, $|v, N-3\rangle$ and $|b, N\rangle$ corresponds to the RWA [100], which necessitates that the neglected states are far-detuned from resonance [6]. This, we will for this example assume to be true.

The starting point is Eq. (1.8), i.e. the TDSE for the Floquet Hamiltonian. Through the discussed truncation of the infinite Floquet Hamiltonian, we obtain a 3×3 Hamiltonian for the three Floquet states $|a, N\rangle$, $|v, N-1\rangle$ and $|b, N-2\rangle$ with coefficients $c_{a,N}(t)$, $c_{v,N-1}(t)$ and $c_{b,N-2}(t)$. By shifting the zero-point energy to the quasi-energy of $|a, N\rangle$, i.e. $N\omega_0 + E_a$ (via the unitary transformation $\exp[-\mathrm{i}(N\omega_0 + E_a)t]$), we can state the full coupled equations for the three-level system:

$$\mathrm{i}\dot{c}_{a,N}(t) = \frac{1}{2}\mathcal{E}_0 z_{av} c_{v,N-1}(t), \tag{1.18}$$

$$\mathrm{i}\dot{c}_{v,N-1}(t) = [-\omega_0 + (E_v - E_a)]c_{v,N-1}(t) + \frac{1}{2}\mathcal{E}_0 z_{va} c_{a,N}(t) + \frac{1}{2}\mathcal{E}_0 z_{vb} c_{b,N-2}(t), \tag{1.19}$$

$$\mathrm{i}\dot{c}_{b,N-2}(t) = [-2\omega_0 + (E_b - E_a)]c_{b,N-2}(t) + \frac{1}{2}\mathcal{E}_0 z_{bv} c_{v,N-1}(t). \tag{1.20}$$

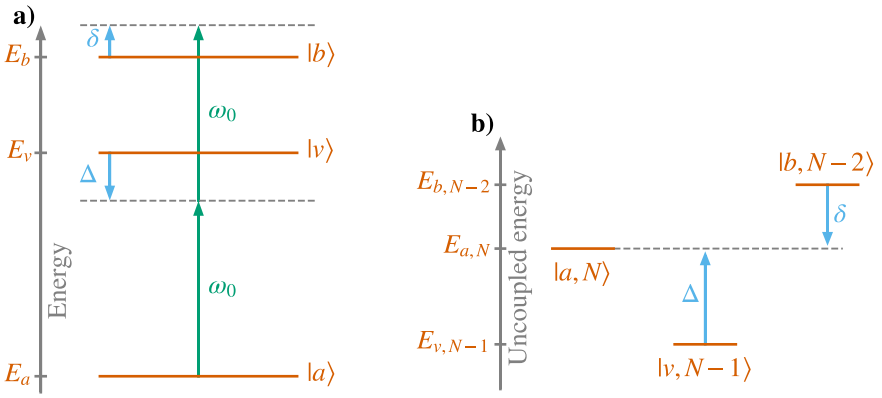

Figure 1.1: Illustrations of a three-level system with two photons of frequency ω_0 with an **a)** absolute energy scale with the energies E_a, E_v and E_b and **b)** uncoupled energy scale with uncoupled energies $E_{a,N}$, $E_{v,N-1}$ and $E_{b,N-2}$. The one-photon detuning is given by $\Delta = \omega_0 - \omega_{va}$ and the two-photon detuning by $\delta = 2\omega_0 - \omega_{ba}$, where $\omega_{jk} = E_j - E_k$ is the energy gap of the respective levels.

A few abbreviations are introduced:

- The energy difference $\omega_{jk} \coloneqq E_j - E_k$
- The one-photon detuning $\Delta \coloneqq \omega_{va} - \omega_0$ and two-photon detuning $\delta \coloneqq \omega_{ba} - 2\omega_0$
- The Rabi frequency $\Omega_{jk} \coloneqq \mathcal{E}_0 z_{jk}$ (also referred to as the coupling)
- The coefficients $a(t) \coloneqq c_{a,N}(t)$, $v(t) \coloneqq c_{v,N-1}(t)$, and $b(t) \coloneqq c_{b,N-2}$, and analogously the states $|a\rangle \coloneqq |a, N\rangle$, $|v\rangle \coloneqq |v, N-1\rangle$ and $|b\rangle \coloneqq |b, N-2\rangle$[4]

The final equations for the three-level system are now cast into a familiar form [25, 34, 59, 60],

$$\mathrm{i}\dot{a}(t) = \frac{1}{2}\Omega_{av} v(t), \tag{1.21}$$

$$\mathrm{i}\dot{v}(t) = \Delta v(t) + \frac{1}{2}\Omega_{va} a(t) + \frac{1}{2}\Omega_{vb} b(t), \tag{1.22}$$

$$\mathrm{i}\dot{b}(t) = \delta b(t) + \frac{1}{2}\Omega_{bv} v(t). \tag{1.23}$$

They are in fact the equations one would obtain from the usual interaction picture Hamiltonian within the RWA. The equations can easily be solved for a given initial condition using any numerical integration scheme, e.g. 4th order Runge Kutta [123].

When describing the dynamics of this system, two different regimes for the population transfer from $|a\rangle$ to $|b\rangle$ can be identified: the *sequential* and *non-sequential* regime. In the sequential regime, the one-photon detuning $|\Delta|$ is small compared to the couplings $|\Omega_{va/vb}|$ and thus, the transition from $|a\rangle$ to $|b\rangle$ is facilitated via two sequential one-photon transitions, first from $|a\rangle$ to $|v\rangle$ and, then, from $|v\rangle$ to $|b\rangle$. The populations $|a(t)|^2$, $|v(t)|^2$, and $|b(t)|^2$ will look similar to those shown in Figure 1.2a). In the sequential process, the state $|v\rangle$ is significantly populated.

[4] We are dropping all reference to the photon number here since each state corresponds to a different photon number. Of course, we are still dealing with Floquet states and their energies.

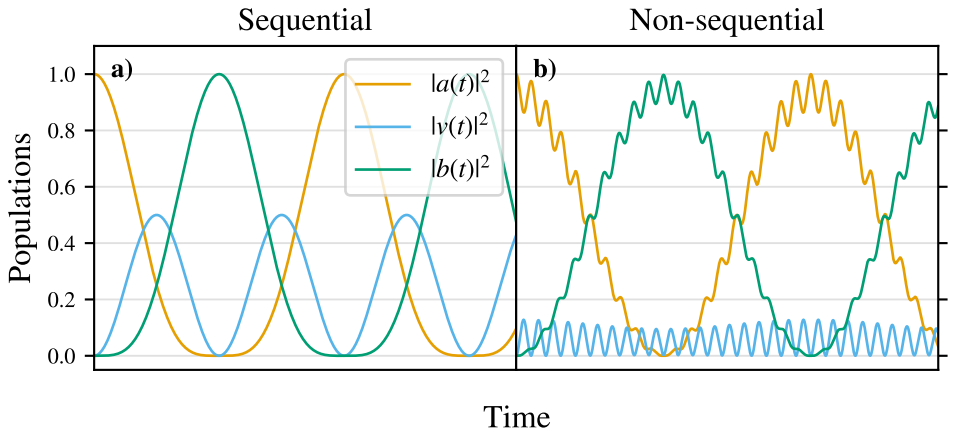

Figure 1.2: Illustration of the population dynamics in a three-level system with two photons for the **a)** sequential process and **b)** non-sequential process. These figures do not represent the dynamics of a specific atomic system and the time units are thus arbitrary and omitted. The parameters were chosen so that for **a)** the detunings $\Delta = 0$ and $\delta = 0$ and that for **b)** the condition $|\Omega_{av}| \ll |\Delta|$ is barely fulfilled (by choosing $\Omega_{av} = 0.4\Delta$ and $\Omega_{vb} = 0.3\Delta$), as well as choosing $\delta = (\Omega_{vb}^2 - \Omega_{av}^2)/4\Delta$ in order to compensate the Stark shifts (see Section 1.5.2). The populations in **b)** are modulated by rapid oscillations. These modulations are due to the sudden turn-on of the field at the initial time. For a discussion, see Appendix A.

Conversely, when $|\Omega_{va/vb}| \ll |\Delta|$, the one-photon transition from $|a\rangle$ to $|v\rangle$ cannot be driven. Still, we may see Rabi oscillations between $|a\rangle$ and $|b\rangle$, as shown schematically in Figure 1.2b). This is the non-sequential regime, where two photons are absorbed and emitted at once. The populations are modulated by fast oscillations. These are due to the sudden turn-on of the field at the initial time, as discussed in Appendix A. In the two-photon process, the intermediate level does not acquire population and is sometimes referred to as a *virtual level*. This virtual level is crucial for the two-photon Rabi cycling, yet the resulting populations look like that of a 2-level system. Thus, it is only natural to ask if we could describe the system dynamics as that of an approximate effective 2-level system, with an effective Hamiltonian H_{eff}. Obtaining this effective Hamiltonian can be achieved via adiabatic elimination and is explored in the following sections and thoroughly in Chapter 2.

1.5.2 The naïve version of adiabatic elimination

Eliminating the virtual states in the description of multiphoton processes is known as adiabatic elimination. Through adiabatic elimination, the effect of the intermediate states on the essential states (i.e. the multiphoton resonant states) is parametrized via effective coupling between the essential states.

Adiabatic elimination has been subject to debate in recent history [59–65]. In many works, e.g. [14, 120, 121], a naïve version of adiabatic elimination is employed which, while often yielding sensible results, suffers from inconsistencies and, for certain parameter regimes, inaccuracy. Thus, rigorous implementations of adiabatic elimination and more accurate procedures have been proposed. In this section, the naïve version is presented so that subsequently in Section 1.5.3,

the criticisms can be elaborated upon and in the following Sections 1.5.4 and 1.5.5 be addressed.

The motivation for the naïve implementation of adiabatic elimination is the following. If the couplings Ω_{av} and Ω_{vb} are energetically much smaller than the one-photon detuning,

$$|\Omega_{av}| \ll |\Delta| \qquad \text{and} \qquad |\Omega_{vb}| \ll |\Delta|, \tag{1.24}$$

the intermediate state $v(t)$ will be barely populated and thus change only negligibly throughout propagation. Hence, it may seem reasonable to simply set $\dot{v}(t) \approx 0$ [61]. When we apply this to Eq. (1.22), we can rearrange to $v(t)$,

$$v(t) = -\frac{1}{2\Delta}\left[\Omega_{va}a(t) + \Omega_{vb}b(t)\right], \tag{1.25}$$

and insert into Eq. (1.21) and (1.23) in order to obtain two coupled equations of $a(t)$ and $b(t)$:

$$\mathrm{i}\dot{a}(t) = -\frac{|\Omega_{av}|^2}{4\Delta}a(t) - \frac{1}{2}\frac{\Omega_{av}\Omega_{vb}}{2\Delta}b(t), \tag{1.26}$$

$$\mathrm{i}\dot{b}(t) = -\frac{1}{2}\frac{\Omega_{bv}\Omega_{va}}{2\Delta}b(t) + \left(\delta - \frac{|\Omega_{bv}|^2}{4\Delta}\right)b(t). \tag{1.27}$$

Introducing the Stark shifts $S_a := -|\Omega_{av}|^2/4\Delta$ and $S_b := -|\Omega_{bv}|^2/4\Delta$, as well as the effective coupling $\Omega_{\text{eff}} := -\Omega_{bv}\Omega_{va}/2\Delta$ [34, 57, 63], the equations are cast into

$$\mathrm{i}\dot{a}(t) = S_a a(t) + \frac{1}{2}\Omega_{\text{eff}}^* b(t), \tag{1.28}$$

$$\mathrm{i}\dot{b}(t) = \frac{1}{2}\Omega_{\text{eff}} b(t) + (\delta + S_b)\, b(t). \tag{1.29}$$

In other words, the dynamics of the three-level system has been reduced to the dynamics of a two-level system coupled effectively by Ω_{eff}, where the ground state is shifted by S_a and the excited state by $\delta + S_b$. These equations can easily be integrated analytically. Using the initial condition $b(t=0) = 0$ and $a(t=0) = 1$ we obtain the populations

$$|a(t)|^2 = \left|\frac{\Omega_{\text{eff}}}{W}\right|^2 \cos^2\left(\frac{W}{2}t\right) + \left(1 - \left|\frac{\Omega_{\text{eff}}}{W}\right|^2\right), \tag{1.30}$$

$$|b(t)|^2 = \left|\frac{\Omega_{\text{eff}}}{W}\right|^2 \sin^2\left(\frac{W}{2}t\right), \tag{1.31}$$

where

$$W = \sqrt{(S_a - S_b - \delta)^2 + |\Omega_{\text{eff}}|^2} \tag{1.32}$$

is the generalized Rabi frequency [22, 25].

In Fig. 1.2b), the population dynamics for the full three-level system in the non-sequential regime is shown. We can now use Eq. (1.25), (1.30), and (1.31) to obtain the effective two-level dynamics for this particular system. These results are shown in Fig. 1.3. It is evident that for the chosen parameter regime, the approximation is good, but not "great". The oscillations for the exact and adiabatically eliminated system go out of sync after just a few periods. This is due to the parameter choice: $\Omega_{av} = 0.4\Delta$ and $\Omega_{vb} = 0.3\Delta$ do not fulfill the conditions Eq. (1.24)

well. We could of course have chosen more suitable parameters. It is however instructive to show a parameter regime where we are severely pushing the limits of the approximation so that the effectiveness of a higher-order method can be demonstrated for this example in Section 1.5.5.

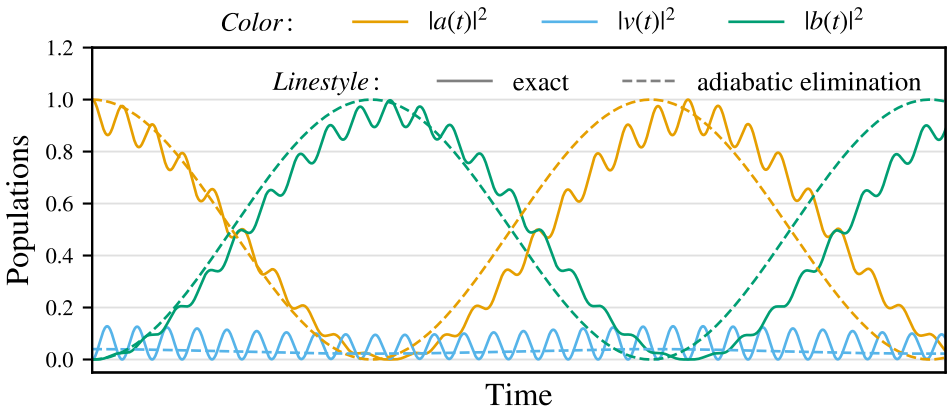

Figure 1.3: The three-level system with non-sequential dynamics. The exact solution (solid) is the same as provided in Fig. 1.2b). The adiabatic elimination (dashed) was performed using Eq. (1.25) , (1.30) and (1.31). Due to the parameter choice ($\Omega_{av} = 0.4\Delta$ and $\Omega_{vb} = 0.3\Delta$), the condition for adiabatic elimination Eq. (1.24) is not well fulfilled and thus, the approximation is far from perfect.

1.5.3 Criticism of the naïve implementation of adiabatic elimination

What then is the criticism of this implementation of adiabatic elimination? Paulisch *et al.* bring forward four points [60]:

1. Setting $\dot{v}(t) \approx 0$ is questionable. While $v(t) \approx 0$ if the coupling is "small", it does not imply that its derivative is also small. In fact, for rectangular pulses, $v(t)$ oscillates rapidly (see Fig. 1.2b)) and yet, adiabatic elimination still yields good results. Furthermore, the relation ≈ 0 is not well-defined (one must insist on $\gg$ or $\ll$) and it is not clear in the naïve implementation where the well-defined condition Eq. (1.24) appears.
2. The normalisation of the wavefunction is inconsistent: We see from Eq. (1.30) and (1.31) that $|a(t)|^2 + |b(t)|^2 = 1$, implying that $|v(t)|^2 = 0$. On the other hand, due to Eq. (1.25) we must have $|v(t)|^2 > 0$, clearly a contradiction. This argument can also be seen visually in Fig. 1.3, where the sum of the populations exceeds one, $|a(t)|^2 + |b(t)|^2 + |v(t)|^2 > 1$.
3. The choice of the interaction picture matters for the accuracy of the solution [59]. Applying an energy shift with the unitary transformation $\exp[-\mathrm{i}\zeta t]$ will change the result.
4. If the detunings of the intermediate states $|v_i\rangle$ are of similar magnitude as the couplings to $|v_i\rangle$, the accuracy of the approximation suffers greatly (as examplified in Fig. 1.3). This makes a higher-order adiabatic elimination procedure desirable.

Paulisch *et al.* propose such a higher-order procedure, which is summarised in Section 1.5.5. Other approaches for higher-order adiabatic elimination can be found in Ref. [33, 63–66]. Note

that the research community of light-matter interaction has, with some exceptions (e.g. Ref. [33, 64]), so far largely ignored the formal theory of effective Hamiltonians, which was developed predominantly from 1958 to the end of the 1990s in nuclear theory, as well as atomic and molecular structure theory (see e.g. Ref. [36, 69, 70, 73–75, 124–131]). A possible explanation for this may be that these theoretical developments were frequently aimed towards high-precision calculations, whereas effective Hamiltonians in light-matter interaction fulfill the role of qualitatively modeling time-dependent phenomena.

1.5.4 Formal adiabatic elimination using the resolvent operator

Elimination of non-resonant quantum states within the resolvent formalism is a well-known procedure [33, 35, 36]. In the specific context of adiabatic elimination, Brion *et al.* showed in 2007 that the pole approximation within the resolvent formalism produces results that agrees with the naïve implementation of adiabatic elimination, while not suffering from inconsistencies, such as having to set $\dot{v}(t) = 0$, or having to worry about the choice of the interaction picture [59]. In this section, adiabatic elimination in the resolvent operator formalism will be discussed in detail, since it is central to both new theoretical developments presented in Chapter 2 and the model system employed in Chapter 3.

The usefulness of the resolvent formalism for this problem is enabled by the projection operator technique, where the Hilbert space is partitioned into an essential and a non-essential subspace, $\mathcal{P}$ and $\mathcal{Q}$ respectively (see Section 1.4.2). Naturally, in adiabatic elimination, the to-be-eliminated states should be in $\mathcal{Q}$, while the essential states are those that are significantly populated. Hence, for the three-level system, we define our essential states as $|a\rangle$ and $|b\rangle$ while the non-essential state is $|v\rangle$, leading to projection operators $P = |a\rangle\langle a| + |b\rangle\langle b|$ and $Q = |v\rangle\langle v|$.

The starting point is the resolvent operator in $\mathcal{P}$, i.e. $PG(z)P$, see Eq. (1.13). For this resolvent, we identified the effective Hamiltonian $H_{\text{eff}}(z) = PH_0P + PR(z)P$. The z-dependence prevented us from using this Hamiltonian in the TISE. The most natural approximation is to simply evaluate $R(z)$ at the two-photon resonance, i.e. at $z = 0$, yielding

$$H_{\text{eff}}(z=0) \equiv H_{\text{eff}}^{(0)} = PH_0P + PR(0)P = PHP - PV\frac{1}{QHQ}VP, \tag{1.33}$$

where $PHP = PH_0P + PVP$. Note that for multiphoton transitions, $PVP = 0$. The matrix $PV[QHQ]^{-1}VP$ contains the influence of the non-essential states on the essential states. Evaluating $R(z = 0)$ corresponds to the pole approximation [33, 35, 55, 59]. The poles due to the non-essential states are regarded as too far from resonance to contribute. For our three-level system with only one non-essential state, the pole is located at $z = \Delta$.

The approximation is easy to visualize by plotting matrix elements of the level-shift operator $PR(z)P$ against z and comparing them to their value at $z = 0$. This is shown in Fig. 1.4 for the three-level ladder system with parameters $\Delta = 0.1$, $\Omega_{av} = \Omega_{va} = \frac{\Delta}{8}$, $\Omega_{bv} = \Omega_{vb} = \frac{\Delta}{6}$, and $\delta = 0$. The value $PR(0)P$, corresponding to the pole approximation, is marked as a horizontal dashed line. One sees that the approximation is valid in a small z-interval around $z = 0$. Further out, at $z = \Delta$, there is a pole due to the resonance with $|v\rangle$. Brion *et al.* showed for a three-level lambda system that the validity of the pole approximation can be traced back to the condition

$\left|\frac{\Omega}{\Delta}\right| \ll 1$, which is precisely the requirement for the naïve adiabatic elimination procedure to be valid [59]. Applied to the three-level ladder system, Eq. (1.33) is quite easy to evaluate since

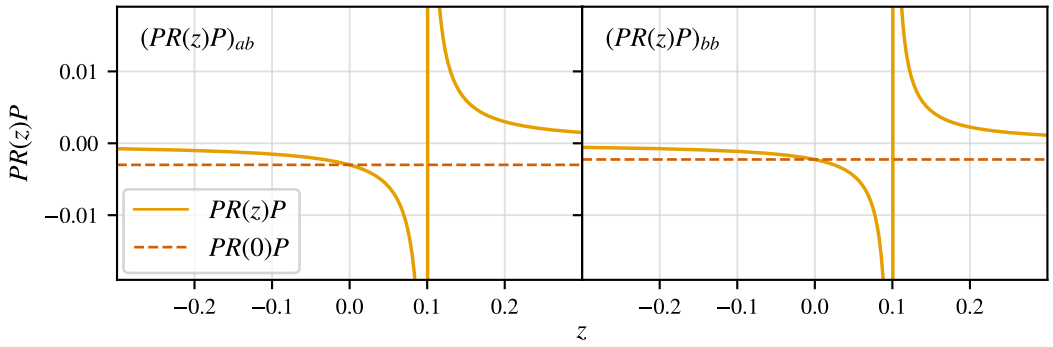

Figure 1.4: Matrix elements $(PR(z)P)_{ab/bb}$ of the level-shift operator, plotted against the energy z (solid, yellow) and compared against the respective pole approximation $(PR(0)P)_{ab/bb}$ (dashed, red). The diagonals correspond to the Stark shifts and the off-diagonals to the couplings. The pole location $z = \Delta = 0.1$ is due to the resonance of $|v\rangle$.

only one state is in $\mathcal{Q}$. As such, $\frac{1}{QHQ} = \frac{1}{\Delta}|v\rangle\langle v|$. With

$$PVQ = \frac{\Omega_{av}}{2}|a\rangle\langle v| + \frac{\Omega_{bv}}{2}|b\rangle\langle v| \quad \text{and} \quad QVP = \frac{\Omega_{va}}{2}|v\rangle\langle a| + \frac{\Omega_{vb}}{2}|v\rangle\langle b|\,, \tag{1.34}$$

one readily obtains

$$PV\frac{1}{QHQ}VP = \frac{|\Omega_{av}|^2}{4\Delta}|a\rangle\langle a| + \frac{|\Omega_{bv}|^2}{4\Delta}|b\rangle\langle b| + \frac{1}{2}\left[\frac{\Omega_{av}\Omega_{vb}}{2\Delta}|a\rangle\langle b| + h.c.\right], \tag{1.35}$$

where $h.c.$ denotes the Hermitian conjugate. Using the quantities S_a, S_b, and Ω_{eff} defined in Section 1.5.2, we obtain the effective Hamiltonian as

$$H_{\text{eff}}^{(0)} = PH_0P + PR(0)P = PHP - PV\frac{1}{QHQ}VP = \begin{pmatrix} S_a & \frac{1}{2}\Omega_{\text{eff}}^* \\ \frac{1}{2}\Omega_{\text{eff}} & \delta + S_b \end{pmatrix}. \tag{1.36}$$

This is identical to the system of equations given by Eq. (1.28) and (1.29).

1.5.5 Higher-order adiabatic elimination using Markov approximations

In 2014, Paulisch *et al.* proposed a rigorous implementation of adiabatic elimination that generalizes to higher orders [60]. Like Brion *et al.* [59], they split the system into essential and non-essential states. Paulisch *et al.* however stay in a time-dependent frame. In this section, their results are restated in our notation of the projection operator technique, i.e. for the Hamiltonian $H = H_0 + V$ in terms of the projection operators P and Q.[5] In Chapter 2, it is shown how their implementation has its counterpart in the energy domain, which is the resolvent formalism.

Paulisch *et al.* start out with the TDSE, Eq. (1.1), for the Hamiltonian $H \equiv H_0 + V$ and split the wavefunction into essential and non-essential states $P|\Psi(t)\rangle$ and $Q|\Psi(t)\rangle$. This yields

[5] Their notation in terms of the objects $\mathbf{\Omega}$, $\boldsymbol{\omega}$, and $\mathbf{\Delta}$ has direct correspondence to my notation: $QHP = QVP \equiv \mathbf{\Omega}^\dagger/2$, $PHQ = PVQ \equiv \mathbf{\Omega}/2$, $PHP \equiv \boldsymbol{\omega}$ and $QHQ \equiv \mathbf{\Delta}$.

two state equations, one for the essential and one for the non-essential states,

$$\mathbb{i}\frac{\mathrm{d}}{\mathrm{d}t}P\left|\Psi(t)\right\rangle = PHP\left|\Psi(t)\right\rangle + PVQ\left|\Psi(t)\right\rangle, \tag{1.37}$$

$$\mathbb{i}\frac{\mathrm{d}}{\mathrm{d}t}Q\left|\Psi(t)\right\rangle = QVP\left|\Psi(t)\right\rangle + QHQ\left|\Psi(t)\right\rangle. \tag{1.38}$$

They integrate over Eq. (1.38):

$$\mathbb{i}Q\left|\Psi(t)\right\rangle = \int_0^t \mathrm{d}t'\,\mathrm{e}^{-\mathbb{i}QHQ(t-t')}QVP\left|\Psi(t')\right\rangle. \tag{1.39}$$

The usual adiabatic elimination, which they refer to as the *zeroth-order Markov approximation*, is obtained by setting $P\left|\Psi(t')\right\rangle \approx P\left|\Psi(t)\right\rangle$, i.e. neglecting the "history" of $P\left|\Psi(t')\right\rangle$ before t. This results in

$$\mathbb{i}Q\left|\Psi(t)\right\rangle \approx \int_0^t \mathrm{d}t'\,\mathrm{e}^{-\mathbb{i}QHQ(t-t')}QVP\left|\Psi(t)\right\rangle = \frac{1-\mathrm{e}^{-\mathbb{i}QHQt}}{\mathbb{i}QHQ}QVP\left|\Psi(t)\right\rangle. \tag{1.40}$$

Noting that time scales of order $\|QHQ\|^{-1}$ are not resolved, $\mathrm{e}^{-\mathbb{i}QHQt}$ averages out over coarsed-grained time intervals, i.e.

$$Q\left|\Psi(t)\right\rangle \approx -\frac{1}{QHQ}VP\left|\Psi(t)\right\rangle \tag{1.41}$$

Inserting in Eq. (1.37) then yields the zeroth-order effective Hamiltonian

$$H_{\mathrm{eff}}^{(0)} = PHP - PV\frac{1}{QHQ}VP, \tag{1.42}$$

which is equivalent to $H_{\mathrm{eff}}^{(0)}$ from Eq. (1.33) by Brion *et al.* [59].[6]

For the *first-order Markov-approximation*, Paulisch *et al.* propose to take into account a linear memory of $P\left|\Psi(t')\right\rangle$ by expanding

$$P\left|\Psi(t')\right\rangle \approx P\left|\Psi(t)\right\rangle - (t-t')P\frac{\mathrm{d}}{\mathrm{d}t}\left|\Psi(t)\right\rangle. \tag{1.43}$$

Inserting this into Eq. (1.39) and coarse-graining again, they arrive at the first-order effective Hamiltonian

$$H_{\mathrm{eff}}^{(1)} = \left(\mathbb{1}_P + PV[QHQ]^{-2}VP\right)^{-1}H_{\mathrm{eff}}^{(0)}, \tag{1.44}$$

where $\mathbb{1}_P \coloneqq P\mathbb{1}P$ is the unity matrix in $\mathcal{P}$. Note that $H_{\mathrm{eff}}^{(1)}$ is non-Hermitian. The non-Hermiticity of higher-order effective Hamiltonians is well-known (see e.g. Ref. [73, 75, 125]). While the eigenfunctions $\left|\Psi_n\right\rangle$ of the full Hamiltonian H (i.e. $H\left|\Psi_n\right\rangle = E_n\left|\Psi_n\right\rangle$) are orthogonal, their projections $P\left|\Psi_n\right\rangle$ onto $\mathcal{P}$ are generally not – hence, the operator H_{eff} associated with these eigenstates will usually be non-Hermitian (an exception is the zeroth-order $H_{\mathrm{eff}}^{(0)}$). Note that the eigenvalues of $H_{\mathrm{eff}}^{(1)}$ are still real [125]. Paulisch *et al.* introduce a modified inner product to render $H_{\mathrm{eff}}^{(1)}$ Hermitian:

$$(P\Psi_1, P\Psi_2) \coloneqq \left\langle\Psi_1\right|\left(\mathbb{1}_P + PV[QHQ]^{-2}VP\right)\left|\Psi_2\right\rangle. \tag{1.45}$$

[6] It is prudent to note that Macrì *et al.* (2023) have shown that the assumption of Markovianity is not required: A correct result for the effective Hamiltonian can be obtained solely by leveraging coarse-graining [65].

They furthermore propose a Hermitian effective Hamiltonian by employing a symmetrical splitting,

$$H_{\text{eff}}^{(1)} = \left(1 + PV[QHQ]^{-2}VP\right)^{-\frac{1}{2}} H_{\text{eff}}^{(0)} \left(1 + PV[QHQ]^{-2}VP\right)^{-\frac{1}{2}}. \tag{1.46}$$

The eigenvalues of the non-Hermitian and Hermitian $H_{\text{eff}}^{(1)}$ coincide, but the eigenvectors of the Hermitian $H_{\text{eff}}^{(1)}$ are no longer simply the projections of the full eigenstates, but rather the most similar possible orthonormal constructions [75]. There have been previous discussions about the use of non-Hermitian H_{eff} as modelling tools [125, 132] – some are still occuring today [133–135]. In light-matter interaction, where populations of electronic states are of special interest (rather than just the spectrum of the H_{eff}), Hermitian H_{eff} seem preferrable, since non-Hermitian H_{eff} will not conserve the norm [64]. Note that Hermitian effective Hamiltonians $H_{\text{H, eff}}$ can in zeroth order be obtained from non-Hermitian effective Hamiltonians $H_{\text{nH, eff}}$ simply by the Hermitisation $H_{\text{H, eff}} \approx \left(H_{\text{nH, eff}} + H_{\text{nH, eff}}^{\dagger}\right)/2$ [126].

Since the dynamics of the non-essential states is given by

$$Q\,|\Psi(t)\rangle = -\frac{1}{QHQ} VP\,|\Psi(t)\rangle\,, \tag{1.47}$$

it follows that with the first-order $H_{\text{eff}}^{(1)}$, norm conservation is guaranteed in the entire Hilbert space $\mathcal{H} = \mathcal{P} \oplus \mathcal{Q}$,

$$\langle\Psi|P|\Psi\rangle + \langle\Psi|Q|\Psi\rangle = 1. \tag{1.48}$$

The efficacy of the first-order effective Hamiltonian can easily be demonstrated by repeating the calculations for Fig. 1.3 with $H_{\text{eff}}^{(1)}$. This yields Fig. 1.5. It is apparent that the first-order results (dashed-dotted) are in much better agreement with the exact results (solid) than the zeroth-order results (i.e. conventional adiabatic elimination). Note that due to Eq. (1.48), $|a(t)|^2 + |b(t)|^2 < 1$ for the higher-order effective Hamiltonian, which is consistent with some population being trapped in $\mathcal{Q}$.

1.6 Ionisation and non-Hermitian effective Hamiltonians

Quantum dynamics with intense fields necessitates accounting for ionisation, i.e. transitions the continuum. Ionisation is conveniently modeled as a decay process, i.e. a process that decreases the norm of the quantum system. This leads to a non-Hermitian quantum theory.

Non-Hermitian quantum theory has a long history: As early as 1928, Gamow introduced an imaginary decay term to model α-decay in nuclei [136]. Another milestone came in 1947 with the Fock-Krylov theorem which states that any quantum state coupled to an energy-conserving continuum undergoes irreversible decay, i.e. that the norm of the state approaches zero as $t \to \infty$ [137, 138]. Still, non-Hermitian quantum mechanics was slow to be embraced, even being deemed unpopular at some point in time [139]. For the study of ionisation, we can classify two implementations yielding non-Hermitian Hamiltonians.

The first approach is to take the entire Hilbert space (with discrete and continuous spectrum) and project out the continuous states using a suitable outgoing boundary condition [35]. Among many others, this approach was taken by Lambopolous [140], Beers and Armstrong [40], McClean

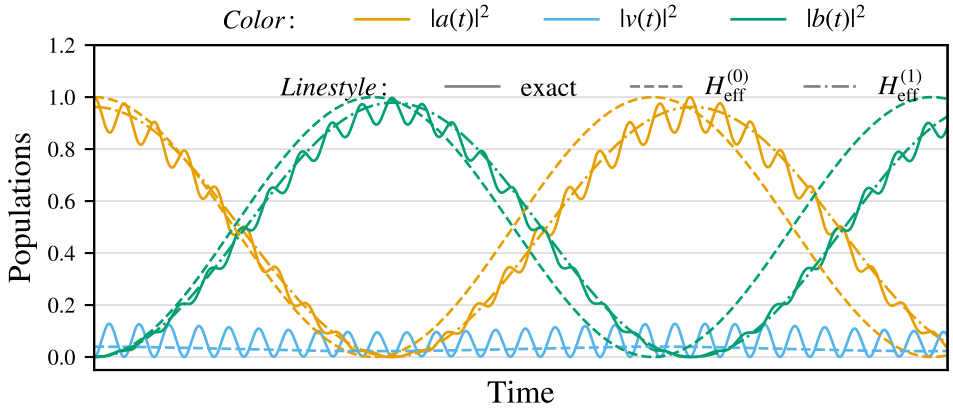

Figure 1.5: Dynamics of the three-level ladder system of Fig. 1.3, where the parameters are left unchanged ($\Omega_{av} = 0.4\Delta$ and $\Omega_{vb} = 0.3\Delta$). The exact solution (solid) and zeroth-order adiabatic elimination ($H_{\text{eff}}^{(0)}$, dashed) thus are the same as those in Fig. 1.3. In dashed-dotted, the results for the first-order effective Hamiltonian $H_{\text{eff}}^{(1)}$ are included. The first-order effective Hamiltonian is significantly better at capturing the quantitative dynamics than the zeroth-order.

and Swain [141], Faisal and Moloney [142] and Baker [138, 143, 144]. In the context of this thesis, the model system of Beers and Armstrong for describing resonant multiphoton ionisation may be highlighted [40].

The second approach is to introduce complex scaling transformations, such as uniformly scaling the radial coordinate $r \to re^{\mathrm{i}\theta}$. Applied to the full Floquet Hamiltonian $H^{(F)}$, this will yield a rotated Floquet Hamiltonian $H_\theta^{(F)}$, which is non-Hermitian [80]. Due to the complex scaling, the continuous spectrum of the rotated Floquet Hamiltonian can be discretized through projection onto L^2-integrable functions, amounting to a quadrature of the integrals governing the continuum dynamics [145]. Contributions to this approach include Maquet *et al.* [81], Holt *et al.* [41], and Telnov and Chu [146]. For an exemplary use of the approach, see Dörr *et al.* [56]. Especially noteworthy is the investigation of resonant N-photon ionisation in hydrogen by Holt *et al.*, where non-Hermitian effective Hamiltonians in the spirit of Beers and Armstrong are obtained by diagonalisation of the rotated Floquet Hamiltonian [41]. An advantage of the complex scaling transform is the avoidance of cumbersome principal value calculations that appear in the calculation of bound-continuum dipole transition matrix elements [81]. Other complex scaling transform include *exterior complex scaling* (ECS) [147].

By now, both approaches are well-established [33, 148] and are used to address current research problems in quantum information [149], multiphoton XUV ionisation [43–45, 55, 98, 99] and chemical physics [150], among others. In Chapter 3, we will take the second approach, namely to calculate complex-scaled field-free atomic parameters using ECS, and to use these parameters to construct the rotated Floquet Hamiltonian, from which we will through the projection operator technique obtain non-Hermitian effective Hamiltonians.

According to Beers and Armstrong, an atom with two unperturbed bound states, $|a, N\rangle \equiv |a\rangle$ and $|b, N - M\rangle \equiv |b\rangle$, that are coupled resonantly via M photons can be described by a 2×2

non-Hermitian (complex-symmetric) effective Hamiltonian [40, 41] (compare with Eq. (1.36)):

$$H_{\text{eff}} = \begin{pmatrix} (E_a + N\omega) + S_a - \frac{\mathrm{i}}{2}\gamma_a & (\Omega + \mathrm{i}\beta)/2 \\ (\Omega + \mathrm{i}\beta)/2 & (E_b + (N-M)\omega) + S_b - \frac{\mathrm{i}}{2}\gamma_b \end{pmatrix}. \tag{1.49}$$

All parameters are real, but the matrix elements are complex. E_a and E_b are the unperturbed energies of $|a\rangle$ and $|b\rangle$ (for the three-level system, we chose the zero-point of the energy so that $E_a = 0$ and $\delta \coloneqq E_b - E_a - 2\omega$). S_a and S_b are the Stark shifts of $|a\rangle$ and $|b\rangle$, while Ω is the effective coupling between $|a\rangle$ and $|b\rangle$. These parameters were introduced for the three-level system in Section 1.5. The conceptually new parameters are γ_a, γ_b and β. The parameters γ_a and γ_b are the ionisation rates describing a process of the atom transitioning from $|a\rangle$ or $|b\rangle$ to a continuum state. The imaginary Rabi frequency β describes a process of the atom transitioning between $|a\rangle$ and $|b\rangle$ via some continuum [41]. It may be interpreted as a measure of the interference between the resonant and non-resonant ionisation process [40]. The β parameter is physically constrained by γ_a and γ_b. It was shown for low-order perturbation theory that with only one continuum available, $\beta = \pm\sqrt{\gamma_a \gamma_b}$ (in other words, β is the geometric mean of the ionisation rates γ_a and γ_b) [40, 41, 55].

2 Higher-order adiabatic elimination in the resolvent formalism

In this chapter, a method for systematically deriving higher-order corrections to adiabatic elimination within the resolvent operator formalism is presented. When Brion *et al.* in 2007 proposed to employ the resolvent operator in the pole approximation to implement adiabatic elimination (Section 1.5.4), their focus was to show that their implementation yielded the same results as the naïve approach (Section 1.5.2), and improved upon its inconsistencies. Recently (Section 1.5.5), Paulisch *et al.* proposed to employ Markov approximations to systematically incorporate higher-order corrections to adiabatic elimination [60]. Paulisch *et al.* stay in the time domain, whereas the resolvent operator formalism takes place in the energy domain. Thus, the question naturally arises if one can incorporate higher-order corrections to adiabatic elimination within the resolvent operator formalism. As will be shown, the answer is in the affirmative and reveals fascinating ties between the pole approximation and the Markov approximation.

The structure of the chapter is as follows. In Section 2.1, it will be motivated how a systematic improvement to the pole approximation can be obtained and how this will correspond to higher-order corrections to adiabatic elimination within the resolvent formalism. The main result of this section will be to derive the first-order effective Hamiltonian of Paulisch *et al.* within the resolvent formalism. In Section 2.2, we will move beyond the first-order correction. The proposals of Faisal [33] and Paulisch *et al.* [60] to obtain higher-order effective Hamiltonians are largely analogous and rely on iterative procedures. We will motivate a novel procedure to obtain a second-order effective Hamiltonian and apply the procedure in a special case to a four-level ladder system. The approach offers a new and deeper perspective on higher-order adiabatic elimination.

2.1 First-order effective Hamiltonian from the resolvent formalism

To summarise the results of Paulisch *et al.*, in the first-order Markov approximation, their effective Hamiltonian reads $H_{\text{eff}}^{(1)} = \left(1 + PV[QHQ]^{-2}VP\right)^{-1} H_{\text{eff}}^{(0)}$, Eq. (1.44), while the dynamic of the non-essential states is given by $Q\,|\Psi(t)\rangle = -[QHQ]^{-1}VP\,|\Psi(t)\rangle$, Eq. (1.47). In the following, it will be shown how these expressions can be obtained within the resolvent operator formalism.

Starting out with the full Hamiltonian $H = H_0 + V$, the resolvent operator in the model space $\mathcal{P}$ reads

$$PG(z)P = \frac{P}{z - PH_0P - PR(z)P}, \tag{2.1}$$

with the level-shift operator

$$R(z) = V + V\frac{Q}{z - QHQ}V. \tag{2.2}$$

In the zeroth-order adiabatic elimination, one would now evaluate at a fixed z value (in our case $z = 0$) [59], corresponding to the pole approximation. The visual intuition behind the pole approximation was provided by Fig. 1.4, where it was clear from Fig. 1.4 that the pole approximation is only valid if the slope of the level-shift operator around $z = 0$ is negligible, which will be the case when the influence of the nearest $\mathcal{Q}$-space pole on the region around $z = 0$ is small.

For higher-order corrections to adiabatic elimination, we seek to improve upon the pole approximation. To this end, the $PR(z = 0)P$ term can be interpreted as the zeroth-order term of an expansion of the level-shift operator around $z = 0$:

$$PR(z)P = PVP + PV\frac{Q}{z - QHQ}VP, \tag{2.3}$$

$$\approx \underbrace{PVP - PV\frac{1}{QHQ}VP}_{PR(0)P} \underbrace{-z\,PV\left(\frac{1}{QHQ}\right)^2 VP}_{\text{linear}} \underbrace{-z^2\,PV\left(\frac{1}{QHQ}\right)^3 VP}_{\text{quadratic}} - \dots\,. \tag{2.4}$$

The expansion in the energy z, first proposed by Brandow [77], is a well-known procedure which connects Brillouin-Wigner Perturbation theory (BWPT) [76] to General Rayleigh-Schrödinger perturbation theory (GRSPT) [36]. In the particular context of multiphoton processes, the expansion is discussed for instance by Faisal (1987) in Ref. [33]. It is perhaps best understood visually. Let us use the 3-level ladder system from Fig 1.4 in Section 1.5.4. Now, let us not only plot $PR(z)P$ and $PR(0)P$, but also the linear and quadratic approximations. This yields Fig. 2.1. There, we can see how the first-order correction (blue, dashed-dotted) takes into account the slope of the level-shift operator and how the second-order correction (green, dotted) takes into account also the curvature. Which correction is required will largely depend on how big the impact of the $\mathcal{Q}$-space pole is on the level-shift operator around $z = 0$.

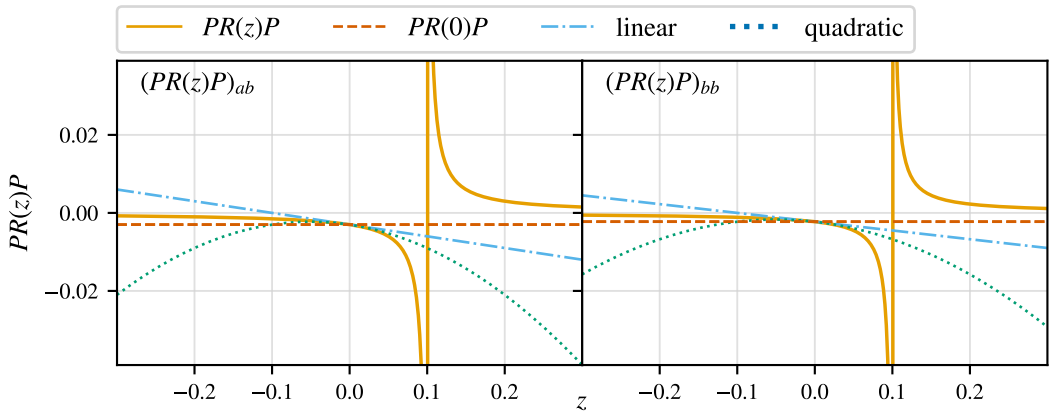

Figure 2.1: Matrix elements $(PR(z)P)_{ab/bb}$, plotted against z, for the 3-level ladder system from Fig 1.4 in Section 1.5.4. $PR(z)P$ (solid, yellow) is compared with $PR(0)P$ (dashed, red), the linear approximation (dashed-dotted, blue) and the quadratic approximation (dotted, green).

Employing the linear expansion of $R(z)$ in $PG(z)P$ yields

$$PG(z)P = \frac{P}{z\,(\mathbb{1}_P + PV[QHQ]^{-2}VP) - (PH_0P - PR(0)P)}, \tag{2.5}$$

$$= (\mathbb{1}_P + \underbrace{PV[QHQ]^{-2}VP}_{C})^{-1} \frac{P}{z - (\mathbb{1}_P + \underbrace{PV[QHQ]^{-2}VP}_{C})^{-1} H_{\text{eff}}^{(0)}}, \tag{2.6}$$

where we identified the zeroth-order effective Hamiltonian $H_{\text{eff}}^{(0)} = PH_0P - PR(0)P$. We define the identity matrix $\mathbb{1}_P$ in $\mathcal{P}$ via $\mathbb{1}_P \coloneqq P\mathbb{1}P$, and furthermore $C \coloneqq PV[QHQ]^{-2}VP$. Note that we could also have factored out to the right,

$$PG(z)P = \frac{P}{z - H_{\text{eff}}^{(0)}\,(\mathbb{1}_P + C)^{-1}} (\mathbb{1}_P + C)^{-1}, \tag{2.7}$$

or employed a symmetric splitting,

$$PG(z)P = (\mathbb{1}_P + C)^{-1/2} \frac{P}{z - (\mathbb{1}_P + C)^{-1/2}\, H_{\text{eff}}^{(0)}\, (\mathbb{1}_P + C)^{-1/2}} (\mathbb{1}_P + C)^{-1/2}\,. \tag{2.8}$$

From Eq. (2.6) and (2.7), we can identify the non-Hermitian first-order effective Hamiltonians

$$H_{\text{eff}}^{(1)} = (\mathbb{1}_P + C)^{-1}\, H_{\text{eff}}^{(0)} \quad \text{and} \quad H_{\text{eff}}^{(1)} = H_{\text{eff}}^{(0)}\, (\mathbb{1}_P + C)^{-1}\,, \tag{2.9}$$

and from Eq. (2.8) the Hermitian first-order effective Hamiltonian

$$H_{\text{eff}}^{(1)} = (\mathbb{1}_P + C)^{-1/2}\, H_{\text{eff}}^{(0)}\, (\mathbb{1}_P + C)^{-1/2}\,. \tag{2.10}$$

For a discussion on the Hermiticity of effective Hamiltonians, see Section 1.5.5.

The effective Hamiltonians in Eq. (2.9) and (2.10) are equivalent to the results obtained by Paulisch *et al.*, Eq. (1.44), a result not yet noted in the literature. Furthermore, this equivalence demonstrates a previously (to my best knowledge) unnoticed analogy between the energy expansion of the level-shift operator and the Markov approximation. Where the first-order Markov approximation takes into account a "linear history" of the wavefunction around $t' = t$, i.e.

$$P\,|\Psi(t')\rangle \approx P\,|\Psi(t)\rangle - (t - t')\frac{\mathrm{d}}{\mathrm{d}t}\,|\Psi(t')\rangle\Big|_{t'=t}, \tag{2.11}$$

this expansion finds its direct counterpart in the energy domain by taking into account the slope of the level-shift operator around an expansion point z_0:

$$R(z) \approx R(z_0) + (z - z_0)\frac{\mathrm{d}}{\mathrm{d}z}R(z)\Big|_{z=z_0}. \tag{2.12}$$

For the asymmetric variants Eq. (2.6) and (2.7), the resolvent operator in subspace $\mathcal{P}$ has $(\mathbb{1}_P + C)^{-1}$ as a factor, either to the left, or to the right. Without loss of generality, we will discuss the left case. When obtaining the time-evolution operator $U_{\text{eff}}^{(1)}(t, t_0) \coloneqq PU(t, t_0)P$ via

integration over z, the factor is simply moved outside the integral:

$$U_{\text{eff}}^{(1)}(t,t_0) = \underbrace{(\mathbb{1}_P + C)^{-1}}_{=:\mathcal{N}^{(1)}} \mathrm{e}^{-\mathrm{i}H_{\text{eff}}^{(1)}(t-t_0)}. \tag{2.13}$$

$U_{\text{eff}}^{(1)}(t,t_0)$ of Eq. (2.13) is not unitary. Unitarity is achieved via the definition of a modified inner product,

$$(\Psi_1, \Psi_2) \coloneqq \langle\Psi_1| \left(\mathbb{1}_P + C\right) |\Psi_2\rangle\,, \tag{2.14}$$

which was proposed by Paulisch *et al.* [60]. In contrast, $U_{\text{eff}}^{(1)}(t,t_0)$ obtained via the symmetric splitting, Eq. (2.8), is unitary. In any case, no matter which of the three variants (left, right, symmetric) is used, $U_{\text{eff}}^{(1)}(t_0,t_0) \neq \mathbb{1}$; the norm in $\mathcal{P}$ is less than one. This is due to the matrix $\mathcal{N}^{(1)}$. Since $\mathcal{N}^{(1)}$ will yield the normalisation $\langle\Psi\,|\,P\,|\,\Psi\rangle + \langle\Psi\,|\,Q\,|\,\Psi\rangle = 1$, we will in the following call it the normalisation of the time-evolution operator.

To complete the equivalence to the results of Paulisch *et al.*, we need to determine the time-evolution of the non-essential states within the resolvent formalism.[1] This will lead us to their conclusion that with the first-order effective Hamiltonian, the norm of the entire Hilbert space $\mathcal{P} \oplus \mathcal{Q}$ is conserved, as opposed to only in $\mathcal{P}$ [60]. Deriving the non-essential state dynamics is as simple as calculating the resolvent operator $QG(z)P$ from Eq. (1.16), and applying the pole approximation on the $\mathcal{Q}$-space dynamics:

$$QG(z)P = \frac{Q}{z - QHQ} VPG(z)P \approx -\frac{1}{QHQ} VPG(z)P \tag{2.15}$$

Integration yields the time-evolution operator $QU(\tau)P$ (remember that $\tau \coloneqq t - t_0$):

$$QU(\tau)P = \frac{1}{2\pi\mathrm{i}} \int_{C_+ \cup C_-} \mathrm{d}z\, \mathrm{e}^{-\mathrm{i}z\tau} QG(z)P, \tag{2.16}$$

$$= -\frac{1}{QHQ} V \left(\frac{1}{2\pi\mathrm{i}} \int_{C_+ \cup C_-} \mathrm{d}z\, \mathrm{e}^{-\mathrm{i}z\tau} PG(z)P \right), \tag{2.17}$$

$$= -\frac{1}{QHQ} VPU(\tau)P. \tag{2.18}$$

We can now use $QU(t,t_0)P$ to obtain the non-essential state dynamics from the essential state dynamics. For this we calculate $Q\,|\Psi(t)\rangle$ via

$$Q\,|\Psi(t)\rangle = QU(t,t_0)P\,|\Psi(t_0)\rangle = -\frac{1}{QHQ} VPU(t,t_0)P\,|\Psi(t_0)\rangle = -\frac{1}{QHQ} VP\,|\Psi(t)\rangle\,. \tag{2.19}$$

This result is once again equivalent to Paulisch *et al.*, i.e. Eq. (1.47). Thus, their argument on norm conservation applies to us too. The norm of the non-essential states is given by

$$\langle\Psi(t)|Q^\dagger Q|\Psi(t)\rangle = \langle\Psi|Q|\Psi\rangle = \langle\Psi|\, PV[QHQ]^{-2}VP\,|\Psi\rangle\,. \tag{2.20}$$

[1] Somewhat surprisingly, I have not been able to find this short derivation in the literature. I would speculate that this is due to the non-essential states being regarded as uninteresting to study, given that they are literally non-essential. However, in recent applications interest is rising for such observables, including photoelectron emission [55].

We know that with the modified inner product $(\Psi, \Psi) = 1$. Thus,

$$1 = (\Psi, \Psi) \coloneqq \langle\Psi| \left(\mathbb{1}_P + PV[QHQ]^{-2}VP\right) |\Psi\rangle\,, \tag{2.21}$$

$$= \langle\Psi|P|\Psi\rangle + \langle\Psi| PV[QHQ]^{-2}VP\,|\Psi\rangle\,, \tag{2.22}$$

$$= \langle\Psi|P|\Psi\rangle + \langle\Psi|Q|\Psi\rangle = \langle\Psi|\Psi\rangle\,, \tag{2.23}$$

which is just our usual normalization condition (i.e. the norm of the wavefunction in the entire Hilbert space is 1). Thus, propagation with the first-order effective Hamiltonian preserves the norm in the whole Hilbert space $\mathcal{P} \oplus \mathcal{Q}$. In contrast, the zeroth-order effective Hamiltonian preserves the norm in the subspace $\mathcal{P}$.

2.2 Higher-order effective Hamiltonians beyond first order

We have seen in the previous section how the first-order correction, using an expansion beyond the pole approximation, yields the equivalent results to the Markov approximation proposed by Paulisch *et al.* [60]. The expansion can be carried out to higher orders than this. However, it becomes seemingly impossible to obtain any exact formula for the effective Hamiltonian beyond first order. To quickly demonstrate this, we consider the Feshbach operator $H_{\text{eff}}(E) = PH_0P + PR(E)P$ of BWPT.[2] By expanding the $PR(E)P$ in E as in Eq. (2.4), we obtain

$$H_{\text{eff}}(E) = PH_0P + PR(E)P \tag{2.24}$$

$$\approx \underbrace{PHP - PV[QHQ]^{-1}VP}_{H_{\text{eff}}^{(0)}} - EPV[QHQ]^{-2}VP - E^2PV[QHQ]^{-3}VP - \dots\,. \tag{2.25}$$

Inserting $H_{\text{eff}}(E)$ into the model space TISE, $EP\,|\Psi\rangle = H_{\text{eff}}(E)P\,|\Psi\rangle$, it is obvious that only for linear order in E can we rearrange to a proper Schrödinger equation where the Hamiltonian does not depend on the energy:

$$EP\,|\Psi\rangle = \underbrace{\left(\mathbb{1}_P + PV[QHQ]^{-2}VP\right)^{-1} H_{\text{eff}}^{(0)}}_{H_{\text{eff}}^{(1)}} P\,|\Psi\rangle + \mathcal{O}(E^2)P\,|\Psi\rangle\,. \tag{2.26}$$

Second- and higher-order corrections can e.g. be obtained iteratively [33, 60]. For the TISE $EP\,|\Psi\rangle = H_{\text{eff}}(E)P\,|\Psi\rangle$, we notice that, formally, $E = H_{\text{eff}}(E)$. Thus, we can approximate the higher-order effective Hamiltonians by reinserting $H_{\text{eff}}(E)$ into itself and, at some sufficient depth, truncating by letting $E \approx H_{\text{eff}}^{(0)}$, yielding $H_{\text{eff,it.}}$ (where "it." stands for iterative):

$$EP\,|\Psi\rangle = H_{\text{eff}}(E)P\,|\Psi\rangle = H_{\text{eff}}(H_{\text{eff}}(\cdots H_{\text{eff}}(E)))P\,|\Psi\rangle \approx \underbrace{H_{\text{eff}}(H_{\text{eff}}(\cdots H_{\text{eff}}(H_{\text{eff}}^{(0)})))}_{=:H_{\text{eff,it.}}} P\,|\Psi\rangle\,. \tag{2.27}$$

[2] The variable switch $z \to E$ is possible here because in BWPT we use $H_{\text{eff}}(z)$ not in the resolvent, $PG(z)P = P[z - H_{\text{eff}}(z)]^{-1}P$, but in the TISE, $H_{\text{eff}}(z)P\,|\Psi\rangle = EP\,|\Psi\rangle$. While $PG(z)P$ is mathematically not defined on the spectrum of $H_{\text{eff}}(z)$, which we denote by E, the TISE with $H_{\text{eff}}(E)P\,|\Psi\rangle = EP\,|\Psi\rangle$ is well-defined (and more pleasant for the eye).

Depending on the order E^n in which the level-shift operator is expanded in Eq. (2.25), one can then through Eq. (2.27) calculate energy-independent higher-order effective Hamiltonians $H^{(n)}_{\text{eff,it.}}$. This fixed-point iteration procedure has one clear disadvantage, which is that it only reveals the higher-order effective Hamiltonian, but not the normalisation $\mathcal{N}$ of the time-evolution operator that will lead to $\langle\Psi|P|\Psi\rangle + \langle\Psi|Q|\Psi\rangle = 1$ (see Eq. (2.13)). Furthermore, one will find it hard to formulate convergence conditions for Eq. (2.27) since these might strongly depend on the starting guess for the energy.

In the following, a novel approach to obtain second-order effective Hamiltonians is presented. After the main idea is presented, we will focus on a special case in which certain operators commute. For this case, we can analytically obtain the second-order effective Hamiltonian and the normalisation $\mathcal{N}^{(2)}$ of the time-evolution operator. The approach can also be generalized in the non-commuting case, but this is beyond the scope of this work.

2.2.1 A block partial-fraction expansion of the resolvent operator

We start as always with the Hermitian Hamiltonian $H = H_0 + V$ and assume a discrete spectrum. We project onto the subspaces $\mathcal{P}$ and $\mathcal{Q}$ using the projection operators P and Q. For the second-order expansion of the level-shift operator, Eq. (2.4), the model space resolvent is given by

$$PG(z)P = \frac{P}{z^2 \underbrace{PV[QHQ]^{-3}VP}_{=:C_2} + z \underbrace{\left(\mathbb{1}_P + PV[QHQ]^{-2}VP\right)}_{=:C_1} - \underbrace{H^{(0)}_{\text{eff}}}_{=:-C_0}}. \tag{2.28}$$

We note that the denominator is a *quadratic matrix polynomial* $T_2(z) \coloneqq C_2 z^2 + C_1 z + C_0$. The resolvent operator is related to the time-evolution operator through a Fourier transform – yet, Fourier transforming $PG(z)P \equiv PT_2^{-1}(z)P$ seems daunting. To rise to this challenge, we will in the following employ a *block partial-fraction expansion* [78] of the resolvent operator. This algebraic technique (the matrix analogue of the scalar partial fraction expansion) has (to my best knowledge) hitherto not been applied to the resolvent.

Firstly, we transform $T_2(z)$ to a *monic* matrix polynomial (i.e. the leading coefficient is the identity matrix):

$$M_2(z) = C_2^{-1}T_2(z) = z^2 + C_2^{-1}C_1 z + C_2^{-1}C_0 \equiv z^2 + D_1 z + D_0 \tag{2.29}$$

For our problems, the non-singularity of C_2 is (except for systems with very specific symmetries) essentially guaranteed in all systems with $\dim\{\mathcal{Q}\} \geq 2$. We furthermore define the set of *right solvents* $\{X_i\}$ as all the matrices X_i that solve

$$M_2(X_i) = X_i^2 + D_1 X_i + D_0 = 0. \tag{2.30}$$

The set of *left solvents* is obtained by switching $D_1 X_i \to X_i D_1$. We consider only right solvents without loss of generality (the block partial-fraction expansion using left solvents proceeds analogously [78]). The existence of a solvent is mathematically not guaranteed; furthermore there could exist infinitely many [151]. We will in the following assume that $\{X_i\}$ is a finite non-empty set. As a further research goal, one might attempt to prove existence properties for the solvents

of $M_2(z)$ by considering the Hermiticity of the coefficients C_i [152, 153].

With the entire set of right solvents $\{X_i\}$ obtained, the block partial-fraction expansion of the resolvent operator then reads [78]:

$$PG(z)P = PC_2^{-1}\frac{1}{M_2(z)}P = PC_2^{-1}\sum_{i=1}^{\sigma}\sum_{j=1}^{m_i}(z - X_i)^{-1}F_{i,j}P, \tag{2.31}$$

where $F_{i,j}$ are *matrix residues*, σ is the number of distinct right solvents, and m_i denotes the multiplicity of the solvent X_i. The matrices $F_{i,j}$ can be explicity calculated; see Ref. [78]. Via Fourier transformation, we can now trivially obtain the time-evolution of the system as

$$PU(\tau)P = PC_2^{-1}\sum_{i=1}^{\sigma}\sum_{j=1}^{m_i}\mathrm{e}^{-\mathrm{i}X_i\tau}F_{i,j}P. \tag{2.32}$$

At this point, many questions are left unanswered. For instance: How are the solvents obtained? How many are there and what is their multiplicity? How do the left and right solvents relate to each other? Where does the second-order effective Hamiltonian emerge from the expansion? In the general case of Eq. (2.31), the answers to these questions are beyond the scope of this work. However, for the special case in which left and right solvents coincide, we will in the following discover that $M_2(z)$ has exactly two solvents: One corresponds to the second-order effective Hamiltonian, while the other solvent does not, on average, contribute to the time-evolution and can be neglected.

2.2.2 The special case of commuting matrix coefficients

The expansion proposed in Eq. (2.31) is very general. The missing puzzle piece are the solvents. It is at this point that we will introduce a very restrictive assumption: For the rest of this section, we will assume that the coefficients of the matrix polynomial commute, i.e. $[C_i, C_j] = 0$ and subsequently $[D_0, D_1] = 0$. This will make the notion of left and right solvents unnecessary; in the commuting case they coincide. Furthermore, a quadratic matrix polynomial with commuting coefficients has exactly two solvents that can be calculated analytically through the quadratic formula [151]. The case of commuting coefficients is restrictive since it only applies for quantum systems with very specific symmetries.[3] The atomic systems that are studied in Chapter 3 do not possess this symmetry. Still, the special case provides a good intuition of what one might expect from the general case of Eq. (2.31).

Proceeding with the commuting case, we can factorise $M_2(z)$ into its two solvents, $X_\pm$,

$$M_2(z) = z^2 + D_1 z + D_0 = (z - X_+)(z - X_-). \tag{2.33}$$

Since $[D_1, D_0] = 0$, the quadratic formula can be used to obtain the solvents:

$$X_\pm = -\frac{1}{2}D_1 \pm \Big(\underbrace{\frac{1}{4}D_1^2 - D_0}_{=:Y}\Big)^{1/2}. \tag{2.34}$$

[3] For a practical example where such symmetries can be found, see e.g. Ref. [154], Table 1 (ethylene and the allyl radical), and compare to Table 2 (butadiene), where these symmetries are lacking.

Note that this formula is only applicable when the matrix square root $Y^{1/2}$ exists and is unique [151], which is the case when Y is positive semi-definite. To understand this, we realize that Y is Hermitian (since C_i and thus D_i are Hermitian), and it is thus diagonalisable and has real eigenvalues. If, and only if, all eigenvalues are non-negative (i.e. Y is positive semi-definite), there exists exactly one Hermitian positive semidefinite matrix Z such that $Y = ZZ$ [155]. If one eigenvalue becomes negative, the square-root is no longer uniquely defined. This is a failure point of this particular method to obtain the two solvents.

Using the complete set of solvents $\{X_+, X_-\}$, we carry out the block partial-fraction expansion of the resolvent operator [78], yielding

$$PG(z)P = PC_2^{-1}\left[\frac{A_+}{z - X_+} + \frac{A_-}{z - X_-}\right]P, \tag{2.35}$$

where $A_\pm$ are the residuals of the expansion. A quick calculation based on Ref. [78] reveals that

$$A_\pm = \pm\left(X_+ - X_-\right)^{-1}, \tag{2.36}$$

with which we obtain the final result

$$PG(z)P = PC_2^{-1}\frac{1}{M_2(z)}P = PC_2^{-1}(X_+ - X_-)^{-1}\left[\frac{1}{z - X_+} - \frac{1}{z - X_-}\right]P. \tag{2.37}$$

Since the resolvent operator relates to the time-evolution operator via Fourier transform, we can trivially obtain the time-evolution from Eq. (2.37) as

$$PU_\pm^{(2)}(\tau)P = \underbrace{PC_2^{-1}(X_+ - X_-)^{-1}}_{=:\mathcal{N}^{(2)}}\left[\mathrm{e}^{-\mathrm{i}X_+\tau} - \mathrm{e}^{-\mathrm{i}X_-\tau}\right]P, \tag{2.38}$$

and identify the normalisation $\mathcal{N}^{(2)}$. In what follows, it will be shown that X_+ acts as a second-order effective Hamiltonian $H_{\text{eff}}^{(2)}$, while X_- is responsible for rapid oscillations.

2.2.3 Application to a four-level ladder system

The above claim that $X_+ \equiv H_{\text{eff}}^{(2)}$ is best demonstrated by application to a physical model system. Let us calculate the effective Hamiltonians for a four-level ladder system displaying three-photon Rabi oscillations. We call the states $|0\rangle$, $|1\rangle$, $|2\rangle$, and $|3\rangle$. The full Hamiltonian is given by

$$H = \begin{pmatrix} 0 & \Omega_0/2 & 0 & 0 \\ \Omega_0/2 & \Delta_0 & \Omega_1/2 & 0 \\ 0 & \Omega_1/2 & \Delta_1 & \Omega_2/2 \\ 0 & 0 & \Omega_2/2 & \delta \end{pmatrix}. \tag{2.39}$$

We choose $\Delta_0 = \Delta_1 = 0.1$, $\delta = 0$ and $\Omega_0 = \Omega_2 = 0.8\Delta_0$ as well as $\Omega_1 = 0.6\Delta_0$. The parameters are chosen so that

1. the coefficients in Eq. (2.33) commute, $[D_0, D_1] = 0$, and
2. both zeroth and first-order adiabatic elimination produce unsatisfying results.

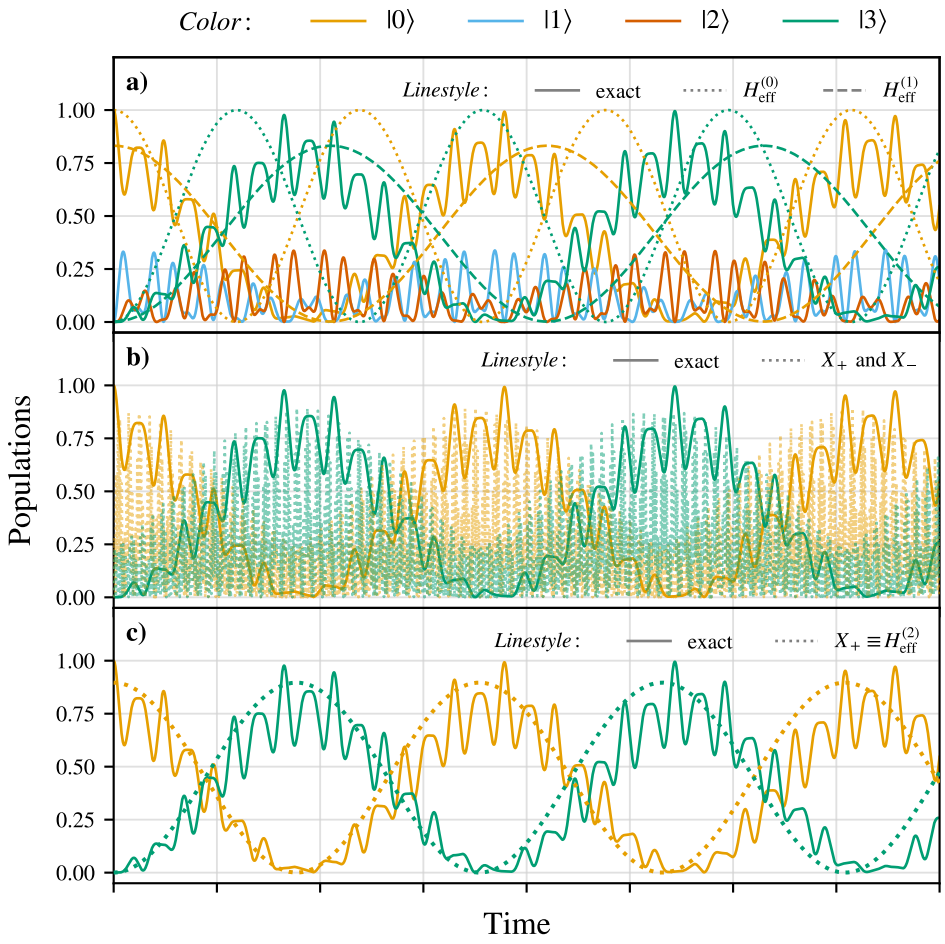

Figure 2.2: Populations for four-level system defined by the Hamiltonian Eq. (2.39). In panel **a)**, the exact solution (solid) is compared with the populations due to $H_{\text{eff}}^{(0)}$ (dotted) and $H_{\text{eff}}^{(1)}$ (dashed). Both effective Hamiltonians produce less-than-stellar results. In panel **b)**, the propagation with the time-evolution operator Eq. (2.38) is shown (dashed-dotted). The slow oscillations (due to X_+) are modulated by rapid oscillations (due to X_-). In panel **c)**, only the propagation with the effective Hamiltonian $H_{\text{eff}}^{(2)} \equiv X_+$ based on Eq. (2.41) is shown (dashed-dotted). This yields a better estimate than either $H_{\text{eff}}^{(0)}$ or $H_{\text{eff}}^{(1)}$. The states $|1\rangle$ and $|2\rangle$ are omitted from panel **b)** and **c)**.

Fig. 2.2a) shows the exact time evolution (solid), obtained by numerical integration with 4th order Runge-Kutta, together with the approximations obtained via $H_{\text{eff}}^{(0)}$ (dotted) and $H_{\text{eff}}^{(1)}$ (dashed). $H_{\text{eff}}^{(1)}$ gives a better estimate, but underestimates the effective Rabi frequency, whereas $H_{\text{eff}}^{(0)}$ overestimates it. Fig. 2.2b) shows the exact solution (solid) together with the solution obtained via propagation with Eq. (2.38) (dashed-dotted), i.e.

$$P\,|\Psi(t)\rangle = PU_{\pm}^{(2)}(t,t_0)P\,|\Psi(t_0\rangle\,. \tag{2.40}$$

We can see that this solution oscillates on two different time scales: First, slow oscillations on the timescale of the effective Rabi frequency, and second, extremely rapid oscillations. The slow oscillations are due to X_+ while the fast oscillations are due to X_-. A quick numerical calculation reveals that $X_+ = H_{\text{eff, it.}}^{(2)}$ from Eq. (2.27). Thus, we identify X_+ as the exact second-

order effective Hamiltonian $H_{\text{eff}}^{(2)}$ and call X_- the non-essential solvent. An intuitive calculation showing why X_+ must be the effective Hamiltonian is shown in Appendix B.

Plotting the time evolution due to $H_{\text{eff}}^{(2)}$, i.e. using

$$PU_{\text{eff}}^{(2)}(\tau)P := \mathcal{N}^{(2)}\mathrm{e}^{-\mathbb{i}X_+\tau}, \tag{2.41}$$

yields Fig. 2.2c) (dashed-dotted), which when compared to the exact solution (solid) is a good estimate and significantly better than $H_{\text{eff}}^{(1)}$.

Why are we able to separate the second-order effective Hamiltonian X_+ from the non-essential solvent X_- using the block partial-fraction expansion of the resolvent operator? We can understand it by noting that the dominator of the resolvent operator in the pole approximation, $PG(z)P = P(z - H_{\text{eff}}^{(0)})^{-1}P$, is a monic Hermitian matrix polynomial $T_1(z)$, which is already trivially block partial-fraction expanded. Thus, $H_{\text{eff}}^{(0)}$ is by definition the solvent for $T_1(X) = 0$. If we search for a higher-order correction to $H_{\text{eff}}^{(0)}$, what we want to correct is the location of this particular solvent. With the linear correction, this is exactly what occurs: The solvent is improved upon by $(\mathbb{1}_P + PV[QHQ]^{-2}VP)^{-1}$. Starting with the quadratic correction, we introduce new solvents: Analogously to the fact that a quadratic polynomial has two roots, the quadratic Hermitian matrix polynomial with commuting coefficients has two solvents.

It is not immediately obvious if X_- and its the time-evolution operator $\exp[-\mathbb{i}X_-t]$ represent a physical process. Intuitively, X_- may represent the time-evolution due to phenomena that couple $\mathcal{P}$ and $\mathcal{Q}$. In that sense, if X_- is big, the associated resolvent $(z - X_-)^{-1}$ will be small around $z = 0$ and hence, the transition probabilities due to $\exp[-\mathbb{i}X_-t]$ will average to zero for large t. If X_- becomes small, this may be indicative of a breakdown of the effective Hamiltonian formalism.

Note that $PU_{\text{eff}}^{(2)}P$ of Eq. (2.41) is structurally analogous to $PU_{\text{eff}}^{(1)}(\tau)P$ of Eq. (2.13) in the sense that the normalisation $\mathcal{N}^{(2)}$ makes the norm in subspace $\mathcal{P}$ less than one. Furthermore, note that X_-, while not contributing to the transition probability, does appear in $\mathcal{N}^{(2)}$.

The concepts explored in this chapter can be generalised both for the non-commuting case, and for higher orders, $H_{\text{eff}}^{(n\geq 3)}$. For both generalisations, the difficult always lies in obtaining the entire set of solvents. One may either construct them based on the eigenvalues and eigenvectors of the matrix polynomial [151, 152], or one can attempt to solve them numerically [151, 156–159]. The block partial-fraction expansions with either the left or right solvents seem to be the higher-order analoga of the two non-Hermitian first-order effective Hamiltonians in Eq. (2.9) (where $(1 + C)^{-1}$ was applied to $H_{\text{eff}}^{(0)}$ either from the left, or from the right). It will be interesting to explore if a symmetric variant also exists. Such generalisations will become the subject of future work.

3 Two-photon Rabi oscillations in hydrogen

In this chapter, the effective Hamiltonian formalism will be employed to describe coherent multiphoton processes in hydrogen. We study in particular the time-evolution due to medium- to high-intensity deep-UV pulses (usually $I_0 < 1 \times 10^{13}\,\mathrm{W \cdot cm^{-2}}$ and $\omega \simeq 5\,\mathrm{eV}$ for the 1s-2s two-photon transition, or $\omega \simeq 6\,\mathrm{eV}$ for the 1s-3s/d two-photon transition). It will be shown that within the applicable parameter regimes, the obtained effective Hamiltonians describe the atom-field dynamics very accurately. They allow us to make meaningful physical interpretations, such as disentangling competing contributions to multiphoton transitions, studying the state-resolved ionisation rates, or quantifying the damping of Rabi oscillations.

There exists a trove of research on the light-matter dynamics on hydrogen. Yet, two-photon Rabi oscillations in hydrogen are barely explored. One important exception is the study by Dörr *et al.* [56]. They conclude that two-photon Rabi oscillations cannot be observed between 1s and 2s, no matter the intensity, since the ionisation from the 2s state is too strong. We will come to the same conclusion using our model system. However – and this has not been previously reported – Rabi oscillations are indeed possible to drive between the 1s and 3s/d states. This is the key finding that is discussed in this chapter.

The structure of the chapter is as follows. In Section 3.1, the model system will be explained in detail. As a case study, the 1s-2s two-photon transition is explored in Section 3.2. Since this system yields a 2-level effective Hamiltonian, the time-dependent Schrödinger equation can be solved analytically, yielding insights into the different contributions to the excited state population. Section 3.3 forms the center of this chapter, containing the study of the 1s-3s/d two-photon transition in hydrogen. It will be shown using TDSE and model system calculations that two-photon Rabi oscillations can be driven in this system. Parameter regimes for these oscillations will be discussed. Furthermore, a bright-dark state analysis of the Hilbert space allows us to further approximate the 3-level effective Hamiltonian by a 2-level effective Hamiltonian, once again enabling us to analytically study the properties of the system. Lastly, in Section 3.4, the model system is used to update and supplement effective Hamiltonians parameters for resonant multiphoton ionisation in hydrogen that were previously calculated by Holt *et al.* [41].

3.1 The model system

The description of resonant ionisation has a long history. Observing current research trends, one will see many models relying on several of the following approximations [43–48, 98, 160–162]:

1. The RWA, which neglects the contribution of off-resonant states and allows for a transformation to an interaction picture in which the Hamiltonian is time-independent.[1]
2. Only states accessible from the essential states via a one-photon transition are included as intermediate states (i.e. for a two-photon transition between 1s and 2s in hydrogen, we would only include p-states as intermediate states).
3. Adiabatic elimination of intermediate states, yielding Stark shifts and effective couplings. Due to the above point, these usually correspond to second-order perturbation theory.
4. The local approximation [164], which eliminates the continuum states in a similar spirit to adiabatic elimination. There are several ways to eliminate continuum states [48]; the common denominator is the reliance on the assumption of a flat continuum.

Other approximations may include the neglect of continuum-continuum couplings and neglect of the ground-state ionisation rate. The latter assumption also makes $\beta = 0$ (where β is the imaginary Rabi frequency describing the interference between different ionisation pathways). Depending on the system studied, all these approximations can be highly useful and valid. For our purposes, we want a model, which

1. describes physics beyond the RWA, since for many multiphoton transitions, the counter-rotating terms contribute massively to the dynamics (see e.g. the two-photon transition between 1s and 2s in hydrogen, where there are no clear resonant intermediate states available),
2. if required, can account for the impact of states not directly dipole-coupled to the essential states but rather accessible via two-photon transitions (e.g. d-states for the two-photon transition from 1s to 2s),
3. does adiabatic elimination of intermediate and off-resonant states rigorously,
4. eliminates continuum states (in some manner analogous to the local approximation), and yields not only all state-resolved ionisation rates but also the imaginary Rabi frequency β, introduced in Section 1.6 and discussed in Ref. [40, 41, 55],
5. is flexible enough to take into account many Rydberg states and different continuum channels.

Gratifyingly, by combining the concepts of Floquet theory (Section 1.3), complex scaling techniques (Section 1.6) and the effective Hamiltonian approach within the resolvent formalism (Sections 1.4, 1.5.4 and 2.1), the above requirements can be fulfilled. Put most concisely, the model system that we are going to use for this chapter is based on the explicit construction of a rotated Floquet Hamiltonian that is both truncated and discretized. From this Hamiltonian, using the effective Hamiltonian formalism detailed in Sections 1.5.4 and 2.1, we can through straight-forward matrix arithmetic obtain few-level effective Hamiltonians.

[1] Possibly the most famous appearance of the RWA is in the Jaynes-Cumming model, which has been central to many theoretical developments in light-matter interaction [163]. For two-photon transitions, there exists a generalisation called the two-photon RWA, which yields time-dependent effective Hamiltonians [62]. The applicability of RWA to multiphoton transitions has been a point of contention, especially in the context of adiabatic elimination [61].

3.1.1 Constructing the rotated Floquet Hamiltonian from atomic parameters

For the linearly polarised, monochromatic electric field $\mathcal{E}(t) = \mathcal{E}_0 \cos(\omega_0 t)$, using Eq. (1.8), we can write the infinitely-dimensional Floquet Hamiltonian as a matrix with the following block structure,

$$H^{(F)} = \begin{pmatrix} \ddots & & \ddots & & \ddots & & & & \\ & 0 & V & H_0 + (N+1)\omega & V & 0 & 0 & 0 & \\ \cdots & 0 & 0 & V & H_0 + N\omega & V & 0 & 0 & \cdots \\ & 0 & 0 & 0 & V & H_0 + (N-1)\omega & V & 0 & \\ & & & & \ddots & & \ddots & & \ddots \end{pmatrix}, \tag{3.1}$$

where H_0 is the field-free Hamiltonian (which is a diagonal matrix) and $V \equiv \mathcal{E}_0 \overline{z}/2$ is the interaction representing the absorption (lower triangle of $H^{(F)}$) or emission (upper triangle of $H^{(F)}$) of a single photon ($\overline{z}$ is the transition dipole matrix with matrix elements z_{nm}). The terms $(N+M)\omega$ are scalars ($N, M \in \mathbb{Z}$) that are added to all matrix elements of H_0. As discussed in Section 1.3, we can write $H^{(F)} \equiv H_0^{(F)} + V^{(F)}$ in a perturbative ansatz, where $H_0^{(F)}$ is diagonal in the basis of the Floquet states.

The Floquet Hamiltonian $H^{(F)}$ is not only infinitely-dimensional (both with respect to the expansion in the photon number $N + M$, and with respect to the angular momentum l), but it has also inherits the properties of H_0: It has a mixed discrete and continuous spectrum where the continuum eigenfunctions are not L^2-integrable. These properties prevent explicit construction of $H^{(F)}$ a matrix. In the following, each point will be addressed.

The most involved task is the discretisation of the continuum. The method was discussed in Section 1.6. In short, the continuum eigenfunctions can be damped through a complex scaling transform, which makes them L^2-integrable and transforms $H^{(F)}$ to the rotated Floquet Hamiltonian $H_\theta^{(F)}$, which has the same block structure as $H^{(F)}$ [81]. By expanding the eigenfunctions in a finite basis, the continuum is discretised [145], yielding a rotated, discretized Floquet Hamiltonian.

The infinite dimension due to the angular momentum l is simply addressed by truncating the angular momentum space with a maximum angular momentum $l_{\max}$. Similarly, the infinite dimension due to the photon number is addressed by choosing a finite Floquet state basis. How to choose this basis based on physical considerations is the topic of the following section. Put together, L^2-discretisation and truncation (through $l_{\max}$ and the finite Floquet state basis) yields the rotated Floquet Hamiltonian as a finite-dimensional matrix with complex-scaled dipole matrix elements $z_{nm} \in \mathbb{C}$ between different Floquet states on the off-diagonals, and the complex-scaled energies $E_n - \frac{\mathrm{i}}{2}\gamma_n$ ($E_n, \gamma_n \in \mathbb{R}$) of the Floquet states on the diagonals.

The finite Floquet state basis is made up of states denoted $|nl, N+M\rangle$. Here, $l \geq 0$ is the angular momentum quantum number (by convention, $l = 0, 1, 2, 3, 4$ correspond to the letters s, p, d, f, g, respectively), $N + M \in \mathbb{Z}$ the photon number (where M denotes the "excursion" from N [81]), and n the label of the discretised states for a given angular momentum, with $l + 1 \leq n \leq n_{\max}$, where $n_{\max}$ is the maximum number of states per angular momentum

channel. It is determined by the Floquet state basis. Note that n and $n_{\max}$ do not necessarily correspond to the principal quantum number since the labelling goes over both bound states and discretised continuum states. This is a necessary consequence of expanding the wavefunction on a finite radial grid. For the following investigations, the essential states (1s, 2s, 3s, and 3d) will however be low-energy bound states, where n can without concern be interpreted as the principal quantum number.

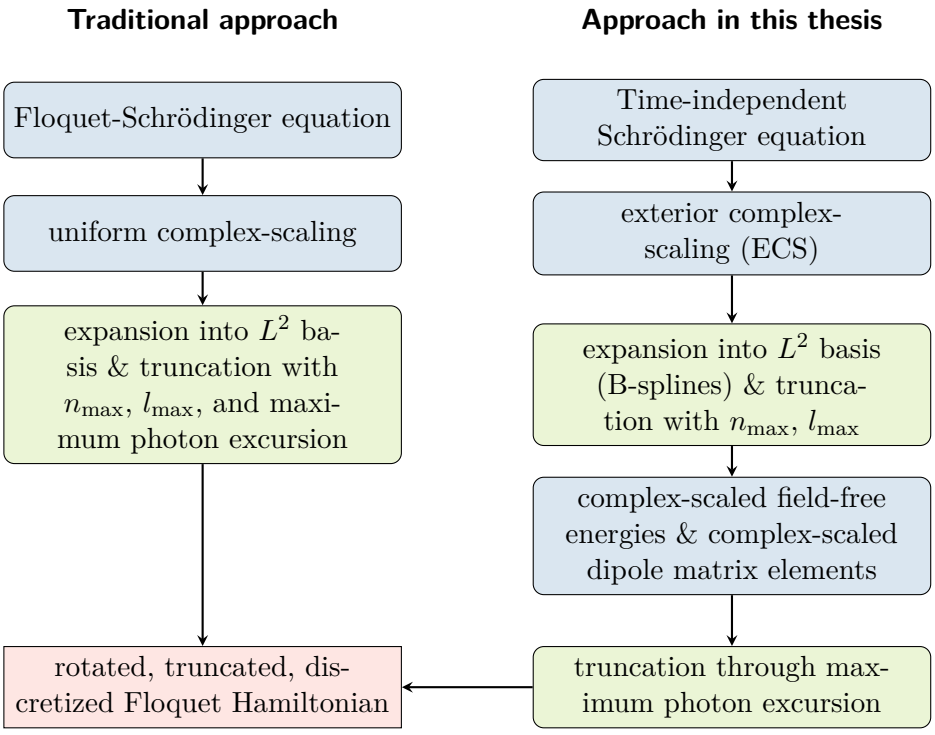

Figure 3.1: Visualisation of two approaches which yield the rotated Floquet Hamiltonian in a truncated and discretized form. Left is the approach commonly used in the 1980s, for example by Maquet *et al.* [81]. Right is the approach pursued in this chapter.

Let us summarize the traditional procedure: The Floquet-Schrödinger equation is transformed through uniform complex-scaling $r \to r\mathrm{e}^{\mathrm{i}\theta}$ and subsequently, via projection onto a finite basis (i.e. truncation with respect to $n_{\max}$, $l_{\max}$, and the maximum photon excursion), truncated and discretised. This approach is visualised as a flowchart in Fig. 3.1.

In the implementation that was done for this chapter, the Floquet formalism only appears at a later stage. First, the TISE is solved on a grid with B-splines with ECS [147, 165, 166]. Here, the B-splines act as a finite L^2-basis, where the size of the grid determines $n_{\max}$ (the larger the grid, the higher $n_{\max}$). Furthermore, $l_{\max}$ is chosen (see next section). This calculation yields the complex-scaled energies $E_n - \frac{\mathrm{i}}{2}\gamma_n$ and, through the determined eigenstates, allows for the calculation of complex-scaled dipole matrix elements $z_{nm} \in \mathbb{C}$. Solving the TISE was done with a code available in Dahlström's group. The complex-scaled parameters were then used to directly construct the rotated, truncated, discretised Floquet Hamiltonian $H_\theta^{(F)}$ (choosing a maximum photon excursion beforehand) in a Python code written by this author. This approach is also visualised in the flowchart, Fig. 3.1.

3.1.2 Choosing the Floquet state basis

The truncation of the rotated Floquet Hamiltonian must necessarily be based on physical considerations. The underlying intuition is that the Floquet state basis must include all states that one may expect to reach via absorption or emission from a given set of essential states. This intuition we formalise by introducing the truncation number $N_{\text{trunc}} \in \mathbb{N}^+$. Given a choice of N_{trunc} and a set of essential states $|nl, N+M\rangle$, we include all states in the Floquet state basis that can be reached via an up to N_{trunc}-photon transition. For instance, we can reach all states $|n'(l\pm1), N+M\pm1\rangle$ through a one-photon transition (here, $n' \in \mathbb{N}^+$ is arbitrary, and $l \geq 0$). Thus, N_{trunc} defines the maximum allowed photon excursion, i.e. how many photon transitions from an essential state will be accounted for.

Since this is an important point, let us go through the example of a 1s-2s two-photon transition. We define the essential states as $|1\text{s}, N\rangle$ and $|2\text{s}, N-2\rangle$. Choosing $N_{\text{trunc}} = 1$, the Floquet basis will consist of the following states $|nl, N+M\rangle$ and state manifolds $|l, N\rangle$:[2]

$$\text{Floquet basis} = \{|\text{p}, N+1\rangle, |1\text{s}, N\rangle, |\text{p}, N-1\rangle, |2\text{s}, N-2\rangle, |\text{p}, N-3\rangle\}.$$

Thus, the Floquet basis consists of the essential states plus all possible states reachable via a one-photon transition from one of the essential states. Choosing $N_{\text{trunc}} = 2$, the Floquet basis will consist of the following state manifolds:

$$\begin{aligned}\text{Floquet basis} = \{&|\text{s}, N+2\rangle, |\text{d}, N+2\rangle, |\text{p}, N+1\rangle, |\text{s}, N\rangle, |\text{d}, N\rangle, |\text{p}, N-1\rangle, \\ &|\text{s}, N-2\rangle, |\text{d}, N-2\rangle, |\text{p}, N-3\rangle, |\text{s}, N-4\rangle, |\text{d}, N-4\rangle\}.\end{aligned}$$

Now, the Floquet basis consists of the essential states (included in the state manifolds $|\text{s}, N\rangle$ and $|\text{s}, N-2\rangle$), plus all possible states reachable via a one-photon or two-photon transition from one of the essential states. The two bases for $N_{\text{trunc}} = 1$ and $N_{\text{trunc}} = 2$ are visualised in Fig. 3.2.

Note that it is generally impossible to *a priori* predict the lowest suitable choice of N_{trunc}. For the two-photon transitions investigated in this thesis, $N_{\text{trunc}} = 2$ yielded reliable results for all systems. For the 1s-2s transition in particular, $N_{\text{trunc}} = 1$ was sufficient.

Not yet discussed is the maximum number of states $n_{\max}$ per angular momentum channel that is considered in the state manifolds. The parameter $n_{\max}$ directly corresponds to some maximum energy $E_{\max}$ of the field-free eigenstates. Physically, the parameter $n_{\max}$ should thus be chosen so that at least the first continuum resonance is included. Choosing a very high $n_{\max}$ just increases the computational cost.

As soon as the basis of Floquet states is determined through the choices of N_{trunc} and $n_{\max}$, the rotated Floquet Hamiltonian $H_\theta^{(F)}$ can be constructed as a matrix using the complex-scaled parameters $E_n - \frac{\mathrm{i}}{2}\gamma_n$ and z_{nm}. Through the perturbative *ansatz* $H_\theta^{(F)} := H_{0,\theta}^{(F)} + V_\theta^{(F)}$, the truncated rotated Floquet Hamiltonian is amenable to the effective Hamiltonian formalism detailed in Section 1.5 and Chapter 2, yielding the effective Hamiltonians

$$H_{\text{eff}}^{(0)} = PH_\theta^{(F)}P - PV_\theta^{(F)}\frac{1}{QH_\theta^{(F)}Q}V_\theta^{(F)}P, \tag{3.2}$$

[2] A state manifold $|l, N+M\rangle$ is a shorthand for the entire set of states $|nl, N+M\rangle$ with $l+1 \leq n \leq n_{\max}$.

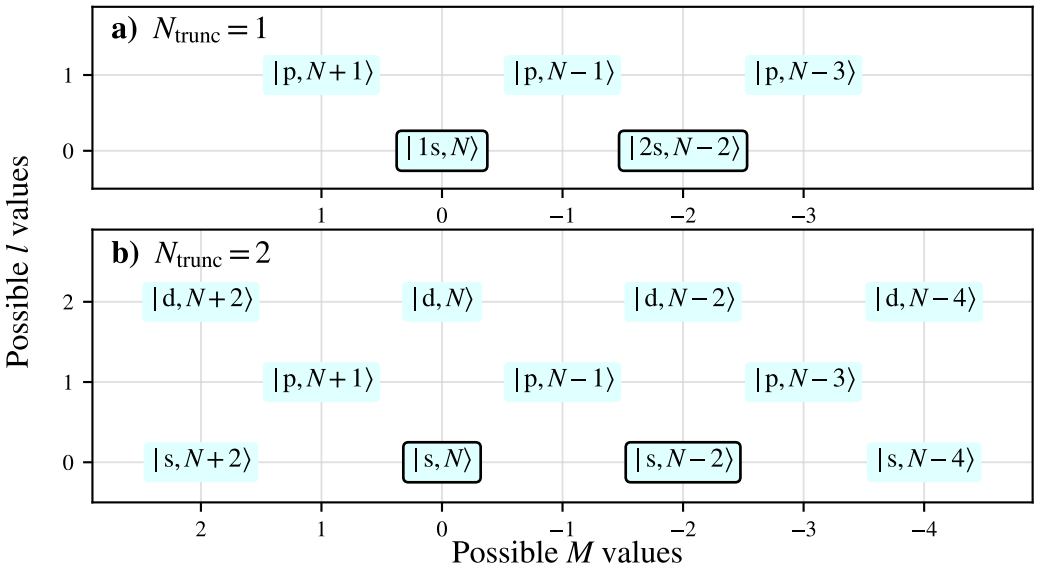

Figure 3.2: Illustration of the Floquet basis for the 1s-2s transition with essential states $|1\text{s}, N\rangle$ to $|2\text{s}, N-2\rangle$ (black outline), with **a)** $N_{\text{trunc}} = 1$ and **b)** $N_{\text{trunc}} = 2$. For $N_{\text{trunc}} = 2$, all $|\text{s}, N\rangle$ and $|\text{s}, N-2\rangle$ states are part of the Floquet basis while for $N_{\text{trunc}} = 1$, only $|1\text{s}, N\rangle$ and $|2\text{s}, N-2\rangle$ are. Note that for a given M value, the Floquet basis can only have either odd or even parity states.

$$H_{\text{eff}}^{(1)} = \left(\mathbb{1}_P + PV_\theta^{(F)}\left[QH_\theta^{(F)}Q\right]^{-2}V_\theta^{(F)}P\right)^{-1/2} \cdot H_{\text{eff}}^{(0)}\left(\mathbb{1}_P + PV_\theta^{(F)}\left[QH_\theta^{(F)}Q\right]^{-2}V_\theta^{(F)}P\right)^{-1/2}, \tag{3.3}$$

which will both be employed in the following investigations. Note that the symmetric splitting is used for Eq. (3.3). This is to ensure that the effective Hamiltonian is complex-symmetric.

3.1.3 Limitations of the model system

When applying the effective Hamiltonian formalism, one must remember that the pole approximation and its first-order correction can in certain scenarious break down. Thus, a central question is the validity of the formalism and how to formulate a mathematical relation that expresses it. Studies in the 1970s and 80s concluded that the effective Hamiltonian formalism breaks down when the spectrum of the model space $\mathcal{P}$ overlaps with the $\mathcal{Q}$-space spectrum [64, 74, 110, 167–170].

A visualisation for this breakdown is easy to provide within the dressed-state picture for two essential states. The dressed states $|+\rangle$ and $|-\rangle$ (eigenstates of the effective 2-level Hamiltonian) are split by the effective Rabi frequency Ω_{eff}, which for a two-photon transition will scale (approximately) quadratically with the field strength [41]. Approximating the non-essential states as the field-free eigenstates of $H_0^{(F)}$, we can formulate the failure point of the effective Hamiltonian formalism as the point where the quasi-energies of either $|+\rangle$ or $|-\rangle$ cross with the energy Δ_{min} of the energetically closest perturbed state $|v_{\text{min}}\rangle \in \mathcal{Q}$. This is illustrated in Fig. 3.3.

The most exact way to formulate the breakdown is to define a critical bound state $|c, N_c\rangle \in \mathcal{Q}$

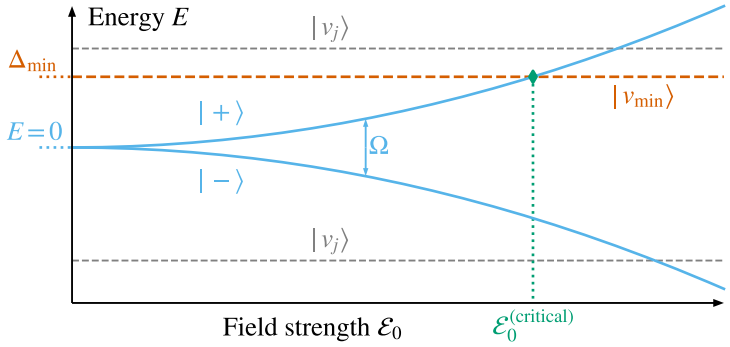

Figure 3.3: Illustration of the breakdown of the model when one of the dressed states $|\pm\rangle$ (separated by the coupling Ω) crosses a perturbatively treated state $|v_{\min}\rangle$ in energy (with other non-essential states $|v_j\rangle$ above and below). We call $|v_{\min}\rangle$ the critical state, with energy $\Delta_{\min}$, and the field strength at which it crosses with $|+\rangle$ the critical field strength $\mathcal{E}_0^{(\text{critical})}$. When $|v_{\min}\rangle$ crosses $|+\rangle$, the spectral components of the $\mathcal{P}$ and $\mathcal{Q}$ space overlap, which leads to the failure of the effective Hamiltonian formalism [33, 60, 64]. In the theory of effective Hamiltonians, the state $|v_{\min}\rangle$ is called the *intruder state* [74, 168, 169].

with photon number N_c, which is responsible for the breakdown of the formalism.[3] The critical state is the state which maximizes $|\Omega_{\text{eff}}/\Delta_c|$, where Ω_{eff} is the effective coupling from $|c, N_c\rangle$ to any essential state and $\Delta_c \coloneqq E_c - N_c\omega_0$ is the detuning of the state. Note that Ω_{eff} depends on the field strength $\mathcal{E}_0$, and it can be, but does not have to be, a single-photon coupling. A simpler form of this condition can be found in Faisal's *Theory of Multiphoton Processes* (Ch. 7), where he approximates Ω_{eff} with the atomic dipole $a_0 e$ (with Bohr length a_0 and elementary charge e; both are 1 in atomic units) and thus states the condition

$$\mathcal{E}_0 \ll |\Delta_{\min}|, \tag{3.4}$$

for the field strength $\mathcal{E}_0$, where $\Delta_{\min}$ is simply the minimal detuning of any non-essential bound state [33]. This condition is very easy to check and yields reasonable intensity limits. As such, it will be used in the following calculations.

3.2 Study of the 1s-2s two-photon transition in hydrogen

The two-photon transition from 1s to 2s in hydrogen, due to its extremely narrow natural linewidth, may be the experimentally most-studied multiphoton transition in physics, giving access to precise measurements of the 1s lamb shift and the Rydberg constant [171–177]. These measurements are of course perturbative: The population of the 2s state remains negligible throughout the interaction. In this section, we move beyond the perturbative picture and show that the model system of Section 3.1 reproduces the important conclusion of Dörr *et al.* that two-photon Rabi oscillations cannot be observed between 1s and 2s [56].

Naturally, a model system requires a benchmark to compare against. These might either be experimental data or, if the system allows for it, high-fidelity numerical simulations. For this

[3] Continuum states will not yield singularities due to their complex energies.

thesis, the model systems are verified by comparing the results to TDSE simulations in the EDA. These simulations are carried out using the same codebase of Jan Marcus Dahlström's group which previously yielded the complex-scaled parameters for the rotated Floquet Hamiltonian.

The model system in this section is set up with the essential states $|1s, N\rangle$ and $|2s, N-2\rangle$. The Floquet Hamiltonian is truncated with $N_{\text{trunc}} = 1$, see Fig 3.2a) for an illustration of the Floquet state basis. A higher N_{trunc} does not worsen the results, but is simply unnecessary for this problem. The maximum number of states per angular momentum channel included in the following calculations is $n_{\max} = 150$, which for the chosen grid corresponds to energies 331 eV bigger than the ground-state energy. [4]

Let us show exemplary results of the model system. As pulse parameters, we choose $I_0 = 4 \times 10^{12}\,\text{W} \cdot \text{cm}^{-2}$ and $\omega_0 = 5.1151\,\text{eV}$. The frequency ω_0 is not exactly two-photon resonant, but slightly detuned so the Stark shift is compensated for. The optimal detuning is best found "brute-force" by varying ω_0 (something that, due to computational cost, is not practical with the TDSE). Applying the condition Eq. (3.4) to the rotated Floquet Hamiltonian, the limit of the model system can easily be found to be $I_0 \ll 1 \times 10^{14}\,\text{W} \cdot \text{cm}^{-2}$, where the limiting state is a Rydberg state of the $|p, N-1\rangle$ manifold. Thus, we are comfortably within the region where the model is applicable. Calculating the zeroth and first-order effective Hamiltonians $H_{\text{eff}}^{(0)}$ and $H_{\text{eff}}^{(1)}$ using Eq. (3.2) and (3.3) respectively, we receive two 2-level effective Hamiltonians for the essential states, which are of the form Eq. (1.49).

Let us abbreviate $|a\rangle \equiv |1s, N\rangle$ and $|b\rangle \equiv |2s, N-2\rangle$. We now propagate with the effective Hamiltonian with the initial condition $a(t) = 1$, $b(t) = 0$ and compare the populations to those obtained by exact numerical TDSE populations in Fig. 3.4. Evidently, we see fantastic agreement for both $H_{\text{eff}}^{(0)}$ and $H_{\text{eff}}^{(1)}$ with the TDSE. All yellow lines, corresponding to the 1s populations, are on top of each other, and so are all blue lines, corresponding to the 2s populations. Since we are so far from the limits of the model system ($I_0 \ll 1 \times 10^{14}\,\text{W} \cdot \text{cm}^{-2}$), it is intuitive that the zeroth-order effective Hamiltonian should be sufficient. The decay of the 2s state is so rapid that no Rabi oscillations are possible for these parameters.

Fig. 3.4 provides a proof-of-concept for the effective Hamiltonian scheme, but does not reveal particularly many insights. One fruitful analysis is to relate the time scales of the parameters to the intensity. The time-scale of ionisation is the inverse of the ionisation rates $\tau_{1s} := 1/\gamma_{1s}$ and $\tau_{2s} = 1/\gamma_{2s}$, while the natural time-scale of the two-photon Rabi oscillations is the two-photon Rabi period, defined by $2\pi/|\Omega_{\text{eff}}|$. We ignore the impact of β in this discussion for simplicity. The ultimate limit is the spontaneous lifetime of the 2s state. Since there are no states available with which the 2s state can couple resonantly, the 2s state is metastable, i.e. has a long lifetime of 122 ms [173]. Through varying the intensity at the two-photon resonance $\omega_0 = (\omega_{2s} - \omega_{1s})/2 = 5.1021\,\text{eV}$, the different effective parameters are obtained as function of I_0 and are shown in Fig. 3.5. Note that the parameters are taken from $H_{\text{eff}}^{(0)}$.

There are several interesting aspects to note. Firstly, $\tau_{2s} < 2\pi/|\Omega_{\text{eff}}|$ for all intensities, i.e. the ionisation lifetime of the 2s level is smaller than the Rabi period. This is a clear indication that Rabi oscillations can never be observed in this system: As soon as we excite to the 2s with

[4] A much smaller $n_{\max}$ would suffice for this problem. However, apart from computational cost – which for this example is still very small – there is no disadvantage in considering higher-lying energies. In general, as long as the computational cost is reasonable, it is my experience to better be safe than sorry with $n_{\max}$.

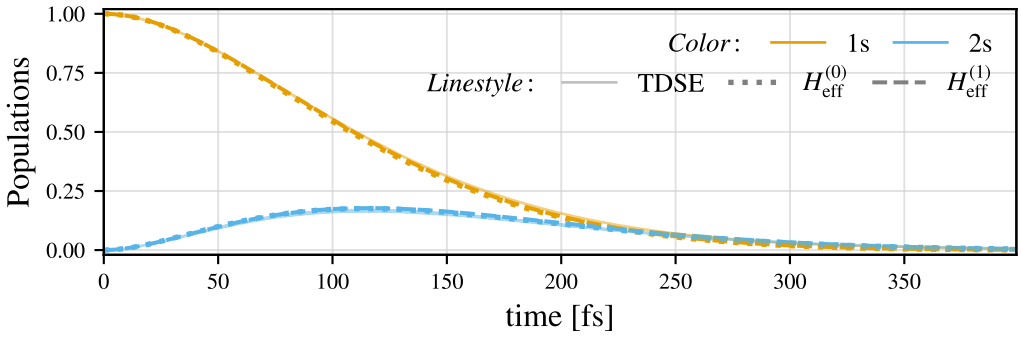

Figure 3.4: Populations of the 1s and 2s states obtained through TDSE simulations (solid) and propagation with $H_{\text{eff}}^{(0)}$ (dotted) and $H_{\text{eff}}^{(1)}$ (dashed). The pulse has intensity $I_0 = 4\times10^{12}\,\mathrm{W\cdot cm^{-2}}$ and frequency $\omega_0 = 5.1151\,\mathrm{eV}$ (chosen so the Stark shift is compensated for). All levels of theory coincide.

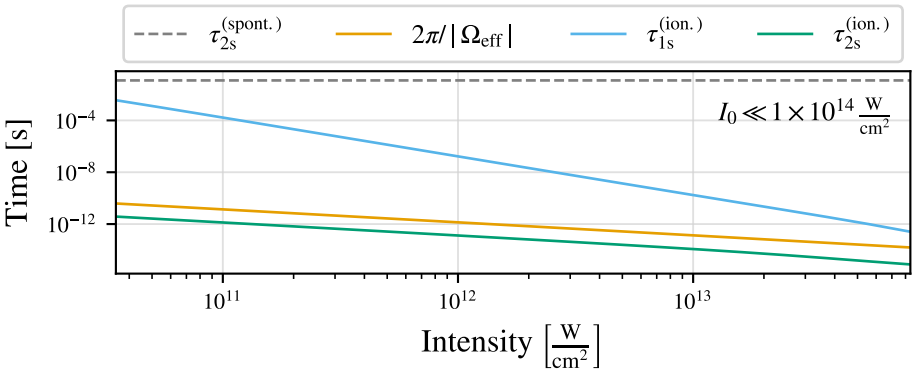

Figure 3.5: Spontaneous lifetime $\tau_{2s}^{(\text{spont.})}$, ionisation lifetimes $\tau_{1s}^{(\text{ion.})}$ and $\tau_{2s}^{(\text{ion.})}$ of the 1s and 2s state and the effective Rabi period $2\pi/|\Omega_{\text{eff}}|$ plotted against the intensity on a log-log scale. As expected from lowest-order perturbation theory, $\tau_{2s}^{(\text{ion.})}$ and $2\pi/|\Omega_{\text{eff}}|$ scale identically with I_0 (linearly, to be exact, or quadratically in the field strength $\mathcal{E}_0$). At some point beyond the intensity limit, the $\tau_{1s}^{(\text{ion.})}$ decay will become dominant since it scales cubically with I_0.

two photons, we will ionise with a third. At low and medium intensities, both τ_{2s} and $2\pi/|\Omega_{\text{eff}}|$ decrease linearly with the same slope. In fact, γ_{2s} and Ω_{eff} scale linearly with the intensity; as might be expected from lowest-order perturbation theory. This was previously noted in the literature [56]. Only at higher intensities do we see τ_{2s} curve downwards, indicating the onset of fourth-order contributions. This onset has not yet been explored. Meanwhile, γ_{1s} scales cubically with the intensity (given that one needs three photons from γ_{1s} to couple resonantly to the continuum and another three to couple back to 1s). This results in a far steeper negative slope. At some intensity $> 1\times10^{14}\,\mathrm{W\cdot cm^{-2}}$, the two ionisation rates will cross, and then the non-resonant ionisation pathway will dominate. The phenomenon of the competition of resonant and non-resonant pathways in multiphoton ionisation has had an upsurge of research interest recently [22, 43, 55, 162] and can be regarded as a fundamental property of resonance-enhanced multiphoton ionisation [40, 41].

The 2-level system can of course be solved analytically [33, 40]. Of interest to us is to obtain a formula for the excited state population $|b(t)|^2$. For the Hamiltonian given by

$$H_{\text{eff}} = \begin{pmatrix} S_a - \frac{\mathbb{i}}{2}\gamma_a & (\Omega + \mathbb{i}\beta)/2 \\ (\Omega + \mathbb{i}\beta)/2 & (S_b + \delta) - \frac{\mathbb{i}}{2}\gamma_b \end{pmatrix}, \tag{3.5}$$

where the zero-point energy has been chosen as the ground-state energy, so that $\delta \coloneqq E_c - 2\omega$, this involves some arithmetic and trigonometrics. First, let us define the auxiliary quantities $\Delta S \coloneqq S_a - (S_b + \delta)$, $\Delta\gamma \coloneqq (\gamma_a - \gamma_b)/2$ and $\Gamma \coloneqq (\gamma_a + \gamma_b)/2$. We identify the generalized Rabi frequency

$$W = \sqrt{(\Delta S - \mathbb{i}\Delta\gamma)^2 + (\Omega + \mathbb{i}\beta)^2} \tag{3.6}$$

$$= \sqrt{(\Delta S)^2 - (\Delta\gamma)^2 + \Omega^2 - \beta^2 - 2\mathbb{i}\,(\Delta S \cdot \Delta\gamma - \Omega\beta)}, \tag{3.7}$$

with which we can calculate the excited state population as

$$|b(t)|^2 = \left|\frac{\Omega}{W}\right|^2 \mathrm{e}^{-\Gamma t}\left[\sinh^2\left(\frac{1}{2}\operatorname{Im}(W)t\right) + \sin^2\left(\frac{1}{2}\operatorname{Re}(W)t\right)\right]. \tag{3.8}$$

An equivalent, but arguably less simple, expression is given in Ref. [33]. The above simple form of $|b(t)|^2$ has, to my best knowledge, not been provided in the literature. It lends itself more easily to the following physical interpretations. In Eq. (3.8), we immediately see that if there is no dissipation, i.e. $\gamma_a = \gamma_b = \beta = 0$, the formula reduces to the well-known Rabi formula, $|b(t)|^2 = |\Omega/W|^2 \sin^2(Wt/2)$. Through further arithmetic, we can obtain analytical expressions for $|\operatorname{Re}(W)|$ and $|\operatorname{Im}(W)|$ (only the absolute value matters for the $\sinh^2$ and $\sin^2$ functions):

$$|\operatorname{Re}(W)| = \frac{1}{\sqrt{2}}\Big|(\Delta S)^2 - (\Delta\gamma)^2 + \Omega^2 - \beta^2 + \sqrt{\left[(\Delta S)^2 - (\Delta\gamma)^2 + \Omega^2 - \beta^2\right]^2 + 4[\Delta S \cdot \Delta\gamma - \Omega\beta]^2}\Big|^{1/2} \tag{3.9}$$

$$|\operatorname{Im}(W)| = \frac{1}{\sqrt{2}}\Big|(\Delta S)^2 - (\Delta\gamma)^2 + \Omega^2 - \beta^2 - \sqrt{\left[(\Delta S)^2 - (\Delta\gamma)^2 + \Omega^2 - \beta^2\right]^2 + 4[\Delta S \cdot \Delta\gamma - \Omega\beta]^2}\Big|^{1/2} \tag{3.10}$$

From these two formulas, which differ only by the sign in front of the root, we can identify

$$|W|^2 = \left|(\Delta S)^2 - (\Delta\gamma)^2 + \Omega^2 - \beta^2\right|. \tag{3.11}$$

Further dissecting Eq. (3.8), we see that it is a sum with two contributions: a damped oscillator and a term involving the multiplication of a damping exponential and a rapidly growing $\sinh^2$. Let us discuss the former, i.e. the contribution

$$f(t) \coloneqq \mathrm{e}^{-\Gamma t}\sin^2\left(\frac{1}{2}\operatorname{Re}(W)t\right). \tag{3.12}$$

Borrowing the well-known concepts from classical mechanics [178], we can identify three regimes:

$$\Gamma > |\operatorname{Re}(W)|, \quad \Rightarrow \text{ overdamped}, \tag{3.13}$$

$$\Gamma = |\operatorname{Re}(W)|, \quad \Rightarrow \text{ critically damped}, \tag{3.14}$$

$$\Gamma < |\operatorname{Re}(W)|, \quad \Rightarrow \text{ underdamped}. \tag{3.15}$$

This gives us a quick way to identify if we can hope to see Rabi oscillations in decaying effective 2-level systems. If one wishes to be able to observe multiple Rabi cycles before the atom is fully ionised, the rule of thumb $\Gamma/|\operatorname{Re}(W)| \leq \frac{1}{10}$ seems reasonable. For Fig. 3.4 (i.e. with $I_0 = 4 \times 10^{12}\,\mathrm{W \cdot cm^{-2}}$), we find that $\Gamma/|\operatorname{Re}(W)| = 1.404$, which thus clearly shows that two-photon Rabi oscillations cannot occur. This conclusion is valid for a broad intensity range, up to the limit of the model system at $I_0 \simeq 1 \times 10^{14}\,\mathrm{W \cdot cm^{-2}}$. A discussion of the second contribution, i.e. the damped $\sinh^2$ term, can be found in Appendix C.

3.3 Two-photon Rabi oscillations between 1s, 3s and 3d in hydrogen

If Rabi oscillations cannot be observed between 1s and 2s in hydrogen, the next step is to go one principal quantum number higher.[5] This changes the situation drastically, since now, there is an "obvious" intermediate state, 2p, that contributes significantly to the two-photon transition. When we are resonant to the $n = 3$ states, there will be three essential states, $|1s, N\rangle$, $|3s, N-2\rangle$, and $|3d, N-2\rangle$, yielding a 3-level effective Hamiltonian. As before, the rotated Floquet Hamiltonian is constructed using complex-scaled atomic parameters. Concerning the truncation, it turns out that $N_{\mathrm{trunc}} = 2$ is necessary for the best agreement (for the 1s-2s transition, $N_{\mathrm{trunc}} = 1$ was easily sufficient). This is related to fourth-order perturbative contributions and is discussed in Appendix D. Th choice of basis is illustrated in Fig. 3.6. Using Eq. (3.4), we identify the critical state as $|4d, N-2\rangle$, which yields $I_0 \ll 2 \times 10^{13}\,\mathrm{W \cdot cm^{-2}}$ as the intensity limit.

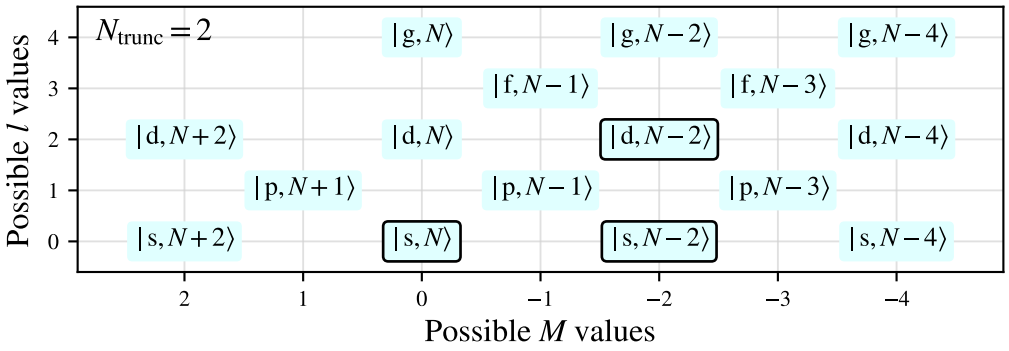

Figure 3.6: Illustration of the Floquet basis for the 1s-3s/d transition with essential states $|1s, N\rangle$, $|3s, N-2\rangle$ and $|3d, N-2\rangle$ (black outline), with $N_{\mathrm{trunc}} = 2$.

[5] The $n = 1$ to $n = 3$ transition in hydrogen has received some attention in spectroscopy [179–181] and was recently used to facilitate air lasing [182–184]. In-depth time-dependent theoretical studies, especially in the strong coupling regime, are lacking.

3.3.1 A three-level system displaying Rabi oscillations

Choosing $I_0 = 4 \times 10^{12}\,\mathrm{W \cdot cm^{-2}}$ and the frequency $\omega_0 = 6.0566\,\mathrm{eV}$ (chosen so that the detuning of the 1s-3d resonance due to the Stark shifts is compensated for), we obtain the following 3-level effective Hamiltonian for the essential states, where we abbreviate $|a\rangle \equiv |1\mathrm{s}, N\rangle$, $|b\rangle \equiv |3\mathrm{s}, N-2\rangle$ and $|c\rangle \equiv |3\mathrm{d}, N-2\rangle$:

$$H_{\mathrm{eff}} = \begin{pmatrix} S_a - \frac{\mathrm{i}}{2}\gamma_a & (\Omega_{ab} + \mathrm{i}\beta_{ab})/2 & (\Omega_{ac} + \mathrm{i}\beta_{ac})/2 \\ (\Omega_{ab} + \mathrm{i}\beta_{ab})/2 & (S_b + \delta_b) - \frac{\mathrm{i}}{2}\gamma_b & (\Omega_{bc} + \mathrm{i}\beta_{bc})/2 \\ (\Omega_{ac} + \mathrm{i}\beta_{ac})/2 & (\Omega_{bc} + \mathrm{i}\beta_{bc})/2 & (S_c + \delta_c) - \frac{\mathrm{i}}{2}\gamma_c \end{pmatrix} \equiv \begin{pmatrix} W_a & X_{ab} & X_{ac} \\ X_{ab} & W_b & X_{bc} \\ X_{ac} & X_{bc} & W_c \end{pmatrix}. \tag{3.16}$$

Note that the ground state energy was chosen as the zero-point energy so that $\delta_b \coloneqq E_b - 2\omega$ and $\delta_c \coloneqq E_c - 2\omega$. We now calculate both $H_{\mathrm{eff}}^{(0)}$ and $H_{\mathrm{eff}}^{(1)}$ using Eq. (3.2) and (3.3). Propagation with the initial conditions $a(t) = 1$, $b(t) = c(t) = 0$ and comparison to an exact TDSE simulation yields the populations shown in Fig. 3.7. The populations undergo two-photon Rabi oscillations. The TDSE populations (solid) match almost perfectly with those predicted by $H_{\mathrm{eff}}^{(1)}$ (dashed), while $H_{\mathrm{eff}}^{(0)}$ (dotted) predicts populations with slightly too high Rabi frequency. That $H_{\mathrm{eff}}^{(1)}$ gives a better estimate should not be too surprising, given that the intensity is reasonably close to the upper-intensity limit.

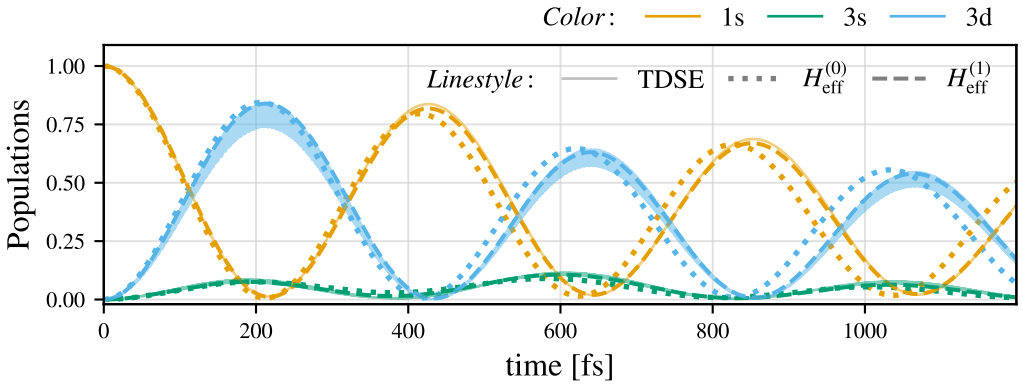

Figure 3.7: Populations of the 1s, 3s, and 3d states obtained through TDSE simulations (solid) and propagation with $H_{\mathrm{eff}}^{(0)}$ (dotted) and $H_{\mathrm{eff}}^{(1)}$ (dashed). The pulse has intensity $I_0 = 4 \times 10^{12}\,\mathrm{W \cdot cm^{-2}}$ and frequency $\omega = 6.0566\,\mathrm{eV}$ (chosen so the Stark shift is compensated for). Clearly, $H_{\mathrm{eff}}^{(0)}$ has lower fidelity than $H_{\mathrm{eff}}^{(1)}$, which coincides very well with TDSE simulations. The fast oscillations of the TDSE simulations are due to counter-rotating contributions.

The higher-order effective Hamiltonian is actually strictly required: $H_{\mathrm{eff}}^{(0)}$ predicts $\Omega_{3\mathrm{s},3\mathrm{d}}$ to change sign at around $I_0 \approx 9 \times 10^{11}\,\mathrm{W \cdot cm^{-2}}$. This sign change does not appear for $H_{\mathrm{eff}}^{(1)}$. Furthermore, $\Omega_{3\mathrm{s},3\mathrm{d}}$ is at $I_0 = 4 \times 10^{12}\,\mathrm{W \cdot cm^{-2}}$ already dominated by fourth-order perturbative contributions of $V^{(F)}$, necessitating the choice $N_{\mathrm{trunc}} = 2$. Both these properties are to some degree surprising: Firstly, one would expect $H_{\mathrm{eff}}^{(0)}$ and $H_{\mathrm{eff}}^{(1)}$ to describe the same physics and only differ in their accuracy – yet, in this case, the sign change predicted by $H_{\mathrm{eff}}^{(0)}$ entails that $\Omega_{3\mathrm{s},3\mathrm{d}}$ vanishes at a certain intensity, whereas $H_{\mathrm{eff}}^{(1)}$ predicts a non-vanishing $\Omega_{3\mathrm{s},3\mathrm{d}}$ for all intensities.

Secondly, the lowest-order perturbative contribution is usually dominant. In Appendix D, the interested reader can find an analysis based on the perturbative expansion of the level-shift operator (Section 1.4.3), in which these findings are elaborated on. For the rest of this section, all further calculations and figures will be obtained using the parameters of $H_{\text{eff}}^{(1)}$.

We can once again calculate how the parameters vary with the intensity at the two-photon resonance $\omega_0 = (\omega_{3s/d} - \omega_{1s})/2 = 6.0470\,\text{eV}$ and relate the time scales of the Rabi period and the ionisation lifetimes to each other. The results can be seen in Fig. 3.8. The ultimate limiting factor is the spontaneous lifetime of the 3d state, which is $\tau_{3d}^{(\text{spont.})} = 1.546 \times 10^{-8}\,\text{s}$ (and thus smaller than that of the 3s state, which is $\tau_{3s}^{(\text{spont.})} = 1.583 \times 10^{-7}\,\text{s}$) [185]. Since there is an obvious relaxation pathway via the 2p state, the spontaneous lifetimes are much shorter than those of the 2s state. However, we need not worry about this, since the time scales of the Rabi periods (and also the ionisation lifetimes) are much shorter. As for the 1s-2s transition, γ_{1s} is very small and scales cubically with I_0 (given that six photons are required to resonantly couple $|1s, N\rangle$ to the continuum and then couple back). The parameters γ_{3s}, γ_{3d}, $\Omega_{1s,3d}$ and $\Omega_{1s,3s}$ all scale linearly with the intensity I_0 (congruent with the perturbative picture, where the lowest-order contribution for all these parameters will be a two-photon transition). One glaring exception is $\Omega_{3s,3d}$, which in the beginning scales linearly with I_0 (i.e. the two-photon process dominates) and for intensities beyond $1 \times 10^{12}\,\text{W} \cdot \text{cm}^{-2}$ begins to scale quadratically with I_0 (i.e. the four-photon process dominates). This is also explained in Appendix D. Fascinatingly, the ionisation lifetime of the 3s state dominates all other time scales. However, since $|\Omega_{1s,3d}| > |\Omega_{1s,3s}|$, the 3s state population is always very small. Thus, given that $\tau_{3d}^{(\text{ion.})} > 2\pi/|\Omega_{1s,3d}|$ we can successfully Rabi cycle between 1s and 3d, while any population that leaks into the 3s state will lead to ionisation.

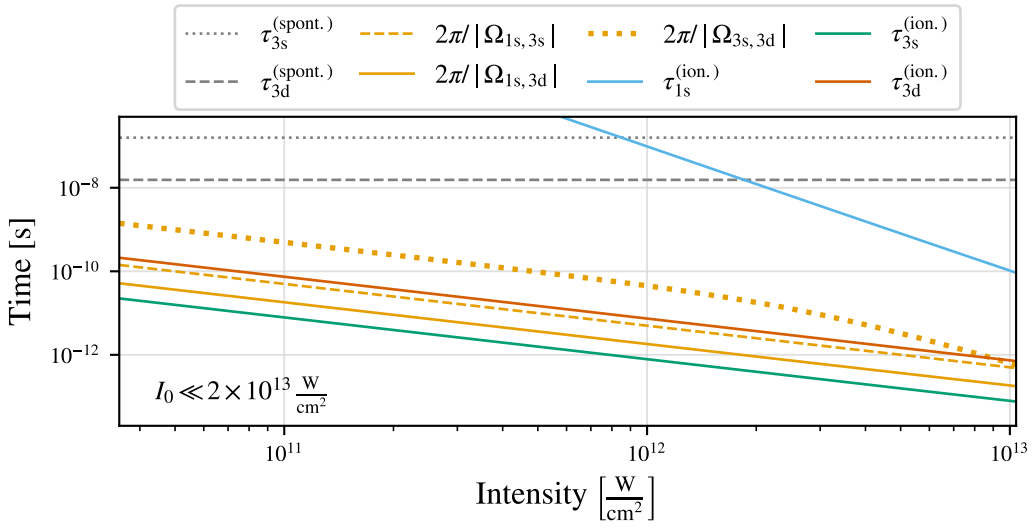

Figure 3.8: Spontaneous lifetimes $\tau_{3s}^{(\text{spont.})}$ and $\tau_{3d}^{(\text{spont.})}$, ionisation lifetimes $\tau_{1s}^{(\text{ion.})}$, $\tau_{3s}^{(\text{ion.})}$ and $\tau_{3s}^{(\text{ion.})}$, and the effective Rabi periods $2\pi/|\Omega_{1s,3s}|$, $2\pi/|\Omega_{1s,3d}|$ and $2\pi/|\Omega_{3s,3d}|$, plotted against the intensity on a log-log scale. All parameters scale as expected from lowest order perturbation theory, except $2\pi/|\Omega_{3s,3d}|$. This case is explored more deeply in Appendix D. Since $|\Omega_{1s,3d}| > |\Omega_{1s,3s}|$ and $\tau_{3d}^{(\text{ion.})} > 2\pi/|\Omega_{1s,3d}|$, we can successfully Rabi cycle between the 1s and 3d states.

Lastly, is is noteworthy that $2\pi/|\Omega_{1s,3d}| \approx 100\,\text{fs}$ for $1 \times 10^{13}\,\text{W}\cdot\text{cm}^{-2}$. For lower intensities, we quickly approach the picosecond regime. These regimes are certainly challenging for experiments. Excimer lasers based on Argon fluoride emit at 193 nm and are worth considering [186]. Furthermore, it has recently become possible to emit high-energy UV pulses through resonant dispersive-wave emission in hollow capillary fibers [187]. Thus, it may be possible with today's experimental capabilities to experimentally drive two-photon Rabi oscillations in hydrogen.

3.3.2 Bright and dark state analysis

While the time-evolution due to a 3-level effective Hamiltonian can in principle still be analysed analytically, the formulas quickly become so convoluted that little insight can be gained. Thus, a simplification is desirable. In this section, we will further approximate the 3-level effective Hamiltonian via a 2-level system by rotating the Hamiltonian into a new basis containing a *bright state* and a *dark state*. This procedure has been proven to be highly useful in STIRAP and is complementary to adiabatic elimination [42, 58, 122, 188].

The starting point is the superposition *ansatz* for the state amplitudes $b(t)$ and $c(t)$ (corresponding to the 3s and 3d states),

$$B(t) \coloneqq b(t)\sin\varphi + c(t)\cos\varphi, \tag{3.17}$$

$$D(t) \coloneqq b(t)\cos\varphi - c(t)\sin\varphi, \tag{3.18}$$

where $B(t)$ is the amplitude corresponding to the bright state $|B\rangle$ and $D(t)$ is the amplitude corresponding to the dark state $|D\rangle$. The reason for the naming convention will become clear shortly. The mixing angle φ is at this point not specified and can in principle be chosen arbitrarily. However, an intentional choice of φ will be shown to simplify the system by decoupling $|a\rangle$ from $|D\rangle$.

The new Hamiltonian in the basis $\{|a\rangle, |B\rangle, |D\rangle\}$, which we will define as $H_{\text{eff}}^{[\varphi]}$, can be obtained from the effective Hamiltonian H_{eff} in the basis $\{|a\rangle, |b\rangle, |c\rangle\}$ via the rotation matrix

$$R(\varphi) \coloneqq \begin{pmatrix} 1 & 0 & 0 \\ 0 & \sin\varphi & \cos\varphi \\ 0 & \cos\varphi & -\sin\varphi \end{pmatrix}, \tag{3.19}$$

and the associated transformation

$$H_{\text{eff}}^{[\varphi]} \coloneqq R(\varphi) H_{\text{eff}} R^T(\varphi). \tag{3.20}$$

For explicit construction of $H_{\text{eff}}^{[\varphi]}$, let us use the notation in Eq. (3.16). We obtain $H_{\text{eff}}^{[\varphi]}$ as

$$H_{\text{eff}}^{[\varphi]} = \begin{pmatrix} W_a & X_{aB} & X_{aD} \\ X_{aB} & W_B & X_{BD} \\ X_{aD} & X_{BD} & W_D \end{pmatrix},$$

where the use of some trigonometric identities reveals that

$$X_{aB} = X_{ab}\sin\varphi + X_{ac}\cos\varphi, \tag{3.21}$$

$$X_{aD} = X_{ab}\cos\varphi - X_{ac}\sin\varphi, \tag{3.22}$$

$$X_{BD} = \frac{1}{2}(W_b - W_c)\sin(2\varphi) + X_{bc}\cos(2\varphi), \tag{3.23}$$

$$W_B = W_b\sin^2\varphi + W_c\cos^2\varphi + X_{bc}\sin(2\varphi), \tag{3.24}$$

$$W_D = W_c\sin^2\varphi + W_b\cos^2\varphi - X_{bc}\sin(2\varphi). \tag{3.25}$$

Further rearrangements are possible, but not necessarily helpful. At this point, no approximations have been made. This change of basis of valid for any φ. In the following, we will motivate a choice for φ and then introduce an approximation that will decouple the dark state from the rest of the system, yielding a 2-level system with states $|a\rangle$ and $|B\rangle$, with the dark state $|D\rangle$ evolving independently.

A good choice for φ is one which makes the coupling from $|a\rangle$ to $|D\rangle$ zero, i.e. $X_{aD} = X_{ab}\cos\varphi - X_{ac}\sin\varphi = 0$. Then, the dark state only couples to the bright state through X_{BD}.[6] The appropriate choice for φ is according to Eq. (3.22) thus

$$\varphi = \arctan\left(\frac{X_{ab}}{X_{ac}}\right) = \arctan\left(\frac{\Omega_{ab} + \mathrm{i}\beta_{ab}}{\Omega_{ac} + \mathrm{i}\beta_{ac}}\right). \tag{3.26}$$

This is still exact. The central approximation that we will now make is to decouple $|B\rangle$ and $|D\rangle$. This is generally possible if $|X_{aB}| \gg |X_{BD}|$. In that case, we may approximate $X_{BD} \approx 0$ and obtain the approximated effective Hamiltonian for $\varphi = \arctan(X_{ab}/X_{ac})$ as

$$H^{[\varphi]}_{\text{eff, approx.}} = \begin{pmatrix} W_a & X_{aB} & 0 \\ X_{aB} & W_B & 0 \\ 0 & 0 & W_D \end{pmatrix}, \tag{3.27}$$

where the 2×2 submatrix $W_a\,|a\rangle\langle a| + X_{aB}(|a\rangle\langle B| + |B\rangle\langle a|) + W_B\,|B\rangle\langle B|$ describes the entire approximate 3-level dynamics under the assumption that either $a(t_0) = 1$ or $B(t_0) = 1$ is chosen as initial condition. The rotation transform yielding $H^{[\varphi]}_{\text{eff}}$ from H_{eff} is illustrated in Fig. 3.9.

Since $H^{[\varphi]}_{\text{eff, approx.}}$ is an effective 2-level system (provided that $D(t_0) = 0$ as initial condition), we can apply the analytical formulas of Section 3.2 in order to calculate $|\operatorname{Re}(W)|$ using Eq. (3.9), and the total ionisation rate $\Gamma = (\gamma_a + \gamma_B)/2$. This allows us to quantify the damping of the oscillations: We receive $|\Gamma/\operatorname{Re}(W)| = 0.0285$, confirming that the oscillation is very underdamped.

We can now compare the populations obtained through propagation with $H^{(1)}_{\text{eff}}$ with those

[6] In particular, $X_{BD} = 0$ if $X_{bc} = 0$ and if $|b\rangle$ and $|c\rangle$ are degenerate in energy, i.e. $W_b = W_c$. The former is usually the case because of selection rules. The latter is the case if the transitions $|a\rangle \leftrightarrow |b\rangle$ and $|a\rangle \leftrightarrow |c\rangle$ are perfectly resonant (i.e. $\delta_b = \delta_c = 0$). If two-color fields are employed (e.g. in STIRAP), this condition can easily be fulfilled [122, 188]. In that case, the 2-level system obtained via the rotation transform contains the exact dynamics of the entire 3-level system.

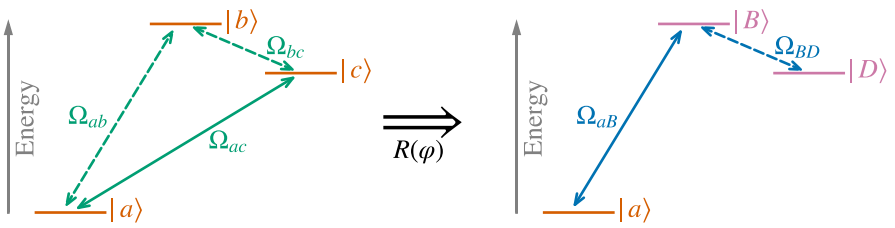

Figure 3.9: Illustration of the three-level systems defined in the basis $\{|a\rangle, |b\rangle, |c\rangle\}$ and the rotated basis $\{|a\rangle, |B\rangle, |D\rangle\}$ with the respective couplings Ω_{ij} between the levels. Weak couplings are indicated via dashed arrows. The rotation transform yields a 2-level system in the limit $\Omega_{BD} \to 0$.

obtained through $H^{[\varphi]}_{\text{eff, approx.}}$. Let us transform back $H^{[\varphi]}_{\text{eff, approx.}}$ to the basis $\{|a\rangle, |b\rangle, |c\rangle\}$ via

$$H_{\text{eff, approx.}} := R^T(\varphi) H^{[\varphi]}_{\text{eff, approx.}} R(\varphi), \tag{3.28}$$

or just via $b(t) = B(t)\sin\varphi$ and $c(t) = B(t)\cos\varphi$. Propagation with $H^{(1)}_{\text{eff}}$ and $H_{\text{eff, approx.}}$ yields Fig. 3.11. Clearly, the approximation was justified. The most obvious difference is that, through the approximation, we enforce the effective Rabi periods of 3s and 3d to be the same.

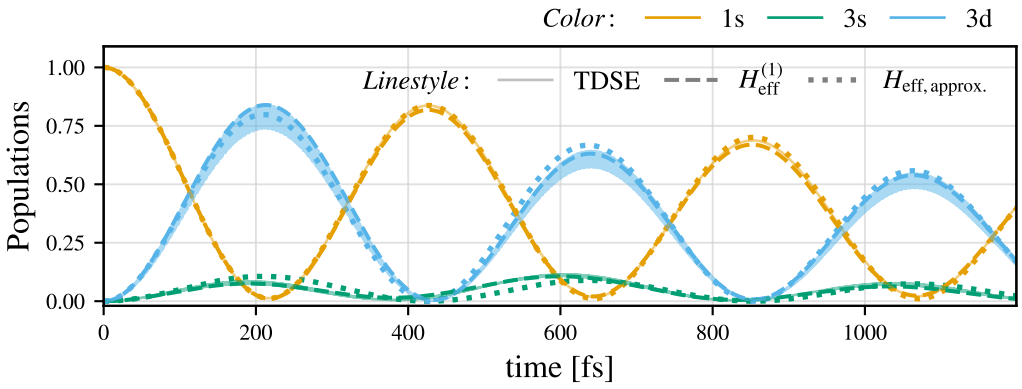

Figure 3.10: Populations of the 1s, 3s and 3d states obtained through TDSE simulations (solid) and propagation with $H^{(1)}_{\text{eff}}$ (dashed) and $H_{\text{eff, approx}}$ (dotted) defined in Eq. (3.28). The parameters are the same as in Fig. 3.7 and as such, the TDSE and $H^{(1)}_{\text{eff}}$ results are left unchanged. Newly added is the approximation $H_{\text{eff, approx}}$. With the rotation transform detailed in this chapter, $H_{\text{eff, approx}}$ is an effective 2-level Hamiltonian in the basis $\{|1s\rangle, |B\rangle\}$.

The parameter plot of Fig. 3.8 can now of course be repeated for the bright and dark state parameters. This is shown in Fig. 3.11. There are several intuitions to be gained: Firstly, $\tau_D^{(\text{ion.})} \approx \tau_{3s}^{(\text{ion.})}$, confirming that the lifetime of the dark state is dominated by the lifetime of the 3s state. Unsurprising is that $\Omega_{1s,3d} \approx \Omega_{1s,B}$; this is just the desired consequence of choosing $\varphi = \arctan(X_{ab}/X_{ac})$. Most interestingly, $2\pi/|\Omega_{1s,3s}| \approx \tau_B^{(\text{ion.})}$. The lifetime of the bright state is thus limited by how efficiently we transfer the population to the 3s state. While this was discussed conceptually in the discussion on Fig. 3.8, the bright-dark state analysis provides clear

mathematical intuition.

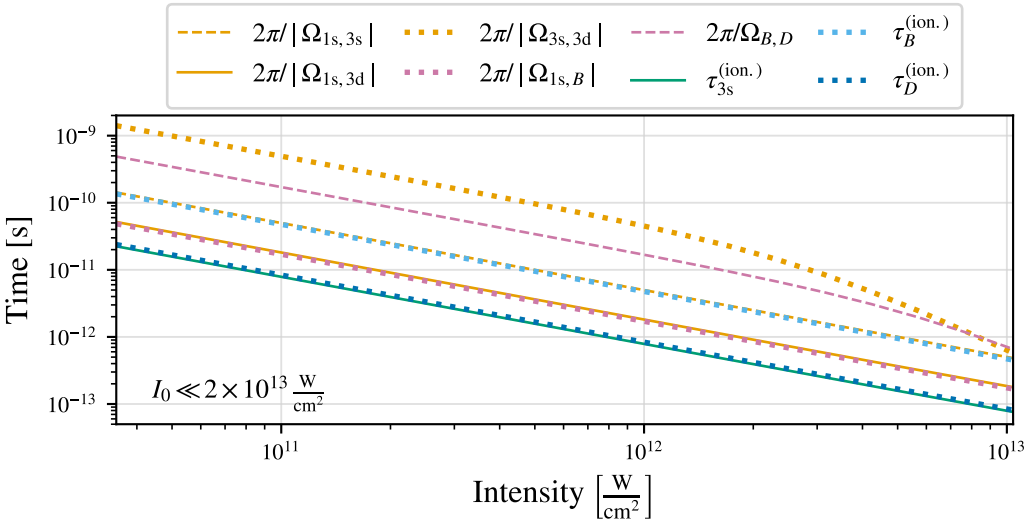

Figure 3.11: Repeat of Fig. 3.8, now additionally with the effective Rabi periods $2\pi/|\Omega_{1s,B}|$ and $2\pi/|\Omega_{B,D}|$, as well as the ionisation lifetimes $\tau_B^{(ion.)}$ and $\tau_D^{(ion.)}$ of the bright and dark states $|B\rangle$ and $|D\rangle$.

3.4 Effective parameters for multiphoton ionisation in hydrogen

Using effective Hamiltonians for the description of resonant multiphoton ionisation has a long history, starting with Beers and Armstrong [40] and being continued by, among others, Holt *et al.* [41]. In particular, Holt *et al.* diagonalized rotated Floquet Hamiltonians to obtain the effective 2-level Hamiltonians for resonant two, three, and four-photon ionisation in hydrogen, where the ground state is $|1s, N\rangle$ and the excited states are $|2p, N-1\rangle$, $|2s, N-2\rangle$ and $|3p, N-3\rangle$ respectively. Their approach, relying on complex scaling of the Floquet Hamiltonian, is very related to the one presented in this thesis. The major difference is that instead of iteratively diagonalizing the rotated Floquet Hamiltonian, the resolvent formalism with projection operator technique was used in this work to obtain the effective Hamiltonian.

In their work, Holt *et al.* print a rather large table with effective Hamiltonian parameters for different pulse frequencies ω and field strengths $\mathcal{E}_0$. For the 1s-2p case, these parameters have previously been found to be slightly inaccurate [55]. In particular – and Holt *et al.* make the reader aware of this themselves – the ground state ionisation rate γ_a and the complex interference term β both suffer from numerical convergence issues in their approach. For this reason, they omit many β and γ_a parameters, and the ones not omitted are unreliable. Additionally (this, they do not note), many of their parameters scale uncomfortably unpredictably with ω (for fixed $\mathcal{E}_0$), whereas one should expect either a slow monotonous increase or decrease with ω.

For this reason, firstly as an update and supplement to their table, and secondly as a suitable demonstration for the broad applicability of the model system presented in this thesis, the reader will find in Appendix E all the parameter sets of Holt compared with values calculated using the

first-order effective Hamiltonian $H_{\text{eff}}^{(1)}$, Eq. (2.10). The defining parameters of the model system, as discussed in Section 3.1, are the truncation number N_{trunc} and the maximum number of states $n_{\max}$ per angular momentum channel that is included. For all these calculations, $N_{\text{trunc}} = 2$ and $n_{\max} = 180$ were chosen. It has to be noted that the choice of $n_{\max}$ is very dependent on the size of the grid on which the wavefunctions are set-up. Also, there is a certain sensitivity of the parameters concerning the complex scaling angle θ. For the following calculations, $\theta = 20°$ was used.

The dimensions of the rotated Floquet Hamiltonians in their truncated and discretised form were

- 2142×2142 for two-photon ionisation, $1s \to 2p \to \epsilon s/d$
- 1969×1969 for three-photon ionisation, $1s \to\to 2s \to \epsilon p$
- 2679×2679 for four-photon ionisation, $1s \to\to\to 3p \to \epsilon s/d$.

This may be compared to Holt *et al.*, who used 400×400 rotated Floquet Hamiltonians. The whole calculation in Python with double precision (`complex128`) took less than 5 min for all parameters on an Intel® Core™ i7-6600U CPU @ 2.60GHz × 4, demonstrating the speed and efficiency of the model system.

Going through the parameters in Appendix E, it is clear that in most cases, they agree well with those of Holt *et al.* The most drastic difference can be found for the small imaginary γ_a and β parameters, which for Holt *et al.* are unreliable and do not scale monotonously with ω, whereas the parameters predicted via $H_{\text{eff}}^{(1)}$ display the expected behaviour. Furthermore, Holt *et al.* were not able to calculate many of the γ_a and β parameters for three- and four-photon ionisation since their numerical scheme did not properly converge on the eigenvalues. This is not an issue for the effective Hamiltonian formalism; there are no convergence issues to be expected for matrix multiplication, and if QHQ is found to be ill-conditioned, its inversion can be avoided by treating $[QHQ]^{-1}VP =: X$ as a set of column-wise linear equations $[QHQ]X = QVP$ and solving for X.[7]

One noteworthy observation is that for four-photon resonant ionisation via the 3p state, $H_{\text{eff}}^{(1)}$ predicts negative coupling constants Ω and negative β parameters, while Holt *et al.* predict both positive coupling constants and positive β parameters. Since the equations for the time evolution only contain the product $\Omega \cdot \beta$, only the sign of $\Omega \cdot \beta$ matters. Due to this, the model systems still yield equivalent results, given that the product is always positive. It is however unclear where the discrepancy originates; it did not appear for the other systems.

[7] In Python, this can be achieved using e.g. `scipy.linalg.solve`. If necessary, more sophisticated solvers can be employed.

Summary, conclusion, and outlook

Higher-order adiabatic elimination in the resolvent formalism

In Chapter 2, a theory for higher-order adiabatic elimination within the resolvent formalism was laid out. The procedure expands the level-shift operator in terms of the energy and has previously been presented by e.g. Faisal with only minor differences [33]. The new contribution to the field is three-fold.

1. It was shown in Sections 2.1 how the expansion of the level-shift operator is the energy domain analogon to the Markov approximation employed by Paulisch *et al.* in the time domain [60]. These fascinating connections have not yet been discussed in the literature.
2. A novel approach to obtain second-order effective Hamiltonians was proposed in Section 2.2. This method is based on the realisation that the expansion of the level-shift operator will yield a matrix polynomial, which can be factorized through its solvents. This renders the resolvent operator in a form accessible to a block partial-fraction expansion. One of the solvents corresponds to a higher-order effective Hamiltonian. In the thesis, we considered a special case in which the coefficients of the matrix polynomial commute. In this case, the second-order effective Hamiltonian can be calculated analytically.
3. It was shown that the block partial-fraction expansion immediately yields the normalisation of the time-evolution operator and thus provides information on how much population resides in the non-essential subspace. This information is to my knowledge not obtainable with previous methods.

There are now several avenues to pursue. Most importantly, in the thesis, only the commuting case was discussed. The more general non-commuting case is therefore the next logical step, and work has already progressed to that end. The crucial step is to obtain the solvents of the matrix polynomial. The most promising option is to obtain those numerically. With a reliable numeric procedure, third and higher-order effective Hamiltonians can be tackled, although it seems questionable to me if it will be worth the effort. A more interesting path may be to generalize the method for complex-symmetric Hamiltonians, i.e. Hamiltonians which describe decay processes. Since the block partial-fraction expansion does not depend on the Hermiticity, it should be straight-forward. These questions may be addressed in future publications.

Two-photon Rabi oscillations in hydrogen

In Chapter 3, two-photon transitions in hydrogen were studied using effective Hamiltonians. As described in Section 3.1, the effective Hamiltonians were obtained by constructing a rotated

Floquet Hamiltonian as a matrix from atomic and pulse parameters and employing the effective Hamiltonian formalism. It was shown that for pulse regimes where the formalism is applicable, the effective Hamiltonians obtained are capable and powerful tools to model and interpret the light-atom dynamics.

Both the 1s-2s and 1s-3s/d two-photon transitions can be described via effective Hamiltonians. The 1s-2s system was shown in Section 3.2 to never Rabi cycle, given that the ionisation lifetime is always smaller than the effective Rabi period for any intensity. This agrees with previous studies [56]. Analytical investigations showed the excited state population to be the sum of a $\sin^2$ and a $\sinh^2$ term, multiplied by an exponential that decays with the mean ionisation rate. The sine contribution allowed us to quantify the dampening of the Rabi periods.

In Section 3.3, it was shown that two-photon Rabi oscillations can be driven between 1s and 3s/d in hydrogen. On the one side, this is intuitive, since the 2p state is now a reasonable intermediate state, whereas the 1s-2s system had no such contributions. On the other side, it is not self-evident that the oscillations are possible. In fact, the limiting factor of the system is the lifetime of the 3s state, which is smaller than all other lifetimes and effective Rabi periods. However, since the 1s state couples much more strongly to the 3d than the 3s state (the coupling from 3s to 3d is even smaller), the 3s state is much less likely to be reached. Thus, Rabi cycling occurs primarily between 1s and 3d, and any population that arrives in the 3s state is ionised directly. One interesting aspect to note is that a proper description of the system is only achieved with the first-order effective Hamiltonian, since the zeroth-order effective Hamiltonian wrongly predicts a sign change of $\Omega_{3s,3d}$ to occur at $I_0 \simeq 9 \times 10^{11}\,\mathrm{W \cdot cm^{-2}}$ (see Appendix D for details).

The 1s-3s/d system is naturally more complicated than the 1s-2s system, given that three essential states are involved. The complexity can however be reduced through a bright-dark state analysis. In the new basis, consisting of the 1s state, a bright state $|B\rangle$ and a dark state $|D\rangle$, the dark state does not couple to the 1s state, and the coupling between $|B\rangle$ and $|D\rangle$ is negligible. Thus, an approximate effective 2-level system can be obtained. This approximation was shown to yield excellent results. Furthermore, there are physical intuitions to be gained from the rotation: The lifetime of the bright state is approximately equal to the Rabi period $2\pi/|\Omega_{1s,3s}|$, which poignantly demonstrates how the transition to the 3s is the dominant cause for ionisation.

Lastly, in Section 3.4, the model system was used to update tables for effective Hamiltonian parameters describing N-photon resonant multiphoton ionisation in hydrogen. These parameters were obtained by Holt *et al.* in 1983 using a much smaller Floquet basis and employing a different approach to obtain an effective Hamiltonian [41]. Their approach suffered from convergence issues for the small imaginary parameters and it is especially these parameters that are much improved by the effective Hamiltonians calculated in this thesis.

Several avenues are open for exploration. Firstly, this thesis has only been interested in the population dynamics. Any photoelectrons were just modeled as a decrease in the norm. However, there is much physics to be learned from the photoelectrons and their energy distribution. Fortunately, if the effective Hamiltonian is known, it is straightforward to obtain the photoelectron spectrum [55].

Secondly, using the SVEA, it should be possible to describe pulse envelopes with the effective

Hamiltonian formalism. Some first tests that I have done seem to confirm this expectation. One might even try to incorporate non-adiabatic corrections containing derivatives of the pulse envelope [33] – pulse shapes such as super-Gaussians may lead to scenarios where corrections upon the SVEA become important in experimental conditions. Envelopes will also open the door to describing STIRAP processes with the effective Hamiltonian formalism, such as Stark-chirped rapid adiabatic passage [32, 189, 190]. In the same vein, including time-dependent phases (i.e. chirped pulses) may be worthwhile [191].

Lastly, through many-mode Floquet theory [34, 51, 103–106], one can obtain time-independent Hamiltonians which describe the interaction of quantum systems with N-color pulses. I have written a code capable of describing two-color $(N + M)$-photon transitions in atoms via the effective Hamiltonian formalism. For multiphoton transitions, many-mode Floquet theory – already for two frequencies – starts to cause issues rather quickly. The central problem is that the Floquet state basis necessary for a sufficient description grows tremendously in size the more modes of the field are included. Furthermore, since there are so many more states accessible, it will come as no surprise that the validity limits of the models are reached at rather low intensities (i.e. the $\mathcal{Q}$-space spectrum overlaps with the model space spectrum). However, there are certain scenarios where I envision that a two-color model system can be successful. Most promising may be the description of pump-probe experiments, especially XUV-XUV, which is regarded as one of the foremost goals of attosecond science [192, 193]. By combining the SVEA (i.e. the ability to model pulse envelopes) with an effective Hamiltonian-based model system capable of describing two-color transitions, it may be possible to elegantly simulate very general pump-probe experiments, crucially including those where the pump and probe pulses overlap significantly, through a minimal-states approach.

We plan to publish the results on the prediction of two-photon Rabi oscillations in hydrogen, and may pursue the aforementioned avenues in future work.

Appendices

A Fast oscillations in three-level system

For the populations of the three-level system, Fig. 1.2b), it was stated that the high-frequency modulations are due to the non-adiabatic pulse turn-on. As a proof of this statement, consider a super-Gaussian pulse, defined by the envelope of the electric field $\mathcal{E}(t)$:

$$g_P(t) = \exp\left[-\ln(2)\cdot\left(\frac{2t}{W}\right)^{2P}\right], \tag{A.1}$$

where W is the FWHM of $g_P(t)$ and P the order of the super-Gaussian. For $P = 1$, the super-Gaussian is just a regular Gaussian while in the limit $P \to \infty$, the super-Gaussian becomes a flat-top pulse. Choosing $P = 10$ and repeating the calculation for Fig. 1.2b) within the SVEA (i.e. the two-photon couplings and Stark shifts are weighted with $[g_{10}(t;W)]^2$), we obtain the populations shown in Fig. A.1. Clearly, the fast oscillations are quenched by the super-Gaussian.

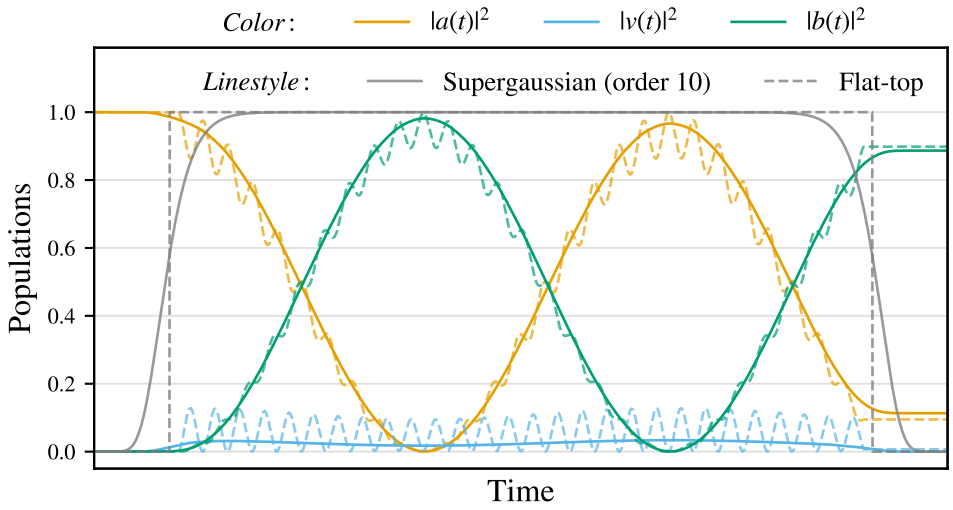

Figure A.1: Two-photon Rabi oscillations in the three-level system employed in Fig. 1.2b) for a flat-top and super-Gaussian pulse envelope. The fast oscillations vanish for the super-Gaussian.

As a mathematical argument, one might integrate the equation for the virtual state $v(t)$ to obtain an approximation and compare the results for a flat-top pulse (i.e. one which starts abruptly at some t_0, rendering the integral for $t < t_0$ zero) and a smooth pulse with zero envelope at $t \to -\infty$ and a slow increase. The flat-top pulse introduces additional oscillatory terms. A related scenario is discussed in Shore's *The Theory of Coherent Atomic Excitation* (Ch. 4) [57].

B Which solvent is essential?

In Section 2.2, it was found that one can block partial-fraction expand the resolvent operator through its solvents. For the second-order expansion of the level-shift operarator with commuting coefficients, $[D_0, D_1] = 0$, there exist two solvents that can be calculated through the quadratic formula:

$$X_\pm = -\frac{1}{2}D_1 \pm \left(\frac{1}{4}D_1^2 - D_0\right)^{1/2}. \tag{B.1}$$

As exemplified for a four-level ladder system, $X_+ \equiv H_{\text{eff}}^{(2)}$ while X_- is responsible for fast modulations. However, a mathematical argument was lacking why X_+ and not X_- should be the effective Hamiltonian. For this argument, let us expand the square root inside $X_\pm$ for small variations around D_0 (remember that $D_0 = -C_2^{-1}H_{\text{eff}}^{(0)}$). This amounts to claiming that the second-order correction is small. In this case,

$$\begin{aligned}
X_\pm &= -\frac{1}{2}D_1 \pm \left(\frac{1}{4}D_1^2 - D_0\right)^{1/2} && \text{(B.2)}\\
&\approx -\frac{1}{2}D_1 \pm \left[\left(\frac{1}{4}D_1^2\right)^{1/2} - \frac{1}{2}\left(\frac{1}{4}D_1^2\right)^{-1/2} D_0\right] && \text{(B.3)}\\
&= -\frac{1}{2}(D_1 \mp D_1) \mp D_1^{-1}D_0 && \text{(B.4)}\\
&= -\frac{1}{2}(D_1 \mp D_1) \mp C_1^{-1}C_0 && \text{(B.5)}
\end{aligned}$$

From this, it is clear that

$$\begin{aligned}
X_+ &\approx -C_1^{-1}C_0 = \left(\mathbb{1}_P + PV[QHQ]^{-2}VP\right)^{-1} H_{\text{eff}}^{(0)} \equiv H_{\text{eff}}^{(1)} && \text{(B.6)}\\
X_- &\approx -D_1 + C_1^{-1}C_0 = -C_2^{-1}C_1 - H_{\text{eff}}^{(1)} && \text{(B.7)}
\end{aligned}$$

and thus, X_+ is the effective Hamiltonian.

C Divergence of populations in non-Hermitian effective 2-level systems

As shown in Section 3.2, the excited state population of the decaying 2-level system can be calculated as

$$|b(t)|^2 = \left|\frac{\Omega}{W}\right|^2 \mathrm{e}^{-\Gamma t}\left[\sinh^2\left(\frac{1}{2}\operatorname{Im}(W)t\right) + \sin^2\left(\frac{1}{2}\operatorname{Re}(W)t\right)\right]. \tag{C.1}$$

In Section 3.2, the dampened oscillation term was discussed. Let us here study the second contribution to Eq. (3.8):

$$f(t) \coloneqq \mathrm{e}^{-\Gamma t}\sinh^2\left(\frac{1}{2}\operatorname{Im}(W)t\right). \tag{C.2}$$

This function has three regimes:

$$\Gamma > |\operatorname{Im}(W)|, \quad \Rightarrow \quad f(t) \to 0,\ t \to \infty, \tag{C.3}$$

$$\Gamma = |\operatorname{Im}(W)|, \quad \Rightarrow \quad f(t) \to \frac{1}{4},\ t \to \infty, \tag{C.4}$$

$$\Gamma < |\operatorname{Im}(W)|, \quad \Rightarrow \quad f(t) \to \infty,\ t \to \infty. \tag{C.5}$$

The rather surprising conclusion from this is that, according to Eq. (C.5), there is the opportunity for 2-level effective Hamiltonians to yield diverging populations. In the following, it will be discussed how the parameters of the zeroth-order effective Hamiltonian $H_{\text{eff}}^{(0)}$ – but not $H_{\text{eff}}^{(1)}$ – seem to be constrained so that $\Gamma \geq |\operatorname{Im}(W)|$ for all systems.

First of all, note that for the perturbatively expanded zeroth-order effective Hamiltonian

$$H_{\text{eff}}^{(0)} = PHP - PV\frac{Q}{H_0}VP + PV\frac{Q}{H_0}V\frac{Q}{H_0}VP. \tag{C.6}$$

it has previously been shown that $\beta = \pm\sqrt{\gamma_a\gamma_b}$, i.e. that β is the geometric mean of the ionisation rates [40, 41, 55]. While I have not endeavoured to formulate a mathematical proof, numerical experiments lead me to the conclusion that this is still the case for the non-perturbative zeroth-order effective Hamiltonian

$$H_{\text{eff}}^{(0)} = PHP - PV\frac{1}{QHQ}VP. \tag{C.7}$$

Still, even when taking $\beta = \pm\sqrt{\gamma_a\gamma_b}$ for granted, it is not obvious that this leads to $\Gamma \geq |\operatorname{Im}(W)|$ for all $\gamma_a, \gamma_b > 0$ and all Ω and ΔS, given how complicated the dependence of $|\operatorname{Im}(W)|$ with respect to its parameters are. I have not yet tried to prove this. I can only offer plausability

arguments based on numerical experiments: We can study $|\mathrm{Im}(W)|$ for fixed ΔS and Ω against varying γ_a/γ_b under the assumption $\beta = \sqrt{\gamma_a\gamma_b}$. This is done for two exemplary ΔS and Ω values in Fig. C.1. There, we see the behaviour that for $\gamma_a/\gamma_b \to \infty$ and for $\gamma_a/\gamma_b \to 0$, $|\mathrm{Im}(W)|$ asymptotically approaches Γ. Empirically, it seems that the condition $|\mathrm{Im}(W)| < \Gamma$ is fulfilled for all ΔS and Ω if $\beta = \pm\sqrt{\gamma_a\gamma_b}$.

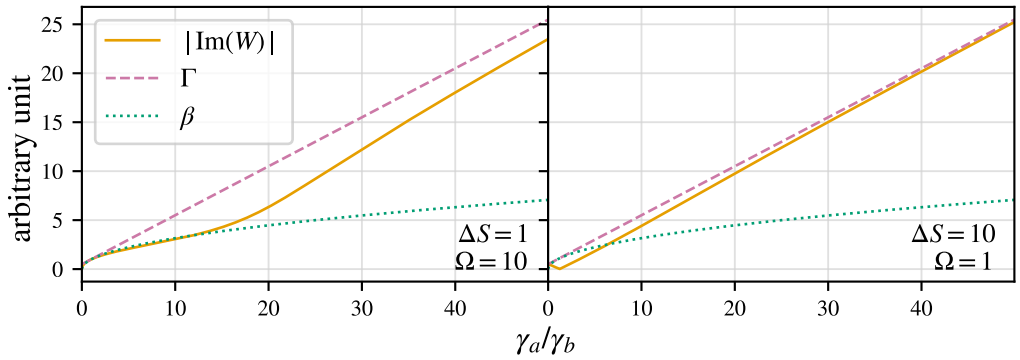

Figure C.1: Comparison of $|\mathrm{Im}(W)|$ from Eq. (3.10), $\Gamma = \gamma_a + \gamma_b$ and $\beta = \sqrt{\gamma_a\gamma_b}$ against varying γ_a/γ_b for fixed ΔS and Ω. As long as $|\mathrm{Im}(W)| < \Gamma$, the populations defined in Eq. (3.8) will not diverge. Numerical epxeriments indicate that the relation indeed holds for all ΔS and Ω.

The reason why this is relevant for this work is that for the first-order effective Hamiltonian $H_{\mathrm{eff}}^{(1)}$ defined by Eq. (2.9), $\beta \neq \pm\sqrt{\gamma_a\gamma_b}$ (as is easily checked numerically for the 1s-2s system). Due to this, $H_{\mathrm{eff}}^{(1)}$ may yield parameters that lead to $\Gamma < |\mathrm{Im}(W)|$ and thus to diverging populations in Eq. (3.8). This seems to occur particularly when a model system approaches the limits of validity (concerning the condition defined in Eq. (3.4)). In principle, since the appearance of the diverging populations coincides with the predicted failure point of the model system, this is not a pressing issue. However, if one wishes to always predict non-divergent populations, one might want to consider a compromise between $H_{\mathrm{eff}}^{(0)}$ and $H_{\mathrm{eff}}^{(1)}$, say an effective Hamiltonian $H_{\mathrm{eff}}^{(0.5)}$, which we define via

$$H_{\mathrm{eff}}^{(0.5)} = (\mathbb{1}_P + \mathrm{Re}(C))^{-1/2}\, H_{\mathrm{eff}}^{(0)}\, (\mathbb{1}_P + \mathrm{Re}(C))^{-1/2}\,, \tag{C.8}$$

where

$$C \coloneqq PV[QHQ]^{-2}VP. \tag{C.9}$$

This higher-order effective Hamiltonian provides corrections to the zeroth-order effective Hamiltonian and at the same time yields parameters constrained so that $\Gamma > |\mathrm{Im}(W)|$.

D Necessity of higher-order effective Hamiltonians for the 1s-3s/d system

For the 3-level system consisting of the $|1\mathrm{s}, N\rangle$, $|3\mathrm{s}, N-2\rangle$ and $|3\mathrm{d}, N-2\rangle$ states, it turns out that the zeroth-order effective Hamiltonian $H_{\mathrm{eff}}^{(0)}$ is not sufficient to describe the dynamics since the effective coupling between 3s and 3d, $\Omega_{3\mathrm{s},3\mathrm{d}}$, is for intensities beyond $I_0 > 3 \times 10^{11}\,\mathrm{W \cdot cm^{-2}}$ dominated by higher-order corrections of the pole approximation. Crucially, this leads to $H_{\mathrm{eff}}^{(0)}$ predicting a sign change of $\Omega_{3\mathrm{s},3\mathrm{d}}$ around $I_0 \approx 9 \times 10^{11}\,\mathrm{W \cdot cm^{-2}}$, whereas the first-order effective Hamiltonian $H_{\mathrm{eff}}^{(1)}$ does not predict such a sign change.

The clearest way to disentangle the different contributions is to calculate $\Omega_{3\mathrm{s},3\mathrm{d}}$ first for $H_{\mathrm{eff}}^{(0)}$ and $H_{\mathrm{eff}}^{(1)}$ (which differ in the expansion in the energy) and then for their second- and fourth-order perturbative approximations, $H_{\mathrm{eff,p2}}^{(0)}$, $H_{\mathrm{eff,p4}}^{(0)}$, $H_{\mathrm{eff,p2}}^{(1)}$ and $H_{\mathrm{eff,p4}}^{(1)}$ (which are further expanded in the interaction V). Remember that $H_{\mathrm{eff}}^{(0)}$ and $H_{\mathrm{eff}}^{(1)}$ are given by

$$H_{\mathrm{eff}}^{(0)} = PHP - PV\frac{1}{QHQ}VP, \tag{D.1}$$

$$H_{\mathrm{eff}}^{(1)} = \left(\mathbb{1}_P + PV[QHQ]^{-2}VP\right)^{-1/2} H_{\mathrm{eff}}^{(0)} \left(\mathbb{1}_P + PV[QHQ]^{-2}VP\right)^{-1/2}. \tag{D.2}$$

To obtain the perturbative approximations for $H_{\mathrm{eff,p2}}^{(0)}$, $H_{\mathrm{eff,p4}}^{(0)}$, $H_{\mathrm{eff,p2}}^{(1)}$ and $H_{\mathrm{eff,p4}}^{(1)}$, we expand the level-shift operator $PR(z)P$ in powers of the interaction V, as shown in Section 1.4.3. Since $PVP = 0$ and all odd orders vanish in our system, the expansion reads up to fourth order:

$$PR(z)P \approx \underbrace{PV\frac{Q}{z-H_0}VP}_{\text{2nd order}} + \underbrace{PV\frac{Q}{z-H_0}V\frac{Q}{z-H_0}V\frac{Q}{z-H_0}VP}_{\text{4th order}}. \tag{D.3}$$

For the perturbative zeroth-order effective Hamiltonians, we apply the pole approximation, $PR(z)P \approx PR(0)P$ and via $H_{\mathrm{eff}}^{(0)} \equiv PH_0P + PR(0)P$ obtain the usual [55]

$$H_{\mathrm{eff,p2}}^{(0)} = PH_0P - PV\frac{Q}{H_0}VP, \tag{D.4}$$

$$H_{\mathrm{eff,p4}}^{(0)} = PH_0P - PV\frac{Q}{H_0}VP - PV\frac{Q}{H_0}V\frac{Q}{H_0}V\frac{Q}{H_0}VP. \tag{D.5}$$

For the perturbative first-order effective Hamiltonians, we expand in linear orders of z and thus get formally z-dependent effective Hamiltonians:

$$H_{\mathrm{eff,p2}}^{(1)}(z) = H_{\mathrm{eff,p2}}^{(0)} - zPV\frac{Q}{H_0^2}VP \equiv H_{\mathrm{eff,p2}}^{(0)} - z \cdot C_2, \tag{D.6}$$

$$H^{(1)}_{\mathrm{eff,p4}}(z) = H^{(0)}_{\mathrm{eff,p4}} - z \cdot C_4, \tag{D.7}$$

with

$$C_4 \coloneqq \left[C_2 + PV\frac{Q}{H_0^2}V\frac{Q}{H_0}V\frac{Q}{H_0}VP + PV\frac{Q}{H_0}V\frac{Q}{H_0^2}V\frac{Q}{H_0}VP + PV\frac{Q}{H_0}V\frac{Q}{H_0}V\frac{Q}{H_0^2}VP\right]. \tag{D.8}$$

The most simple (and thus for this analysis arguably the best) way to eliminate the z-dependence is to replace $z \to H^{(0)}_{\mathrm{eff}}$. This is the approach explained in Section 2.2, particularly Eq. (2.27). One thing to consider is that $[H^{(0)}_{\mathrm{eff}}, C_{2/4}] \neq 0$. Thus, using e.g. $H^{(1)}_{\mathrm{eff,p2}} = H^{(0)}_{\mathrm{eff,p2}} - H^{(0)}_{\mathrm{eff,p2}}C_2$ does not yield a complex-symmetric effective Hamiltonian. The most simple "fix" is to employ a symmetric splitting (see e.g. Ref. [64]), yielding

$$H^{(1)}_{\mathrm{eff,p2}} = H^{(0)}_{\mathrm{eff,p2}} - \frac{1}{2}\left[H^{(0)}_{\mathrm{eff,p2}}C_2 + C_2H^{(0)}_{\mathrm{eff,p2}}\right], \tag{D.9}$$

$$H^{(1)}_{\mathrm{eff,p4}} = H^{(0)}_{\mathrm{eff,p4}} - \frac{1}{2}\left[H^{(0)}_{\mathrm{eff,p4}}C_4 + C_4H^{(0)}_{\mathrm{eff,p4}}\right], \tag{D.10}$$

as the, now complex-symmetric, perturbative first-order effective Hamiltonians. With these preliminaries out of the way, we can calculate $\Omega_{3s,3d}$ for all these six effective Hamiltonians for varying intensity around $I_0 \approx 1 \times 10^{12}\,\mathrm{W \cdot cm^{-2}}$. The results of this calculation are shown in Fig. D.1.

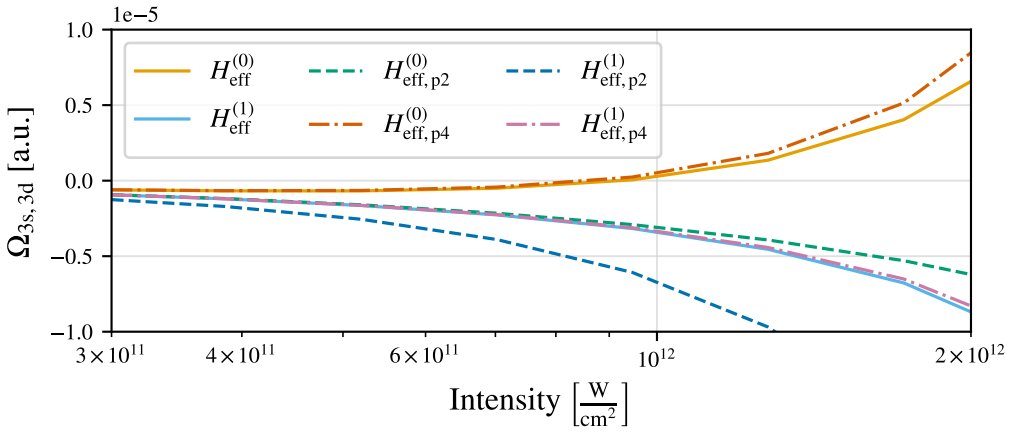

Figure D.1: $\Omega_{3s,3d}$ calculated parametrically for different intensities for the different effective Hamiltonians $H^{(0)}_{\mathrm{eff}}$, $H^{(1)}_{\mathrm{eff}}$, $H^{(0)}_{\mathrm{eff,p2}}$, $H^{(0)}_{\mathrm{eff,p4}}$, $H^{(1)}_{\mathrm{eff,p2}}$ and $H^{(1)}_{\mathrm{eff,p4}}$ defined by Equations (D.1), (D.2), (D.4), (D.5), (D.9) and (D.10) respectively. $H^{(0)}_{\mathrm{eff}}$ predicts a sign change due to the fourth-order perturbative contributions. However, if the slope of the level-shift operator is taken into account by expanding around z, the fourth-order perturbative contributions of $H^{(1)}_{\mathrm{eff,p4}}$ (negative) dominate the fourth-order perturbative contributions of $H^{(0)}_{\mathrm{eff,p4}}$ (positive). Therefore $H^{(1)}_{\mathrm{eff}}$ does not predict the sign change and it is hence required for a proper description of the coupling $\Omega_{3s,3d}$.

In the figure, we see that $H^{(0)}_{\mathrm{eff}}$ and $H^{(1)}_{\mathrm{eff}}$ predict different signs for $\Omega_{3s,3d}$. Both $H^{(0)}_{\mathrm{eff}}$ and $H^{(1)}_{\mathrm{eff}}$ are well-described by their fourth-order perturbative approximations $H^{(0)}_{\mathrm{eff,p4}}$ and $H^{(1)}_{\mathrm{eff,p4}}$, respectively. The second-order perturbative approximations are insufficient at these intensities.

This is unexpected, given that the second-order contribution is the lowest significant contribution and is usually dominant. In this case, the second-order contribution is however rather weak since there are two reasonably resonant contributions that make up most of the effective coupling (these are the contributions that the RWA would retain) and which contribute with opposite signs, i.e. they interfere destructively:

$$|3\mathrm{s}, N-2\rangle \overset{\text{Emission}}{\longrightarrow} |2\mathrm{p}, N-1\rangle \overset{\text{Absorption}}{\longrightarrow} |3\mathrm{d}, N-2\rangle$$
$$|3\mathrm{s}, N-2\rangle \overset{\text{Absorption}}{\longrightarrow} |(n\geq 3)\mathrm{p}, N-3\rangle \overset{\text{Emission}}{\longrightarrow} |3\mathrm{d}, N-2\rangle$$

For this reason, the fourth-order contributions become important already at intensities of $I_0 > 3{\times}10^{11}\,\mathrm{W{\cdot}cm^{-2}}$. And since the fourth-order contribution of $H_{\mathrm{eff}}^{(1)}$ has the opposite sign (negative) as the fourth-order contributions of $H_{\mathrm{eff}}^{(0)}$ (positive), $H_{\mathrm{eff}}^{(1)}$ is required to properly model the coupling $\Omega_{3\mathrm{s},3\mathrm{d}}$. Furthermore, due to the significant fourth-order contributions, $N_{\mathrm{trunc}} = 2$ is required.

E Tables with effective Hamiltonian parameters for resonant multiphoton ionisation in hydrogen

Table E.1: Two-level effective Hamiltonian parameters in atomic units for two-, three-, and four-photon ionisation of the hydrogen ground state for different parameter sets of the pulse frequency ω and field strength $\mathcal{E}_0$. Δ is the detuning (with Stark shifts), Ω the effective Rabi frequency, β the imaginary Rabi frequency, γ_a and γ_b the ionisation rates of the ground state $|a\rangle$ and excited state $|b\rangle$ respectively, and S_a and S_b the Stark shifts of the ground and excited state respectively. The rows are shaded alternatingly in white (Holt's parameters) and light grey (parameters obtained via $H_{\text{eff}}^{(1)}$). Note the abbreviation $x(-n) \equiv x \cdot 10^{-n}$.

ω	Δ	Ω	β	γ_a	γ_b	S_a	S_b
Two-photon ionisation							
$\mathcal{E}_0 = 0.001$							
0.35000	−2.500(−2)	7.450(−4)	3.1(−9)	7.4(−11)	3.53(−7)	−9.33(−7)	3.36(−6)
	−2.500(−2)	7.449(−4)	4.4(−9)	4.1(−11)	3.25(−7)	−9.35(−7)	3.28(−6)
0.36000	−1.500(−2)	7.449(−4)	2.7(−9)	7.6(−11)	3.12(−7)	−9.79(−7)	3.18(−6)
	−1.500(−2)	7.449(−4)	3.7(−9)	3.7(−11)	3.05(−7)	−9.82(−7)	3.15(−6)
0.37000	−5.004(−3)	7.449(−4)	2.5(−9)	1.3(−10)	2.77(−7)	−1.04(−6)	3.01(−6)
	−5.004(−3)	7.449(−4)	3.1(−9)	3.3(−11)	2.76(−7)	−1.04(−6)	3.00(−6)
0.37500	−3.982(−6)	7.449(−4)	2.9(−9)	6.0(−10)	2.61(−7)	−1.07(−6)	2.92(−6)
	−3.999(−6)	7.449(−4)	2.9(−9)	3.1(−11)	2.61(−7)	−1.07(−6)	2.92(−6)
0.38000	4.996(−3)	7.449(−4)	3.2(−9)	1.0(−10)	2.46(−7)	−1.11(−6)	2.84(−6)
	4.996(−3)	7.449(−4)	2.7(−9)	3.0(−11)	2.46(−7)	−1.11(−6)	2.85(−6)
0.39000	1.500(−2)	7.449(−4)	2.8(−9)	4.5(−11)	2.20(−7)	−1.21(−6)	2.70(−6)
	1.500(−2)	7.449(−4)	2.3(−9)	2.7(−11)	2.17(−7)	−1.21(−6)	2.69(−6)
0.40000	2.500(−2)	7.449(−4)	2.4(−9)	3.3(−11)	1.97(−7)	−1.25(−6)	2.57(−6)
	2.500(−2)	7.449(−4)	2.0(−9)	2.5(−11)	1.90(−7)	−1.34(−6)	2.55(−6)
$\mathcal{E}_0 = 0.005$							
0.35000	−2.511(−2)	3.727(−3)	3.9(−7)	4.6(−8)	8.80(−6)	−2.91(−5)	8.38(−5)
	−2.511(−2)	3.723(−3)	5.5(−7)	2.6(−8)	8.10(−6)	−2.33(−5)	8.20(−5)
0.36000	−1.510(−2)	3.726(−3)	3.5(−7)	4.8(−8)	7.77(−6)	−2.42(−5)	7.91(−5)
	−1.510(−2)	3.723(−3)	4.6(−7)	2.3(−8)	7.61(−6)	−2.45(−5)	7.88(−5)

Continued on next page

Table E.1: Continued from previous page

ω	Δ	Ω	β	γ_a	γ_b	S_a	S_b
0.37000	−5.099(−3)	3.725(−3)	3.2(−7)	6.8(−8)	6.87(−6)	−2.51(−5)	7.43(−5)
	−5.101(−3)	3.723(−3)	3.9(−7)	2.1(−8)	6.90(−6)	−2.60(−5)	7.50(−5)
0.37500	−9.711(−5)	3.723(−3)	3.6(−7)	9.1(−8)	6.45(−6)	−2.54(−5)	7.17(−5)
	−9.990(−5)	3.723(−3)	3.6(−7)	2.0(−8)	6.52(−6)	−2.68(−5)	7.31(−5)
0.38000	4.903(−3)	3.721(−3)	3.9(−7)	5.7(−8)	6.12(−6)	−2.70(−5)	7.03(−5)
	4.901(−3)	3.723(−3)	3.4(−7)	1.9(−8)	6.14(−6)	−2.78(−5)	7.11(−5)
0.39000	1.490(−2)	3.720(−3)	3.4(−7)	2.9(−8)	5.48(−6)	−2.99(−5)	6.72(−5)
	1.490(−2)	3.723(−3)	2.9(−7)	1.7(−8)	5.41(−6)	−3.02(−5)	6.73(−5)
0.40000	2.490(−2)	3.720(−3)	3.0(−7)	2.2(−8)	4.91(−6)	−3.34(−5)	6.40(−5)
	2.490(−2)	3.723(−3)	2.5(−7)	1.6(−8)	4.74(−6)	−3.35(−5)	6.37(−5)
			$\mathcal{E}_0 = 0.01$				
0.35000	−2.542(−2)	7.459(−3)	3.1(−6)	7.2(−7)	3.49(−5)	−8.95(−5)	3.32(−4)
	−2.542(−2)	7.434(−3)	4.4(−6)	4.1(−7)	3.22(−5)	−9.30(−5)	3.28(−4)
0.36000	−1.540(−2)	7.457(−3)	2.8(−6)	7.2(−7)	3.07(−5)	−9.25(−5)	3.12(−4)
	−1.541(−2)	7.435(−3)	3.7(−6)	3.7(−7)	3.03(−5)	−9.76(−5)	3.15(−4)
0.37000	−5.385(−3)	7.448(−3)	2.7(−6)	8.4(−7)	2.71(−5)	−9.43(−5)	2.91(−4)
	−5.403(−3)	7.435(−3)	3.1(−6)	3.3(−7)	2.75(−5)	−1.03(−4)	3.00(−4)
0.37500	−3.767(−4)	7.436(−3)	2.8(−6)	8.8(−7)	2.55(−5)	−9.59(−5)	2.81(−4)
	−3.987(−4)	7.435(−3)	2.9(−6)	3.1(−7)	2.60(−5)	−1.07(−4)	2.92(−4)
0.38000	4.624(−3)	7.423(−3)	2.9(−6)	7.3(−7)	2.41(−5)	−1.02(−4)	2.75(−4)
	4.605(−3)	7.434(−3)	2.7(−6)	3.0(−7)	2.45(−5)	−1.11(−4)	2.84(−4)
0.39000	1.462(−2)	7.415(−3)	2.7(−6)	4.7(−7)	2.17(−5)	−1.16(−4)	2.65(−4)
	1.461(−2)	7.433(−3)	2.3(−6)	2.7(−7)	2.16(−5)	−1.20(−4)	2.69(−4)
0.40000	2.462(−2)	7.412(−3)	2.4(−6)	3.5(−7)	1.95(−5)	−1.31(−4)	2.53(−4)
	2.461(−2)	7.432(−3)	2.0(−6)	2.5(−7)	1.89(−5)	−1.34(−4)	2.54(−4)
			Three-photon ionisation				
			$\mathcal{E}_0 = 0.001$				
0.18500	−5.009(−3)	3.980(−6)			6.70(−6)	−1.42(−6)	7.65(−6)
	−5.009(−3)	3.926(−6)	3.0(−10)	2.7(−15)	6.66(−6)	−1.42(−6)	7.64(−6)
0.18650	−2.009(−3)	3.950(−6)			6.52(−6)	−1.43(−6)	7.54(−6)
	−2.009(−3)	3.926(−6)	2.8(−10)	3.0(−15)	6.52(−6)	−1.42(−6)	7.54(−6)
0.18700	−1.009(−3)	3.950(−6)			6.47(−6)	−1.43(−6)	7.50(−6)
	−1.009(−3)	3.927(−6)	2.7(−10)	3.1(−15)	6.47(−6)	−1.43(−6)	7.50(−6)
0.18725	−5.089(−4)	3.930(−6)			6.44(−6)	−1.43(−6)	7.48(−6)
	−5.089(−4)	3.927(−6)	2.7(−10)	3.1(−15)	6.44(−6)	−1.43(−6)	7.48(−6)
0.18745	−1.089(−4)	3.940(−6)			6.42(−6)	−1.42(−6)	7.46(−6)
	−1.089(−4)	3.927(−6)	2.7(−10)	3.1(−15)	6.42(−6)	−1.43(−6)	7.47(−6)

Continued on next page

Table E.1: Continued from previous page

ω	Δ	Ω	β	γ_a	γ_b	S_a	S_b
0.18750	−8.891(−6)	3.930(−6)			6.41(−6)	−1.43(−6)	7.47(−6)
	−8.892(−6)	3.927(−6)	2.7(−10)	3.1(−15)	6.41(−6)	−1.43(−6)	7.46(−6)
0.18775	4.911(−4)	3.930(−6)			6.38(−6)	−1.43(−6)	7.45(−6)
	4.911(−4)	3.927(−6)	2.7(−10)	3.2(−15)	6.38(−6)	−1.43(−6)	7.44(−6)
0.18800	9.911(−4)	3.940(−6)			6.36(−6)	−1.43(−6)	7.42(−6)
	9.911(−4)	3.927(−6)	2.6(−10)	3.2(−15)	6.36(−6)	−1.43(−6)	7.43(−6)
			$\mathcal{E}_0 = 0.005$				
0.18500	−5.227(−3)	9.940(−5)	2.3(−7)		1.67(−4)	−3.55(−5)	1.91(−4)
	−5.226(−3)	9.799(−5)	1.9(−7)	3.5(−11)	1.67(−4)	−3.55(−5)	1.91(−4)
0.18650	−2.224(−3)	9.840(−5)	2.2(−7)		1.63(−4)	−3.56(−5)	1.89(−4)
	−2.224(−3)	9.802(−5)	1.8(−7)	3.9(−11)	1.63(−4)	−3.56(−5)	1.88(−4)
0.18700	−1.223(−3)	9.810(−5)	2.3(−7)		1.62(−4)	−3.57(−5)	1.88(−4)
	−1.223(−3)	9.802(−5)	1.7(−7)	4.1(−11)	1.62(−4)	−3.57(−5)	1.88(−4)
0.18750	−2.225(−4)	9.780(−5)	2.2(−7)		1.60(−4)	−3.58(−5)	1.87(−4)
	−2.224(−4)	9.803(−5)	1.7(−7)	4.2(−11)	1.60(−4)	−3.57(−5)	1.87(−4)
0.18800	7.785(−4)	9.800(−5)	2.6(−7)		1.59(−4)	−3.58(−5)	1.86(−4)
	7.785(−4)	9.803(−5)	1.7(−7)	4.3(−11)	1.59(−4)	−3.58(−5)	1.86(−4)
0.18850	1.779(−3)	9.830(−5)	2.5(−7)		1.58(−4)	−3.59(−5)	1.85(−4)
	1.779(−3)	9.803(−5)	1.6(−7)	4.4(−11)	1.58(−4)	−3.58(−5)	1.85(−4)
0.19000	4.782(−3)	9.930(−5)	2.4(−7)		1.54(−4)	−3.60(−5)	1.82(−4)
	4.782(−3)	9.801(−5)	1.5(−7)	4.7(−11)	1.53(−4)	−3.60(−5)	1.82(−4)
0.19500	1.479(−2)	1.030(−4)	2.1(−7)		1.41(−4)	−3.66(−5)	1.73(−4)
	1.479(−2)	9.783(−5)	1.3(−7)	5.2(−11)	1.37(−4)	−3.66(−5)	1.72(−4)
			$\mathcal{E}_0 = 0.01$				
0.18500	−5.909(−3)	3.930(−4)	3.9(−6)		6.72(−4)	−1.42(−4)	7.67(−4)
	−5.907(−3)	3.900(−4)	3.0(−6)	2.1(−9)	6.67(−4)	−1.42(−4)	7.65(−4)
0.18650	−2.898(−3)	3.890(−4)	3.4(−6)		6.54(−4)	−1.43(−4)	7.55(−4)
	−2.897(−3)	3.903(−4)	2.8(−6)	2.4(−9)	6.53(−4)	−1.43(−4)	7.55(−4)
0.18700	−1.895(−3)	3.880(−4)	3.4(−6)		6.49(−4)	−1.43(−4)	7.52(−4)
	−1.894(−3)	3.903(−4)	2.8(−6)	2.5(−9)	6.48(−4)	−1.43(−4)	7.51(−4)
0.18750	−8.925(−3)	3.870(−4)	3.4(−6)		6.43(−4)	−1.44(−4)	7.49(−4)
	−8.906(−4)	3.904(−4)	2.7(−6)	2.6(−9)	6.43(−4)	−1.43(−4)	7.47(−4)
0.18800	1.129(−4)	3.860(−4)	3.9(−6)		6.33(−4)	−1.43(−4)	7.44(−4)
	1.129(−4)	3.904(−4)	2.7(−6)	2.7(−9)	6.38(−4)	−1.43(−4)	7.44(−4)
0.18850	1.117(−3)	3.870(−4)	4.0(−6)		6.31(−4)	−1.43(−4)	7.44(−4)
	1.117(−3)	3.904(−4)	2.6(−6)	2.7(−9)	6.32(−4)	−1.44(−4)	7.40(−4)

Continued on next page

Table E.1: Continued from previous page

ω	Δ	Ω	β	γ_a	γ_b	S_a	S_b
0.19000	4.126(−3)	3.910(−4)	3.9(−6)		6.16(−4)	−1.44(−4)	7.29(−4)
	4.127(−3)	3.904(−4)	2.5(−6)	2.9(−9)	6.15(−4)	−1.44(−4)	7.28(−4)
0.19500	1.416(−2)	4.050(−4)	3.3(−6)		5.66(−4)	−1.47(−4)	6.95(−4)
	1.416(−2)	3.899(−4)	2.0(−6)	3.2(−9)	5.51(−4)	−1.47(−4)	6.89(−4)
			Four-photon ionisation				
			$\mathcal{E}_0 = 0.001$				
0.14810	−1.582(−4)	2.710(−8)			3.31(−6)	−1.30(−6)	1.24(−5)
	−1.582(−4)	−2.687(−8)	−6.0(−12)	4.1(−16)	3.31(−6)	−1.30(−6)	1.24(−5)
0.14812	−9.816(−5)	2.670(−8)			3.31(−6)	−1.30(−6)	1.24(−5)
	−9.817(−5)	−2.687(−8)	−6.0(−12)	4.1(−16)	3.31(−6)	−1.30(−6)	1.24(−5)
0.14184	−3.816(−5)	2.690(−8)			3.31(−6)	−1.30(−6)	1.24(−5)
	−3.816(−5)	−2.687(−8)	−6.0(−12)	4.1(−16)	3.31(−6)	−1.30(−6)	1.24(−5)
0.14816	2.184(−5)	2.680(−8)			3.30(−6)	−1.30(−6)	1.24(−5)
	2.184(−5)	−2.687(−8)	−6.0(−12)	4.1(−16)	3.31(−6)	−1.30(−6)	1.24(−5)
0.14817	5.184(−5)	2.690(−8)			3.30(−6)	−1.30(−6)	1.24(−5)
	5.184(−5)	−2.688(−8)	−6.0(−12)	4.1(−16)	3.30(−6)	−1.30(−6)	1.24(−5)
0.14820	1.418(−4)	2.690(−8)			3.30(−6)	−1.30(−6)	1.24(−5)
	1.418(−4)	−2.688(−8)	−6.0(−12)	4.1(−16)	3.30(−6)	−1.30(−6)	1.24(−5)
			$\mathcal{E}_0 = 0.005$				
0.14790	−1.083(−3)	3.270(−6)	1.6(−8)		8.27(−5)	−3.24(−5)	3.07(−4)
	−1.087(−3)	−3.335(−6)	−1.9(−8)	3.8(−12)	8.32(−5)	−3.24(−5)	3.10(−4)
0.14822	−1.222(−4)	3.240(−6)	1.7(−8)		8.20(−5)	−3.24(−5)	3.05(−4)
	−1.255(−4)	−3.338(−6)	−1.9(−8)	3.8(−12)	8.26(−5)	−3.24(−5)	3.09(−4)
0.14825	−3.208(−5)	3.240(−6)	1.7(−8)		8.19(−5)	−3.24(−5)	3.05(−4)
	−3.534(−5)	−3.339(−6)	−1.9(−8)	3.8(−12)	8.25(−5)	−3.24(−5)	3.08(−4)
0.14828	5.804(−5)	3.230(−6)	1.6(−8)		8.19(−5)	−3.24(−5)	3.05(−4)
	5.477(−5)	−3.339(−6)	−1.9(−8)	3.8(−12)	8.25(−5)	−3.24(−5)	3.08(−4)
0.14830	1.181(−4)	3.230(−6)	1.6(−8)		8.19(−5)	−3.24(−5)	3.05(−4)
	1.148(−4)	−3.339(−6)	−1.9(−8)	3.8(−12)	8.24(−5)	−3.24(−5)	3.08(−4)
0.14860	1.019(−3)	3.200(−6)	1.7(−8)		8.12(−5)	−3.25(−5)	3.04(−4)
	1.016(−3)	−3.342(−6)	−1.8(−8)	3.9(−12)	8.17(−5)	−3.25(−5)	3.07(−4)
			$\mathcal{E}_0 = 0.01$				
0.14820	−1.092(−3)	2.320(−5)	4.9(−7)		3.20(−4)	−1.30(−4)	1.12(−3)
	−1.121(−3)	−2.607(−5)	−6.0(−7)	9.2(−10)	3.30(−4)	−1.30(−4)	1.15(−3)

Continued on next page

Table E.1: Continued from previous page

ω	Δ	Ω	β	γ_a	γ_b	S_a	S_b
0.14840	$-4.903(-4)$	$2.310(-5)$	$4.9(-7)$		$3.19(-4)$	$-1.30(-4)$	$1.12(-3)$
	$-5.178(-4)$	$-2.607(-5)$	$-5.9(-7)$	$9.3(-10)$	$3.28(-4)$	$-1.30(-4)$	$1.14(-3)$
0.14850	$-1.893(-4)$	$2.300(-5)$	$4.9(-7)$		$3.18(-4)$	$-1.30(-4)$	$1.11(-3)$
	$-2.166(-4)$	$-2.607(-5)$	$-5.9(-7)$	$9.3(-10)$	$3.27(-4)$	$-1.30(-4)$	$1.14(-3)$
0.14870	$4.134(-4)$	$2.290(-5)$	$4.8(-7)$		$3.16(-4)$	$-1.30(-4)$	$1.11(-3)$
	$3.857(-4)$	$-2.606(-5)$	$-5.9(-7)$	$9.4(-10)$	$3.25(-4)$	$-1.30(-4)$	$1.14(-3)$
0.14880	$7.144(-4)$	$2.280(-5)$	$4.8(-7)$		$3.16(-4)$	$-1.30(-4)$	$1.11(-3)$
	$6.866(-4)$	$-2.606(-5)$	$-5.8(-7)$	$9.4(-10)$	$3.24(-4)$	$-1.30(-4)$	$1.14(-3)$
0.14910	$1.618(-3)$	$2.260(-5)$	$4.7(-7)$		$3.13(-4)$	$-1.30(-4)$	$1.11(-3)$
	$1.589(-3)$	$-2.605(-5)$	$-5.7(-7)$	$9.5(-10)$	$3.21(-4)$	$-1.30(-4)$	$1.14(-3)$

Acknowledgments

First, I want to thank you, Marcus: for offering me the topic, for always being available and approachable, for being both helpful and honest in our discussions, and of course for giving extensive feedback on my drafts. I would imagine that supervising students is always a tightrope walk of giving too little and too much freedom – judging by how much fun I had during the last year, I think you struck a perfect balance!

All the members of the TLDM group, I want to thank for your friendliness, and for our many scientific and just as many unscientific discussions! Regarding the science, I want to single out Axel and Edvin; you two helped me a lot both with maths, coding and of course physics. Thank you Axel furthermore for your plentiful helpful comments on my drafts.

My gratitude further extends to Cord Arnold and Chen Guo from the atomic division faculty; they gave me information on current laser capabilities in order to contextualise my research.

Many thanks to my unforgettable roommates in the thesis office at MatFys! And in general, thanks to all of you at MatFys who I've had nice talks with at lunch, not to mention the several of you that I had the privilege of backstabbing in our lasertag games. I would do it again in a heartbeat.

Finally, the only person who I forced to listen to all my frequent musings, complaints and sparsely scattered *heureka* moments (the latter traditionally at inopportune moments) is of course my dearest Anna, who has been my biggest support for, by now, five years. Thank you!

References

[1] Heisenberg, W. Über quantentheoretische Umdeutung kinematischer und mechanischer Beziehungen. *Zeitschrift für Physik* **33**, 879–893 (1925).

[2] Born, M., Heisenberg, W. & Jordan, P. Zur Quantenmechanik. II. *Zeitschrift für Physik* **35**, 557–615 (1926).

[3] Schrödinger, E. Quantisierung als Eigenwertproblem. *Annalen der Physik* **384**, 361–376 (1926).

[4] Maiman, T. H. Stimulated optical radiation in ruby. *Nature* (1960).

[5] Einstein, A. Strahlungs-Emission und Absorption nach der Quantentheorie. *Deutsche Physikalische Gesellschaft* **18**, 318–323 (1916).

[6] Foot, C. J. *Atomic Physics* (OUP Oxford, 2004).

[7] Göppert-Mayer, M. Über Elementarakte mit zwei Quantensprüngen. *Annalen der Physik* **401**, 273–294 (1931).

[8] Franken, P. A., Hill, A. E., Peters, C. W. & Weinreich, G. Generation of Optical Harmonics. *Physical Review Letters* **7**, 118–119 (1961).

[9] Kaiser, W. & Garrett, C. G. B. Two-Photon Excitation in Ca F 2 : Eu 2 +. *Physical Review Letters* **7**, 229–231 (1961).

[10] Saleh, B. E. A. & Teich, M. C. *Fundamentals of Photonics.* Wiley Series in Pure and Applied Optics (Wiley-Interscience, Hoboken, New Jersey, 2007), second edition edn.

[11] Joachain, C. J., Kylstra, N. J. & Potvliege, R. M. *Atoms in Intense Laser Fields* (Cambridge University Press, Cambridge, 2011).

[12] Amini, K. *et al.* Symphony on strong field approximation. *Reports on Progress in Physics* **82**, 116001 (2019).

[13] Krausz, F. & Ivanov, M. Attosecond physics. *Reviews of Modern Physics* **81**, 163–234 (2009).

[14] Kumlin, J. *et al.* Quantum optics with Rydberg superatoms. *Journal of Physics Communications* **7**, 052001 (2023).

[15] Li, R., Qian, J. & Zhang, W. Proposal for practical Rydberg quantum gates using a native two-photon excitation. *Quantum Science and Technology* **8**, 035032 (2023).

[16] Chow, M. N. H. *et al.* First-order crosstalk mitigation in parallel quantum gates driven with multi-photon transitions. *Applied Physics Letters* **124**, 044002 (2024).

[17] Rabi, I. I. Space Quantization in a Gyrating Magnetic Field. *Physical Review* **51**, 652–654 (1937).

[18] Vion, D. *et al.* Manipulating the Quantum State of an Electrical Circuit. *Science* **296**, 886–889 (2002).

[19] Yu, Y., Han, S., Chu, X., Chu, S.-I. & Wang, Z. Coherent Temporal Oscillations of Macroscopic Quantum States in a Josephson Junction. *Science* **296**, 889–892 (2002).

[20] Wong, K. C. Review of NMR Spectroscopy: Basic Principles, Concepts and Applications in Chemistry. *Journal of Chemical Education* **91**, 1103–1104 (2014).

[21] Grover, V. P. *et al.* Magnetic Resonance Imaging: Principles and Techniques: Lessons for Clinicians. *Journal of Clinical and Experimental Hepatology* **5**, 246–255 (2015).

[22] Nandi, S. *et al.* Observation of Rabi dynamics with a short-wavelength free-electron laser. *Nature* **608**, 488–493 (2022).

[23] Gentile, T. R., Hughey, B. J., Kleppner, D. & Ducas, T. W. Experimental study of one- and two-photon Rabi oscillations. *Physical Review A* **40**, 5103–5115 (1989).

[24] Gatzke, M., Baruch, M. C., Watkins, R. B. & Gallagher, T. F. Microwave multiphoton Rabi oscillations. *Physical Review A* **48**, 4742–4749 (1993).

[25] Linskens, A. F., Holleman, I., Dam, N. & Reuss, J. Two-photon Rabi oscillations. *Physical Review A* **54**, 4854–4862 (1996).

[26] Fushitani, M. *et al.* Femtosecond two-photon Rabi oscillations in excited He driven by ultrashort intense laser fields. *Nature Photonics* **10**, 102–105 (2016).

[27] Reetz-Lamour, M., Amthor, T., Deiglmayr, J. & Weidemüller, M. Rabi Oscillations and Excitation Trapping in the Coherent Excitation of a Mesoscopic Frozen Rydberg Gas. *Physical Review Letters* **100**, 253001 (2008).

[28] Huber, B. *et al.* GHz Rabi Flopping to Rydberg States in Hot Atomic Vapor Cells. *Physical Review Letters* **107**, 243001 (2011).

[29] Johnson, T. A. *et al.* Rabi Oscillations between Ground and Rydberg States with Dipole-Dipole Atomic Interactions. *Physical Review Letters* **100**, 113003 (2008).

[30] Kittelmann, O., Ringling, J., Nazarkin, A., Korn, G. & Hertel, I. V. Direct Observation of Coherent Medium Response under the Condition of Two-Photon Excitation of Krypton by Femtosecond UV-Laser Pulses. *Physical Review Letters* **76**, 2682–2685 (1996).

[31] Rickes, T. *et al.* Efficient adiabatic population transfer by two-photon excitation assisted by a laser-induced Stark shift. *The Journal of Chemical Physics* **113**, 534–546 (2000).

[32] Yatsenko, L. P., Romanenko, V. I., Shore, B. W., Halfmann, T. & Bergmann, K. Two-photon excitation of the metastable 2s state of hydrogen assisted by laser-induced chirped Stark shifts and continuum structure. *Physical Review A* **71**, 033418 (2005).

[33] Faisal, F. H. M. *Theory of Multiphoton Processes* (Springer, New York, 1987).

[34] Akulin, V. M. & Karlov, N. V. *Intense Resonant Interactions in Quantum Electronics*. Theoretical and Mathematical Physics (Springer-Verlag Berlin, Heidelberg, 1992), 1 edn.

[35] Cohen-Tannoudji, C., Grynberg, G. & Dupont-Roc, J. *Atom-Photon Interactions: Basic Processes and Applications* (Wiley-VCH, New York, 1998).

[36] Lindgren, I. & Morrison, J. *Atomic Many-Body Theory*, vol. 13 of *Springer Series in Chemical Physics* (Springer, Berlin, Heidelberg, 1982).

[37] Bakos, J. S. Multiphoton Ionization of Atoms. In Marton, L. (ed.) *Advances in Electronics and Electron Physics*, vol. 36, 57–152 (Academic Press, 1975).

[38] Feshbach, H. Unified theory of nuclear reactions. *Annals of Physics* **5**, 357–390 (1958).

[39] Feshbach, H. A unified theory of nuclear reactions. II. *Annals of Physics* **19**, 287–313 (1962).

[40] Beers, B. L. & Armstrong, L. Exact solution of a realistic model for two-photon ionization. *Physical Review A* **12**, 2447–2454 (1975).

[41] Holt, C. R., Raymer, M. G. & Reinhardt, W. P. Time dependences of two-, three-, and four-photon ionization of atomic hydrogen in the ground 1^2S and metastable 2^2S states. *Physical Review A* **27**, 2971–2988 (1983).

[42] Vitanov, N. V. & Stenholm, S. Population transfer by delayed pulses via continuum states. *Physical Review A* **56**, 741–747 (1997).

[43] Zhang, X. *et al.* Effect of nonresonant states in near-resonant two-photon ionization of hydrogen. *Physical Review A* **106**, 063114 (2022).

[44] Tóth, A. & Csehi, A. Probing strong-field two-photon transitions through dynamic interference. *Journal of Physics B: Atomic, Molecular and Optical Physics* **54**, 035005 (2021).

[45] Simonović, N. S., Popović, D. B. & Bunjac, A. Manifestations of Rabi Dynamics in the Photoelectron Energy Spectra at Resonant Two-Photon Ionization of Atom by Intense Short Laser Pulses. *Atoms* **11**, 20 (2023).

[46] Demekhin, P. V. & Cederbaum, L. S. Strong interference effects in the resonant Auger decay of atoms induced by intense x-ray fields. *Physical Review A* **83**, 023422 (2011).

[47] Mouloudakis, G. & Lambropoulos, P. Non-Hermitian landscape of autoionization. *Physical Review A* **108**, 063104 (2023).

[48] Yu, C. & Madsen, L. B. Core-resonant ionization of helium by intense XUV pulses: Analytical and numerical studies on channel-resolved spectral features. *Physical Review A* **98**, 033404 (2018).

[49] Day, H. C., Piraux, B. & Potvliege, R. M. Multistate non-Hermitian Floquet dynamics in short laser pulses. *Physical Review A* **61**, 031402 (2000).

[50] Duncan, D. I., Story, J. G. & Gallagher, T. F. Floquet description of multiphoton processes in Li. *Physical Review A* **52**, 2209–2217 (1995).

[51] Chu, S.-I. Recent Developments in Semiclassical Floquet Theories for Intense-Field Multiphoton Processes. In Bates, D. R. & Bederson, B. (eds.) *Advances in Atomic and Molecular Physics*, vol. 21, 197–253 (Academic Press, 1985).

[52] Chu, S.-I. Generalized Floquet Theoretical Approaches to Intense-Field Multiphoton and Nonlinear Optical Processes. *Advances in Chemical Physics* **73**, 739–799 (2007).

[53] Rosenberg, L. Multiphoton transitions: Approximations for the effective Hamiltonian. *Physical Review A* **14**, 1137–1145 (1976).

[54] Hanson, L. G., Zhang, J. & Lambropoulos, P. Manifestations of atomic and core resonances in photoelectron energy spectra. *Physical Review A* **55**, 2232–2244 (1997).

[55] Olofsson, E. & Dahlström, J. M. Photoelectron signature of dressed-atom stabilization in an intense XUV field. *Physical Review Research* **5**, 043017 (2023).

[56] Dörr, M., Latinne, O. & Joachain, C. J. Time evolution of two-photon population transfer between the 1s and 2s states of a hydrogen atom. *Physical Review A* **55**, 3697–3703 (1997).

[57] Shore, B. W. *The Theory of Coherent Atomic Excitation* (Wiley VCH, New York, 1990).

[58] Shore, B. W. Pre-History Of The Concepts Underlying Stimulated Raman Adiabatic Passage (STIRAP). *Acta Physica Slovaca* **63** (2013).

[59] Brion, E., Pedersen, L. H. & Mølmer, K. Adiabatic elimination in a lambda system. *Journal of Physics A: Mathematical and Theoretical* **40**, 1033 (2007).

[60] Paulisch, V., Rui, H., Ng, H. K. & Englert, B.-G. Beyond adiabatic elimination: A hierarchy of approximations for multi-photon processes. *The European Physical Journal Plus* **129**, 12 (2014).

[61] Fewell, M. P. Adiabatic elimination, the rotating-wave approximation and two-photon transitions. *Optics Communications* **253**, 125–137 (2005).

[62] Kaufman, B., Rozgonyi, T., Marquetand, P. & Weinacht, T. Adiabatic elimination in strong-field light-matter coupling. *Physical Review A* **102**, 063117 (2020).

[63] Torosov, B. T. & Vitanov, N. V. Adiabatic elimination of a nearly resonant quantum state. *Journal of Physics B: Atomic, Molecular and Optical Physics* **45**, 135502 (2012).

[64] Sanz, M., Solano, E. & Egusquiza, Í. L. Beyond Adiabatic Elimination: Effective Hamiltonians and Singular Perturbation. In Anderssen, R. S. *et al.* (eds.) *Applications + Practical Conceptualization + Mathematics = Fruitful Innovation*, Mathematics for Industry, 127–142 (Springer Japan, Tokyo, 2016).

[65] Macrì, N., Giannelli, L., Paladino, E. & Falci, G. Coarse-Grained Effective Hamiltonian via the Magnus Expansion for a Three-Level System. *Entropy* **25**, 234 (2023).

[66] Han, R., Khoon Ng, H. & Englert, B.-G. Raman transitions without adiabatic elimination: A simple and accurate treatment. *Journal of Modern Optics* **60**, 255–265 (2013).

[67] Finkelstein-Shapiro, D. *et al.* Adiabatic elimination and subspace evolution of open quantum systems. *Physical Review A* **101**, 042102 (2020).

[68] Saideh, I., Finkelstein-Shapiro, D., Pullerits, T. & Keller, A. Projection-based adiabatic elimination of bipartite open quantum systems. *Physical Review A* **102**, 032212 (2020).

[69] Bloch, C. Sur la théorie des perturbations des états liés. *Nuclear Physics* **6**, 329–347 (1958).

[70] des Cloizeaux, J. Extension d'une formule de Lagrange à des problèmes de valeurs propres. *Nuclear Physics* **20**, 321–346 (1960).

[71] Krenciglowa, E. M. & Kuo, T. T. S. Convergence of effective hamiltonian expansion and partial summations of folded diagrams. *Nuclear Physics A* **235**, 171–189 (1974).

[72] Lee, S. Y. & Suzuki, K. The effective interaction of two nucleons in the s-d shell. *Physics Letters B* **91**, 173–176 (1980).

[73] Suzuki, K. & Okamoto, R. Degenerate Perturbation Theory in Quantum Mechanics. *Progress of Theoretical Physics* **70**, 439–451 (1983).

[74] Durand, P. Direct determination of effective Hamiltonians by wave-operator methods. I. General formalism. *Physical Review A* **28**, 3184–3192 (1983).

[75] Klein, D. J. Degenerate perturbation theory. *The Journal of Chemical Physics* **61**, 786–798 (1974).

[76] Löwdin, P.-O. Studies in perturbation theory: Part I. An elementary iteration-variation procedure for solving the Schrödinger equation by partitioning technique. *Journal of Molecular Spectroscopy* **10**, 12–33 (1963).

[77] Brandow, B. H. Linked-Cluster Expansions for the Nuclear Many-Body Problem. *Reviews of Modern Physics* **39**, 771–828 (1967).

[78] Leyva-Ramos, J. Partial-fraction expansion in system analysis. *International Journal of Control* **53**, 619–639 (1991).

[79] Shirley, J. H. Solution of the Schrödinger Equation with a Hamiltonian Periodic in Time. *Physical Review* **138**, B979–B987 (1965).

[80] Chu, S.-I. & Reinhardt, W. P. Intense Field Multiphoton Ionization via Complex Dressed States: Application to the H Atom. *Physical Review Letters* **39**, 1195–1198 (1977).

[81] Maquet, A., Chu, S.-I. & Reinhardt, W. P. Stark ionization in dc and ac fields: An L^2 complex-coordinate approach. *Physical Review A* **27**, 2946–2970 (1983).

[82] Griffiths, D. J. *Introduction to Quantum Mechanics* (Prentice Hall International, Upper Saddle River, NJ, 2004), 2nd edition edn.

[83] Cohen-Tannoudji, C., Diu, B. & Laloe, F. *Quantum Mechanics, Vol. 1* (Wiley-VCH, New York, 1977), 1 edn.

[84] Sakurai, J. & Napolitano, J. *Modern Quantum Mechanics* (Cambridge University Press, Cambridge, 2017), 2 edn.

[85] Maxwell, J. C. VIII. A dynamical theory of the electromagnetic field. *Philosophical Transactions of the Royal Society of London* **155**, 459–512 (1865).

[86] Griffiths, D. J. *Introduction to Electrodynamics* (Cambridge University Press, Cambridge, United Kingdom ; New York, NY, 2017), 4. revised edn.

[87] Lamb, W. E. Fine Structure of the Hydrogen Atom. III. *Physical Review* **85**, 259–276 (1952).

[88] Reiss, H. R. Velocity-gauge theory for the treatment of strong-field photodetachment. *Physical Review A* **76**, 033404 (2007).

[89] Reiss, H. R. High-Field Laser Physics (2010).

[90] Reiss, H. R. Limitations of gauge invariance and consequences for laser-induced processes (2010).

[91] Gazibegović-Busuladžić, A., Milošević, D. B. & Becker, W. Gauge dependence of the strong-field approximation: Theory vs. experiment for photodetachment of F-. *Optics Communications* **275**, 116–122 (2007).

[92] Anzaki, R., Shinohara, Y., Sato, T. & Ishikawa, K. L. Gauge invariance beyond the electric dipole approximation. *Physical Review A* **98**, 063410 (2018).

[93] Di Stefano, O. *et al.* Resolution of gauge ambiguities in ultrastrong-coupling cavity quantum electrodynamics. *Nature Physics* **15**, 803–808 (2019).

[94] Vábek, J., Bachau, H. & Catoire, F. Ionization dynamics and gauge invariance. *Physical Review A* **106**, 053115 (2022).

[95] Karaveli, S. & Zia, R. Optical Frequency Magnetic Dipole Transitions. In Bhushan, B. (ed.) *Encyclopedia of Nanotechnology*, 1942–1950 (Springer Netherlands, Dordrecht, 2012).

[96] Reiss, H. R. Theoretical methods in quantum optics: S-matrix and Keldysh techniques for strong-field processes. *Progress in Quantum Electronics* **16**, 1–71 (1992).

[97] Reiss, H. R. Limits on Tunneling Theories of Strong-Field Ionization. *Physical Review Letters* **101**, 043002 (2008).

[98] Tóth, A., Borbély, S., Zhou, Y. & Csehi, A. Role of dynamic Stark shifts in strong-field excitation and subsequent ionization. *Physical Review A* **107**, 053101 (2023).

[99] Zhao, Y. *et al.* Dynamic interference in strong-field multiphoton excitation and ionization. *Physical Review A* **106**, 063103 (2022).

[100] Einwohner, T. H., Wong, J. & Garrison, J. C. Analytical solutions for laser excitation of multilevel systems in the rotating-wave approximation. *Physical Review A* **14**, 1452–1456 (1976).

[101] Schek, I., Sage, M. L. & Jortner, J. Validity of the rotating wave approximation for high-order molecular multiphoton processes. *Chemical Physics Letters* **63**, 230–235 (1979).

[102] Whaley, K. B. & Light, J. C. Rotating-frame transformations: A new approximation for multiphoton absorption and dissociation in laser fields. *Physical Review A* **29**, 1188–1207 (1984).

[103] Ho, T.-S., Chu, S.-I. & Tietz, J. V. Semiclassical many-mode floquet theory. *Chemical Physics Letters* **96**, 464–471 (1983).

[104] Ho, T.-S. & Chu, S.-I. Semiclassical many-mode Floquet theory. II. Non-linear multiphoton dynamics of a two-level system in a strong bichromatic field. *Journal of Physics B: Atomic and Molecular Physics* **17**, 2101 (1984).

[105] Ho, T.-S. & Chu, S.-I. Semiclassical many-mode Floquet theory. III. SU(3) dynamical evolution of three-level systems in intense bichromatic fields. *Physical Review A* **31**, 659–676 (1985).

[106] Ho, T.-S. & Chu, S.-I. Semiclassical many-mode Floquet theory. IV. Coherent population trapping and SU(3) dynamical evolution of dissipative three-level systems in intense bichromatic fields. *Physical Review A* **32**, 377–395 (1985).

[107] Shore, B. W. Coherent manipulations of atoms using laser light. *Acta Physica Slovaca* **58**, 243–486 (2008).

[108] Cohen-Tannoudji, C. Optical Pumping and interactions of atoms with electromagnetic fields. *Cargèse Lectures in Physics* **2**, 347–394 (1968).

[109] Mariño, M. *Advanced Topics in Quantum Mechanics* (Cambridge University Press, Cambridge, 2021).

[110] Schucan, T. H. & Weidenmüller, H. A. Perturbation theory for the effective interaction in nuclei. *Annals of Physics* **76**, 483–509 (1973).

[111] Suzuki, K., Kumagai, H., Okamoto, R. & Matsuzaki, M. Recursion method for deriving an energy-independent effective interaction. *Physical Review C* **89**, 044003 (2014).

[112] Shore, B. W. & Ackerhalt, J. Dynamics of multilevel laser excitation: Three-level atoms. *Physical Review A* **15**, 1640–1647 (1977).

[113] Brune, M., Raimond, J. M. & Haroche, S. Theory of the Rydberg-atom two-photon micromaser. *Physical Review A* **35**, 154–163 (1987).

[114] Davidovich, L., Raimond, J. M., Brune, M. & Haroche, S. Quantum theory of a two-photon micromaser. *Physical Review A* **36**, 3771–3787 (1987).

[115] Narducci, L. M., Scully, M. O., Oppo, G.-L., Ru, P. & Tredicce, J. R. Spontaneous emission and absorption properties of a driven three-level system. *Physical Review A* **42**, 1630–1649 (1990).

[116] Beterov, I. M. & Chebotaev, V. P. Three-level gas systems and their interaction with radiation. *Progress in Quantum Electronics* **3**, 1–106 (1974).

[117] Kuklinski, J. R., Gaubatz, U., Hioe, F. T. & Bergmann, K. Adiabatic population transfer in a three-level system driven by delayed laser pulses. *Physical Review A* **40**, 6741–6744 (1989).

[118] Bechmann-Pasquinucci, H. & Peres, A. Quantum Cryptography with 3-State Systems. *Physical Review Letters* **85**, 3313–3316 (2000).

[119] Chen, X. & Muga, J. G. Engineering of fast population transfer in three-level systems. *Physical Review A* **86**, 033405 (2012).

[120] Vitanov, N. V. Adiabatic population transfer by delayed laser pulses in multistate systems. *Physical Review A* **58**, 2295–2309 (1998).

[121] Sola, I. R. & Malinovsky, V. S. Collapse of the stimulated Raman adiabatic passage due to geometrical factors and how to overcome it. *Physical Review A* **68**, 013412 (2003).

[122] Vitanov, N. V. & Stenholm, S. Population transfer via a decaying state. *Physical Review A* **56**, 1463–1471 (1997).

[123] Širca, S. & Horvat, M. *Computational Methods in Physics: Compendium for Students* (Springer, 2018), 2 edn.

[124] Jørgensen, F. Effective hamiltonians. *Molecular Physics* **29**, 1137–1164 (1975).

[125] Brandow, B. H. Formal theory of effective π-electron hamiltonians. *International Journal of Quantum Chemistry* **15**, 207–242 (1979).

[126] Brandow, B. H. Effective hamiltonian theory: Recent formal results and non-nuclear applications. In Zabolitzky, J. G., de Llano, M., Fortes, M. & Clark, J. W. (eds.) *Recent Progress in Many-Body Theories*, 373–381 (Springer, Berlin, Heidelberg, 1981).

[127] Soliverez, C. E. General theory of effective Hamiltonians. *Physical Review A* **24**, 4–9 (1981).

[128] Durand, P. & Malrieu, J.-P. Effective Hamiltonians and Pseudo-Operators as Tools for Rigorous Modelling. In Lawley, K. (ed.) *Advances in Chemical Physics*, vol. 67, 321–412 (Wiley, 1987), 1 edn.

[129] Suzuki, K. & Okamoto, R. General Structure of Effective Interaction in Degenerate Perturbation Theory. *Progress of Theoretical Physics* **71**, 1221–1238 (1984).

[130] Durand, P. & Paidarová, I. Convergence studies in the theory of effective Hamiltonians. *International Journal of Quantum Chemistry* **58**, 341–350 (1996).

[131] Killingbeck, J. P. & Jolicard, G. The Bloch wave operator: Generalizations and applications: Part I. The time-independent case. *Journal of Physics A: Mathematical and General* **36**, R105 (2003).

[132] Johnson, M. B. Folded diagram theory, time-dependent approach of Johnson and Baranger. In Barrett, B. R. (ed.) *Effective Interactions and Operators in Nuclei*, 25–41 (Springer, Berlin, Heidelberg, 1975).

[133] Shao, W., Wu, C. & Feng, X.-L. Generalized James' effective Hamiltonian method. *Physical Review A* **95**, 032124 (2017).

[134] Rosado, W. & Arraut, I. Comment on "Generalized James' effective Hamiltonian method". *Physical Review A* **108**, 066201 (2023).

[135] Shao, W., Wu, C. & Feng, X.-L. Reply to "Comment on 'Generalized James' effective Hamiltonian method'" (2024). 2312.05732.

[136] Gamow, G. Zur Quantentheorie des Atomkernes. *Zeitschrift für Physik* **51**, 204–212 (1928).

[137] Fock, V. & Krylov, N. On the uncertainty relation between time and energy. *J. Phys. USSR* **11**, 112–120 (1947).

[138] Baker, H. C. & Singleton, R. L. Non-Hermitian quantum dynamics. *Physical Review A* **42**, 10–17 (1990).

[139] Dattoli, G., Torre, A. & Mignani, R. Non-Hermitian evolution of two-level quantum systems. *Physical Review A* **42**, 1467–1475 (1990).

[140] Lambropoulos, P. Theory of multiphoton ionization: Near-resonance effects in two-photon ionization. *Physical Review A* **9**, 1992–2013 (1974).

[141] McClean, W. A. & Swain, S. Theory of resonant two-photon ionisation. *Journal of Physics B: Atomic and Molecular Physics* **11**, 1717 (1978).

[142] Faisal, F. H. M. & Moloney, J. V. Time-dependent theory of non-Hermitian Schrodinger equation: Application to multiphoton-induced ionisation decay of atoms. *Journal of Physics B: Atomic and Molecular Physics* **14**, 3603 (1981).

[143] Baker, H. C. Non-Hermitian Dynamics of Multiphoton Ionization. *Physical Review Letters* **50**, 1579–1582 (1983).

[144] Baker, H. C. Non-Hermitian quantum theory of multiphoton ionization. *Physical Review A* **30**, 773–793 (1984).

[145] Yamani, H. A. & Reinhardt, W. P. L^2 discretizations of the continuum: Radial kinetic energy and Coulomb Hamiltonian. *Physical Review A* **11**, 1144–1156 (1975).

[146] Telnov, D. A. & Chu, S.-I. High-order perturbation expansion of non-Hermitian Floquet theory for multiphoton and above-threshold ionization processes. *Physical Review A* **61**, 013408 (1999).

[147] Simon, B. The definition of molecular resonance curves by the method of exterior complex scaling. *Physics Letters A* **71**, 211–214 (1979).

[148] Moiseyev, N. *Non-Hermitian Quantum Mechanics* (Cambridge University Press, 2011).

[149] Grimaudo, R., Messina, A., Sergi, A., Vitanov, N. V. & Filippov, S. N. Two-Qubit Entanglement Generation through Non-Hermitian Hamiltonians Induced by Repeated Measurements on an Ancilla. *Entropy* **22**, 1184 (2020).

[150] Mayer, N., Moiseyev, N. & Smirnova, O. Enantiosensitive exceptional points (2023). 2306.12293.

[151] Higham, N. J. & Kim, H.-M. Numerical analysis of a quadratic matrix equation. *IMA Journal of Numerical Analysis* **20**, 499–519 (2000).

[152] Tisseur, F. & Meerbergen, K. The Quadratic Eigenvalue Problem. *SIAM Review* **43**, 235–286 (2001). 3649752.

[153] Lancaster, P. & Tisseur, F. Hermitian quadratic matrix polynomials: Solvents and inverse problems. *Linear Algebra and its Applications* **436**, 4017–4026 (2012).

[154] Maynau, D., Durand, Ph., Daudey, J. P. & Malrieu, J. P. Direct determination of effective Hamiltonians by wave-operator methods. II. Application to effective-spin interactions in π-electron systems. *Physical Review A* **28**, 3193–3206 (1983).

[155] Horn, R. A. & Johnson, C. R. *Matrix Analysis* (New York, NY, 2012).

[156] Dennis, J. E., Jr., Traub, J. F. & Weber, R. P. Algorithms for Solvents of Matrix Polynomials. *SIAM Journal on Numerical Analysis* **15**, 523–533 (1978).

[157] Kratz, W. & Stickel, E. Numerical Solution of Matrix Polynomial Equations by Newton's Method. *IMA Journal of Numerical Analysis* **7**, 355–369 (1987).

[158] Bai, Z.-Z. & Gao, Y.-H. Modified Bernoulli Iteration Methods for Quadratic Matrix Equation. *Journal of Computational Mathematics* **25**, 498–511 (2007). 43693387.

[159] Davis, G. J. Numerical Solution of a Quadratic Matrix Equation. *SIAM Journal on Scientific and Statistical Computing* **2**, 164–175 (1981).

[160] Rogus, D. & Lewenstein, M. Resonant ionisation by smooth laser pulses. *Journal of Physics B: Atomic and Molecular Physics* **19**, 3051 (1986).

[161] Demekhin, P. V. & Cederbaum, L. S. Dynamic Interference of Photoelectrons Produced by High-Frequency Laser Pulses. *Physical Review Letters* **108**, 253001 (2012).

[162] Tóth, B., Tóth, A. & Csehi, A. Competition of multiphoton ionization pathways in lithium. *Journal of Physics B: Atomic, Molecular and Optical Physics* **57**, 055002 (2024).

[163] Shore, B. W. & Knight, P. L. The Jaynes-Cummings Model. *Journal of Modern Optics* **40**, 1195–1238 (1993).

[164] Cederbaum, L. S. & Domcke, W. Local against non-local complex potential in resonant electron-molecule scattering. *Journal of Physics B: Atomic and Molecular Physics* **14**, 4665 (1981).

[165] Forster, B., Blu, T. & Unser, M. Complex B-splines. *Applied and Computational Harmonic Analysis* **20**, 261–282 (2006).

[166] Dahlström, J. M., Pabst, S. & Lindroth, E. Attosecond transient absorption of a bound wave packet coupled to a smooth continuum. *Journal of Optics* **19**, 114004 (2017).

[167] Hofmann, H. M., Lee, S. Y., Richert, J., Weidenmüller, H. A. & Schucan, T. H. Nonperturbative approximation schemes for the effective interaction in nuclei. *Annals of Physics* **85**, 410–437 (1974).

[168] Suzuki, K. & Lee, S. Y. Convergent Theory for Effective Interaction in Nuclei. *Progress of Theoretical Physics* **64**, 2091–2106 (1980).

[169] Malrieu, J. P., Durand, P. & Daudey, J. P. Intermediate Hamiltonians as a new class of effective Hamiltonians. *Journal of Physics A: Mathematical and General* **18**, 809 (1985).

[170] Schucan, T. H. & Weidenmüller, H. A. The effective interaction in nuclei and its perturbation expansion: An algebraic approach. *Annals of Physics* **73**, 108–135 (1972).

[171] Andreae, T. *et al.* Absolute frequency measurement of the hydrogen 1S-2S transition and a new value of the Rydberg constant. *Physical Review Letters* **69**, 1923–1926 (1992).

[172] Beyer, A. *et al.* Precision Spectroscopy of Atomic Hydrogen. *Journal of Physics: Conference Series* **467**, 012003 (2013).

[173] Cesar, C. L. *et al.* Two-Photon Spectroscopy of Trapped Atomic Hydrogen. *Physical Review Letters* **77**, 255–258 (1996).

[174] Huber, A., Gross, B., Weitz, M. & Hänsch, T. W. High-resolution spectroscopy of the 1s-2s transition in atomic hydrogen. *Physical Review A* **59**, 1844–1851 (1999).

[175] Parthey, C. G. *et al.* Improved Measurement of the Hydrogen 1s-2s Transition Frequency. *Physical Review Letters* **107**, 203001 (2011).

[176] Schmidt-Kaler, F. *et al.* High-resolution spectroscopy of the 1s-2s transition of atomic hydrogen and deuterium. *Physical Review A* **51**, 2789–2800 (1995).

[177] Zimmermann, C., Kallenbach, R. & Hänsch, T. W. High-resolution spectroscopy of the hydrogen 1s-2stransition in an atomic beam. *Physical Review Letters* **65**, 571–574 (1990).

[178] Morin, D. *Introduction to Classical Mechanics: With Problems and Solutions* (Cambridge University Press, Cambridge, 2008).

[179] Arnoult, O., Nez, F., Schwob, C., Julien, L. & Biraben, F. Towards an absolute measurement of the 1S-3S line in atomic hydrogen. *Canadian Journal of Physics* **83**, 273–281 (2005).

[180] Arnoult, O., Nez, F., Julien, L. & Biraben, F. Optical frequency measurement of the 1S–3S two-photon transition in hydrogen. *The European Physical Journal D* **60**, 243–256 (2010).

[181] Galtier, S. *et al.* Progress in Spectroscopy of the 1S–3S Transition in Hydrogen. *Journal of Physical and Chemical Reference Data* **44**, 031201 (2015).

[182] Ding, P., Ruchkina, M., Liu, Y., Alden, M. & Bood, J. Femtosecond two-photon-excited backward lasing of atomic hydrogen in a flame. *Optics Letters* **43**, 1183–1186 (2018).

[183] Ding, P., Ruchkina, M., Liu, Y., Alden, M. & Bood, J. Gain mechanism of femtosecond two-photon-excited lasing effect in atomic hydrogen. *Optics Letters* **44**, 2374–2377 (2019).

[184] Ruchkina, M., Ding, P., Ehn, A., Aldén, M. & Bood, J. Single-shot, spatially-resolved stand-off detection of atomic hydrogen via backward lasing in flames. *Proceedings of the Combustion Institute* **37**, 1281–1288 (2019).

[185] Cresser, J. D., Tang, A. Z., Salamo, G. J. & Chan, F. T. Lifetime of excited atomic states. *Physical Review A* **33**, 1677–1682 (1986).

[186] Basting, D. & Stamm, U. The Development of Excimer Laser Technology – History and Future Prospects. *Zeitschrift für Physikalische Chemie* **215** (2001).

[187] Travers, J. C., Grigorova, T. F., Brahms, C. & Belli, F. High-energy pulse self-compression and ultraviolet generation through soliton dynamics in hollow capillary fibres. *Nature Photonics* **13**, 547–554 (2019).

[188] Fleischhauer, M. & Manka, A. S. Propagation of laser pulses and coherent population transfer in dissipative three-level systems: An adiabatic dressed-state picture. *Physical Review A* **54**, 794–803 (1996).

[189] Yatsenko, L. P., Unanyan, R. G., Bergmann, K., Halfmann, T. & Shore, B. W. Population transfer through the continuum using laser-controlled Stark shifts. *Optics Communications* **135**, 406–412 (1997).

[190] Yatsenko, L. P., Shore, B. W., Halfmann, T., Bergmann, K. & Vardi, A. Source of metastable H(2s) atoms using the Stark chirped rapid-adiabatic-passage technique. *Physical Review A* **60**, R4237–R4240 (1999).

[191] Saalmann, U., Giri, S. K. & Rost, J. M. Adiabatic Passage to the Continuum: Controlling Ionization with Chirped Laser Pulses. *Physical Review Letters* **121**, 153203 (2018).

[192] Guo, Z. *et al.* Experimental demonstration of attosecond pump–probe spectroscopy with an X-ray free-electron laser. *Nature Photonics* 1–7 (2024).

[193] Kretschmar, M. *et al.* Compact realization of all-attosecond pump-probe spectroscopy. *Science Advances* **10**, eadk9605 (2024).